Strongly interacting systems in AMO physics

A dissertation presented
by

Mohammad Hafezi

to
The Department of Physics
in partial fulfillment of the requirements
for the degree of
Doctor of Philosophy
in the subject of

Physics

Harvard University
Cambridge, Massachusetts
August 2009

Thesis advisor

Mikhail D. Lukin

Author

Mohammad Hafezi

Strongly interacting systems in AMO physics

Abstract

Strong interactions can dramatically change the essence of a physical system. The behavior of strongly interacting systems can be fundamentally different than those where the interaction is absent or treated perturbatively. Many examples are known in solid-state physics including the superconductivity and the Fractional Quantum Hall Effect. At the same time, tremendous developments have been made in manipulating the interaction between light and matter. These advances have paved the way to explore the strongly interacting many-body physics in new regimes. This thesis explores two novel avenues to study strongly interacting systems. First, we investigate the effect of strong interaction between bosons subjected to an effective magnetic field. We show that how a Fractional Quantum Hall state of bosons in an optical lattice can be created, characterized and detected in a realistic experiment. Moreover, we demonstrate that Chern numbers can unambiguously characterize the topological order of such systems. Second, we investigate the effect of strong interaction between photons on their transport properties. We theoretically study the transmission of few-photon quantum fields through a strongly nonlinear optical medium. We develop a general approach to investigate non-equilibrium quantum transport of bosonic fields through a finite-size nonlinear medium and apply it to a recently demonstrated ex-

perimental system where cold atoms are loaded in a hollow-core optical fiber. We show that the photonic field can exhibit either anti-bunching or bunching, associated with the resonant excitation of bound states of photons by the input field. These effects can be observed by probing statistics of photons transmitted through the nonlinear fiber. As an application, we propose a scheme to realize a single-photon gate, where the presence or absence of a single "control" photon regulates the propagation of a "target" photon. Finally, we study optical nonlinearities due to the interaction of weak optical fields with the collective motion of a strongly dispersive ultracold gas. We present a theoretical model that is in good agreement with our experimental observations.

Contents

List of Figures

Citations to Previously Published Work

Parts of Chapter 2 have appeared in the following papers:

> "Fractional quantum Hall effect in optical lattices", Mohammad Hafezi, Anders S. Sørensen, Eugene A. Demler and Mikhail D. Lukin, Phys. Rev. A **76**, 023613 (2007);
>
> "Characterization of topological states on a lattice with Chern number", Mohammad Hafezi, Anders S. Sørensen, Mikhail D. Lukin and Eugene A. Demler, Euro. Phys. Lett. **81**, 1 (2008).

Parts of Chapters 3 and 4 have appeared in the following papers:

> "Photonic quantum transport in a nonlinear optical fiber", Mohammad Hafezi, Darrick E. Chang, Vladimir Gritsev, Eugene A. Demler and Mikhail D. Lukin submitted to Phys. Rev. Lett., (e-print: arXiv:0907.5206).
>
> "Efficient All-Optical Switching Using Slow Light within a Hollow Fiber", Michal Bajcsy, Sebastian Hofferberth, Vladko Balic, Thibault Peyronel, Mohammad Hafezi, Alexander S Zibrov, Vladan Vuletic, Mikhail D Lukin Phys. Rev. Lett. **102**, 203902 (2009).

Parts of Chapter 5 have appeared in the following paper:

> "Optical bistability at low light level due to collective atomic recoil", Mukund Vengalattore, Mohammad Hafezi, Mikhail D. Lukin, Mara Prentiss, Phys. Rev. Lett. **101**, 063901 (2008).

Acknowledgments

During the course of my Ph.D. studies, many individuals provided help and support in various forms. First and foremost, I would like to thank my Ph.D. advisor, Prof. Mikhail Lukin, for his support and encouragement. It was certainly a privilege to be his student. I am indebted to Misha for his dedication and enthusiastic support of my projects and my scientific career.

I would like to thank Prof. Eugene Demler for his help and support. I can hardly think of any meeting that the discussion with him did not add a new physical insight to the problem. I also had the opportunity to discuss and collaborate with Prof. Anders Sørensen on various projects. Most of our discussions were over phone or email, however, his simple yet insightful physical intuitions were undoubtedly instrumental in the progress of my studies. I should also thank Prof. Mara Prentiss, Prof. Vladan Vuletic , Prof. Markus Greiner and Prof. Ron Walsworth for useful discussions and teaching me a great deal of experimental details.

I am very fortunate to have Darrick Chang as a friend and a colleague and to share an office with him (in different locations). I have many good memories with him and Michael Hohensee in those offices. I had the opportunity to collaborate closely with experimentalists and learned something new most of the time we had a meeting together. For that, I should thank Mukund Vengalattore, Sasha Zibrov, Misho Bajcsy, Sebastian Hofferberth, Thibault Peyronel. I would like to thank my other friends and colleagues in the Physic Department and Lukin group members for many stimulating discussions that I had with them: Jacob Taylor, Arjyesh Mukherjee, Roberto Martinez, Liang Jiang, Alexey Gorshkov, Vladimir Gritsev, Adilet Imambekov, Ana-Maria Ray, Axel Andre, Peter Rabl, Gurudev Dutt, Philip Walther, Lily

Childress, Matt Eiseman, Florent Massou, Alex Nemroski, Frank Koppens, Sahand Hormoz, Pablo Londero and Alexey Tonyushkin. Moreover, I would like to gratefully acknowledge fruitful discussions with Michael Fleischhauer, Kun Yang, Yashar Ahmadian, Vahab Mirrokni, Sylvana Kolaczkowska, Senthil Todadri, Steven Girvin, Ignacio Cirac, Shanhui Fan and Peter Zoller. The Physics Department staff at Harvard has been a great source of support and help. I would like to thank in particular Sheila Ferguson, Marilyn O'Connor, Vickie Greene and Adam Ackerman for all their help.

I would also like to thank all my friends and also my earlier professors and teachers. In particular, Prof. Hossein Shojaie who introduced me to physics in the middle school and taught me how to enjoy science. My parents, Manouchehr Hafezi and Fatemeh Jazayeri, have both been a great source of support and encouragement throughout my life and my Ph.D. years have been no exception. Finally, it is hard for me to imagine how I could have finished this thesis without unflagging support of Salome and the peace of mind she gave me.

Dedicated to my mother Fatemeh,
and my father Manouchehr.

Chapter 1

Introduction

1.1 Motivation

Strong interactions can dramatically change the essence of a physical system. The behavior of strongly interacting systems can be fundamentally different than those where the interaction is absent or treated perturbatively. A few hallmarks of such phenomena are the experimental discovery and theoretical understanding of superconductivity [123, 15, 2, 64, 16] and the Fractional Quantum Hall Effect [162, 108], celebrated by several Nobel Prizes. While phenomena involving strongly correlated systems have traditionally been found in electronic systems, the fundamental behavior of strongly interacting systems are ubiquitous and do not critically depend on the constituent particles.

During the past few decades rapid and instrumental advances have been achieved in optical sciences and atomic physics to control and manipulate the interaction between light (photons) and matter (atoms). Examples include, photonic crystals [143],

ultracold gases [172, 25], Cavity QED Physics [20, 86, 134] and slow light [92]. Many of these developments have been dedicated to control the interaction between single atoms and single photons. These have paved the way to explore strongly-interacting many-body physics in new regimes. With these new developments we can not only shed light on unanswered questions that remain in condensed matter physics (particularly those of interacting electrons), but also push the research frontier into novel areas like non-equilibrium dynamics.

This thesis explores two different avenues to reach the regime of strong interaction and investigate the behavior of quantum states of such systems by developing new techniques to characterize and manipulate them.

First, we investigate the effect of strong interaction of bosons under influence of a U(1) gauge field (similar to magnetic field for electrons). This is motivated by recent advances in the ultracold atom science. By providing an unprecedented level of precision and control over interaction, such advances have introduced a playground to test and investigate new condensed matter models.

Second, we investigate the effect of strong interaction between photons in a one-dimensional nonlinear optical fiber. The synergy between the ultracold atom science and the optical fiber technology has opened a new door to manipulate the interaction between light and matter.

1.2 Bosonic Fractional Quantum Hall states

1.2.1 Introduction to Fractional Quantum Hall Physics

The quantization of the Hall conductance was first discovered by von Klitzing *et al.* [97] in 1980. In a two-dimensional electron gas at low temperature and under strong perpendicular magnetic field, von Klitzing *et al.* observed plateaus of Hall conductivity occuring at integral multiples of e^2/h. This quantum effect is called the Integer Quantum Hall Effect (IQHE). In 1982, Tsui, Strömer and Gossard [162] discovered the Fractional Quantum Hall Effect (FQHE) by working with a sample with fewer impurities. Although, both observations seem to be similar, however, the underlying physics of the FQHE and the IQHE are quite different. The IQHE can be explained by a simple single-particle theory considering random impurity potentials, and the FHQE is a many-body effect in which the role of the electron-electron interaction is essential in the phenomenon. In 1983, Laughlin in his seminal paper [108] suggested a wave function to explain the essence of some of the FHQE states.

To understand this phenomenon, we briefly describe the Laughlin wave function. We consider electrons confined in a continuum in x-y plane and are subjected to a magnetic field in the perpendicular direction given by the vector potential $\mathbf{A} = \frac{1}{2}B(x\hat{y} - y\hat{x})$, in the symmetric gauge. The single-particle wave functions are given by Landau levels each separated by the cyclotron energy $\frac{e\hbar B}{m_e c}$, where B is the strength of the magnetic field and m_e is the mass of the electron. The lowest Landau levels (LLL) are eigenfunctions ϕ_m of the orbital angular momentum operator with orbital angular momentum m given by

$$\phi_m(z) = \langle z|m\rangle = \frac{1}{(2\pi l_B 2^m m!)^{1/2}} \left(\frac{z}{l_B}\right)^m e^{-|z^2|/4l_B^2}, \tag{1.1}$$

where the position of the electron is characterized by a complex coordinate $z = x + iy$ and the magnetic length is $l_B = (\frac{\hbar c}{eB})^{1/2}$. We define N_ϕ to be the total number of magnetic flux quanta, i.e. $N_\phi = \frac{A}{2\pi l_B^2}$, where A is the area of the system. It is easy to calculate the diagonal matrix element $\langle m|r^2|m\rangle = 2(m+1)l_B^2$, which means that the area swept by an electron in the state $|m\rangle$ is proportional to m [109]. Since this area should always be smaller than the whole area of the system (i.e., $\pi\langle m|r^2|m\rangle \leq A$), we find out that $m \leq N_\phi - 1$. This shows that the lowest Landau level is N_ϕ-fold degenerate.

If the number of electrons N_e is larger than the degeneracy of the lowest Landau level ($N_e > N_\phi$), then electrons fill the LLL and the remaining electrons jump to the next level. Considering the conductance of localized and extended states, one can explain the origin of the IQHF at integer filling factors $\nu = N_e/N_\phi$. However, if the number of electrons is smaller than the degeneracy of the lowest Landau level ($N_e < N_\phi$), then the free electrons have the freedom to choose any superposition of the states available in LLL. In the presence of interaction, electrons will rearrange themselves in LLL to minimize the interaction energy overhead. Remarkably, if the interaction is a short-range delta-function $H_{int} \propto \sum_{j<k} \delta(z_j - z_k)$, the Laughlin wave function is the *exact* ground state of the system. This can be readily seen from the many-body Laughlin wave function [108]:

$$\Psi_q(z_1, z_2, ..., z_{N_e}) \propto \prod_{j<k}^{N_e} (z_j - z_k)^q \prod_{j=1}^{N_e} \exp^{-|z_j|^2/4l_B^2}, \tag{1.2}$$

where q is an odd integer to satisfy the anti-symmetrization characteristic of fermions.

This wave function has a node anywhere two particles meet each other, therefore, $\langle\Psi_q|H_{int}|\Psi_q\rangle = 0$. If we expand the first product of the wave function in powers of an arbitrary electron position z_i, the highest power of the polynomial in z_i is $q(N_e-1) = N_\phi - 1$ by the area constraint above. Therefore, for large N_e and N_ϕ, the integer q will be given by the inverse of the filling factor $\nu = 1/q = N_e/N_\phi$. These states are responsible for the Hall conductance plateaus which occur at the fractional filling factors $\nu = 1/q$, where q is an odd integer. (For a more detailed introduction and thorough discussion of the FQHE, see e.g. Refs. [133, 35])

1.2.2 Fractional Quantum Hall and Bose-Einstein Condensates

With recent advances in the field of ultracold atomic gases, trapped Bose-Einstein Condensates (BEC's) have become an important platform to study many-body physics, such as quantum phase transitions. In particular, the ability to dynamically control lattice structure, strength of interaction and the disorder in BEC's confined in optical lattices, have led to the recent observation of the superfluid to Mott-insulator transition and many other important many-body phenomena (for a brief review, see Ref. [25]).

One of the most interesting characteristics of a BEC is its response to rotation. Early work on superfluid helium-4 showed that a BEC does not rotate like a conventional fluid [46]. Instead, the rotation of superfluid helium-4 leads to the formation of quantized vortices. Such vortices also appear in type-II superconductors under an applied magnetic field, which may be understood as a BEC of paired (fermionic)

electrons.

During the past decade, there has been a tremendous interest in studying rotating BEC's in harmonic traps. At a sufficient rotation rate, an Abrikosov lattice of quantized vortices has been observed [1]. The Coriolis force in the rotating frame can be considered as the Lorentz force on a charged particle in a uniform magnetic field (Larmor's theorem). Therefore, these vortices can be considered as magnetic fluxes penetrating the system. Consequently, the equivalent of the magnetic filling factor ($\nu = N_e/N_\phi$) in the context of the FQHE, will be the ratio between the number of bosons N_b in the condensate and the number of vortices, $\nu = N_b/N_\phi$, in the BEC context.

Hence, one can imagine the realization of certain strongly correlated quantum states similar to the Fractional Quantum Hall states at high rotation rates when the number of vortices exceeds the number of bosons in the condensate ($N_b > N_\phi$) [176, 38, 141]. While this approach yields a stable ground state separated from all excited states by an energy gap, in practice this gap is rather small because of the weak interactions among the particles in the magnetic traps typically used. In optical lattices the interaction energies are much larger because the atoms are confined in a smaller volume, and the realization of FQHE in optical lattices could therefore lead to a higher energy gap and be much more robust. Note, the rotation of the lattice is not the sole approach to making an artificial magnetic field for a condensate. There have been a number of proposals to implement artificial gauge fields in optical lattices in the past few years [153, 119, 142].

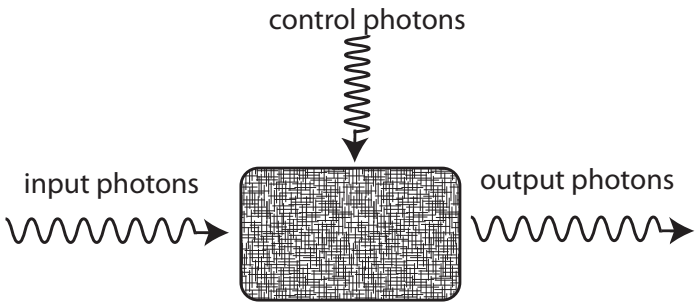

Figure 1.1: Optical nonlinearity

1.3 Strongly interacting photons

Mediated interactions are ubiquitous in physics and, whenever strong, they can fundamentally change the quantum state of a system. A well-known example is the attractive interaction between electrons mediated by phonons which results in the superconductivity [15]. In the case of light, photon-photon interaction can be mediated by atoms or molecules through an electric dipole interaction, causing *optical nonlinearity*. The mediated interaction between photons can be sketched in a simple picture as shown in Fig. 1.1. The control photons change the state of matter. Then, the input photons interact with the matter and *feel* the effect of the control photons. This mediated interaction is usually very small and one needs to use many photons (strong intensities) to observe appreciable effects [27]. Therefore, the main challenge is to increase the interaction between light and matter so that the effective interaction between photons becomes noticeable, even at the level of a few photons. In this spirit, a single-photon switch can be understood as a system where the transport of a single input photon can be blocked by the injection of a single control photon, in direct analogy to an electronic transistor.

There has been great effort to make a large nonlinearity at the level of few photons in the optical frequency domain. As described above, to create this large nonlinearity, the interaction between light and matter should be maximized. One can envisage three avenues to optimize this interaction, which we now briefly describe.

First, the light can be either focused with lenses or guided inside a fiber to more strongly interact with an emitter (see Fig. 1.2a). The emitter can be anything that has an electric dipole interaction with light, such as an atom, molecule, quantum dot, etc. If the wavelength of the resonant light interacting with the emitter is λ and, therefore, the interaction cross section is λ^2 (up to a geometrical factor) and A is the effective area of light in the transverse direction [Fig. 1.2(a)], then the probability of interaction is characterized by the ratio λ^2/A. This probability is always less than one [164], which is a manifestation of the scattering of light into undesired directions. Examples of such systems have been investigated by dye molecules in free space [178, 83], trapped alkaline atoms [159] and quantum dots [9].

Second, we can confine photons inside an optical cavity, so that the chance of interaction with an emitter increases [see Fig. 1.2(b)]. In particular, the chance of interaction will be multiplied by the average number of round trips of a photon makes once it enters the cavity. The average number of around trips is characterized by the finesse $\mathcal{F}$ of the cavity in question. Therefore, once the quantity $\mathcal{F}\lambda^2/A$ is larger than one, we enter the regime of *strong nonlinearity*. This quantity corresponds to the *cooperativity* in the context of Cavity QED [86]. There have been beautiful experiments [134, 23, 147, 59] to reach this regime and to illustrate intriguing physics, such as the Photon-Blockade Phenomenon, where the transmission of a photon is

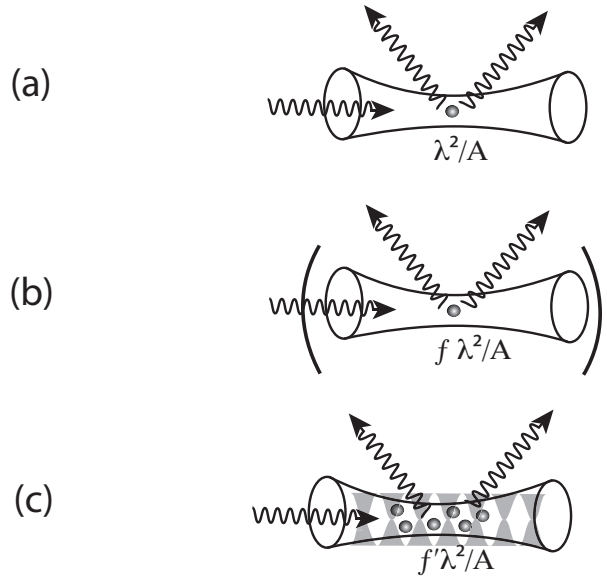

Figure 1.2: Atom-photon interaction: (a) in a free space or inside a waveguide (b) inside a cavity (c) inside a waveguide which confines light in the transverse direction; by using many atoms inside the waveguide one can form a band-gap and trap light also in the longitudinal direction.

blocked due to the presence of another photon.

Third, the light can be confined in the transverse direction to propagation, being guided by a hollow-core fiber, and interact with the emitters inside the empty core [see Fig. 1.2(c)]. In a conventional optical fiber, the light is guided due to total internal reflection, since the fiber core has a higher refractive index than the surrounding cladding. In contrast, in the hollow-core photonic band gap fibers, the light is confined into the empty core of the fiber (see Fig. 1.3). The cladding contains a periodic array of air holes which creates a photonic band gap and guides the light inside the core [98, 143]. The cores can be several microns in diameter which make the effective area (A) small and therefore, the interaction probability λ^2/A larger, even reaching a few percents. Consequently, one can already observe strong nonlinearities by loading atoms in the hollow core [18, 102, 63, 11].

Furthermore, one can use the atoms themselves, to form a photonic band gap in the longitudinal direction. Similar to a photonic bandgap, the periodic array of atoms or the modulated atomic polarization can lead to coupling between forward- and backward-propagating light. Therefore, a band gap structure can form [43, 8]. In particular, using coherent control techniques such as Electromagnetically-Induced Transparency (EIT) [113, 55], one can dynamically control the properties of photonic band gap and thereby manipulate the propagation of light to the point of trapping and releasing a photonic field [12]. Therefore, under certain conditions the system can act as an effective cavity with a finesse $\mathcal{F}'$ and an effective cooperativity $\mathcal{F}'\lambda^2/A$. We also note that there are other possibilities to control the interaction between atoms and guided light by using a nanofiber [93, 121] or surface plasmons [3].

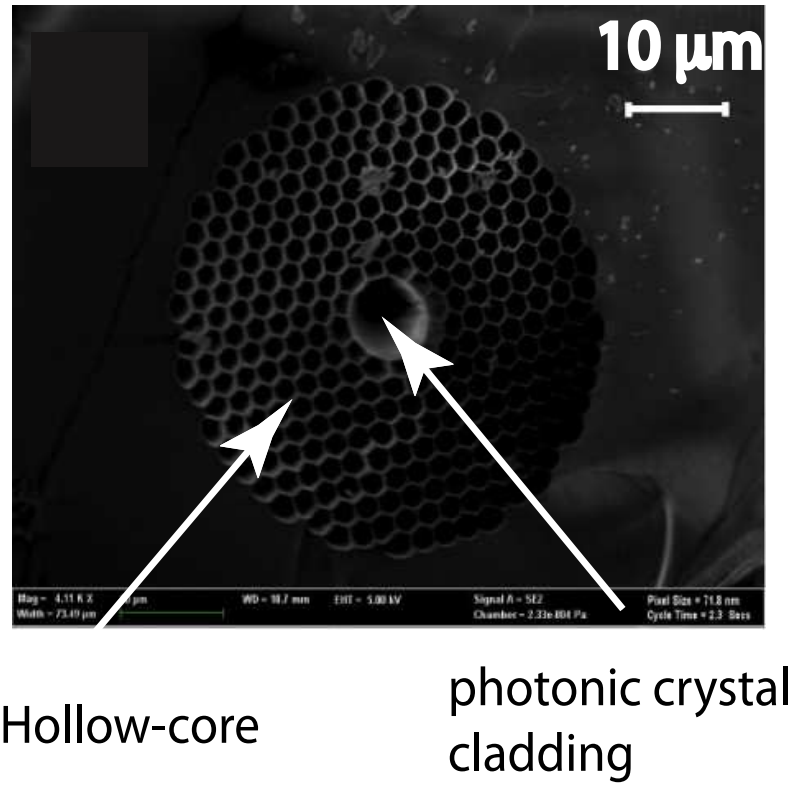

Figure 1.3: Hollow-core photonic band gap fiber. Photonic band gap of the cladding prevents light in the core from escaping in the transverse direction.

1.4 Overview

In Chapter 2, we analyze the feasibility to create Fractional Quantum Hall (FQH) states of atoms confined in optical lattices. We investigate conditions under which the FQHE can be achieved for bosons on a lattice with an effective magnetic field and a finite onsite interaction. Furthermore, we characterize the ground state in these systems by calculating topologically significant numbers, called Chern numbers, which provide direct signatures of topological order. We also discuss various issues which are relevant for the practical realization of such FQH states with ultracold atoms in an optical lattice, including the presence of the long-range dipole interaction, which can improve the energy gap and stabilize the ground state. We also investigate a new detection technique based on Bragg spectroscopy to probe these system in an experimental realization.

As noted above the FQH effect can be realized by rotating and cooling atoms confined in a harmonic trap. In this situation, it can be shown that the Laughlin wave function describes the exact ground state of the many-body system [176, 128]. In optical lattices, on the other hand, there are a number of questions which need to be addressed: First, it is unclear to which extent the lattice modifies the FQH physics. Furthermore, to characterize such states, we investigate a novel procedure for calculating Chern numbers and demonstrate how this method may provide insight into the topological order of the ground state in regimes where other methods (such as overlap calculations) fail to provide an unambiguous glimpse into the nature of the ground state. Additionally, to consider these fundamental features of the FQH states on a lattice, which are applicable regardless of the system being used to realize the

effect, we study a number of questions which are of particular interest to experimental efforts attempting to realize the effect with atoms in optical lattices.

In Chapter 3, we theoretically study the transmission of few-photon quantum fields through a strongly nonlinear optical medium. We develop a general approach to investigate non-equilibrium quantum transport of bosonic fields through a finite-size nonlinear medium and apply it to a recent experiment where cold atoms are loaded in a hollow-core optical fiber [11]. We show that when the interaction between photons is effectively repulsive, the system acts as a single-photon switch. In the case of attractive interaction, the system can exhibit either anti-bunching or bunching, associated with the resonant excitation of bound states of photons by the input field. These effects can be observed by probing statistics of transmitted photons through the nonlinear fiber.

In Chapter 4, we present a scheme to perform a single-photon gate in a nonlinear optical fiber. For this, we evaluate the transport of a single photon in a nonlinear fiber where another photon is previously stored as an atomic spin excitation. We estimate the fidelity of such a gate for different experimental parameters.

In Chapter 5, we demonstrate optical nonlinearities due to interaction of weak optical fields with the collective motion of a strongly dispersive ultracold gas. The combination of a recoil-induced resonance (RIR) in the high gain regime and optical wave-guiding within the dispersive medium enables us to achieve a large collective atomic cooperativity even in the absence of a cavity. As a result, we observe optical bistability at very weak input powers. The present scheme allows for dynamic optical control of the dispersive properties of the ultracold gas using weak pulses of light.

The experimental observations are in good agreement with our theoretical models.

Chapter 2

Fractional quantum Hall state in optical lattices

2.1 Introduction

With recent advances in the field of ultracold atomic gases, trapped Bose-Einstein condensates (BEC's) have become an important system to study many-body physics such as quantum phase transitions. In particular, the ability to dynamically control the lattice structure and the strength of interaction and disorder in BEC's confined in optical lattices, have led to the recent observation of the superfluid to Mott-insulator transition [71, 116, 34, 177, 57]. At the same time, there has been a tremendous interest in studying rotating BEC's in harmonic traps; at sufficient rotation an Abrikosov lattice of quantized vortices has been observed [1] and the realization of strongly correlated quantum states similar to the fractional quantum Hall states has been predicted to occur at higher rotation rates [176, 38, 141]. In these proposals, the

rotation can play the role of an effective magnetic field for the neutral atoms and in analogy with electrons, the atoms may enter into a state described by the Laughlin wave function, which was introduced to describe the fractional quantum Hall effect. While this approach yields a stable ground state separated from all excited states by an energy gap, in practice this gap is rather small because of the weak interactions among the particles in the magnetic traps typically used. In optical lattices, the interaction energies are much larger because the atoms are confined in a much smaller volume, and the realization of the fractional quantum Hall effect in optical lattices could therefore lead to a much higher energy gap and be much more robust. In a recent paper [153], it was shown that it is indeed possible to realize the fractional quantum Hall effect in an optical lattice, and that the energy gap achieved in this situation is a fraction of the tunneling energy, which can be considerably larger than the typical energy scales in a magnetic trap.

In addition to being an interesting system in its own right, the fractional quantum Hall effect, is also interesting from the point of view of topological quantum computation [95]. In these schemes quantum states with fractional statistics can potentially perform fault tolerant quantum computation. So far, there has been no direct experimental observation of fractional statistics although some signatures have been observed in electron interferometer experiments [33, 32]. Strongly correlated quantum gases can be a good alternative where the interaction and disorder in the systems are more controllable. Therefore, realization of fractional quantum Hall states in atomic gases can be a promising resource for topological quantum computation in the future.

As noted above the FQH effect can be realized by simply rotating and cooling

atoms confined in a harmonic trap. In this situation, it can be shown that the Laughlin wave function exactly describes the ground state of the many body system [176, 128]. In an optical lattices, on the other hand, there are a number of questions which need to be addressed. First of all, it is unclear to which extent the lattices modifies the fractional quantum Hall physics. For a single particle, the lattice modifies the energy levels from being simple Landau levels into the fractal structure known as the Hofstadter butterfly [81]. In the regime where the magnetic flux going through each lattice α is small, one expects that this will be of minor importance and in Ref. [153] it was argued that the fractional quantum Hall physics persists until $\alpha \lesssim 0.3$. In this chapter, we extent and quantify predictions carried out in Ref. [153] . Whereas Ref. [153] only considered the effect of infinite onsite interaction, we extent the analysis to finite interactions. Furthermore, where Ref. [153] mainly argued that the ground state of the atoms was in a quantum Hall state by considering the overlap of the ground state found by numerical diagonalization with the Laughlin wave function, we provide further evidence for this claim by characterizing the topological order of the system by calculating Chern numbers. These calculations thus characterize the order in the system even for parameter regimes where the overlap with the Laughlin wave function is decreased by the lattice structure.

In addition to considering these fundamental features of the FQH states on a lattice, which are applicable regardless of the system being used to realize the effect, we also study a number of questions which are of particular interest to experimental efforts towards realizing the effect with atoms in optical lattices. In particular, we show that adding dipole interactions between the atoms can be used to increase the

energy gap and stabilize the ground state. Furthermore, we study Bragg spectroscopy of atoms in the lattice and show that this is a viable method to identify the quantum Hall states created in an experiment, and we discuss a new method to generate an effective magnetic field for the neutral atoms in the lattice.

The chapter is organized as follows: In Sec. 2.2, we study the system with finite onsite interaction. In Sec. 2.3 we introduce Chern numbers to characterize the topological order of the system. The effect of the dipole-dipole interaction has been elaborated in Sec. 2.4.1. Sec. 2.4.2 studies the case of $\nu = 1/4$ filling factor. Sec. 2.5 is dedicated to explore Bragg spectroscopy of the system. Sec. 2.6 outlines a new approach for generating the type of the Hamiltonian studied in this chapter.

2.2 Quantum Hall state of bosons on a lattice

2.2.1 Single particle on a magnetic lattice

In a continuum, single-particle energy eigenstates in the presence of a perpendicular magnetic field are given by Landau levels, where levels are separated by the cyclotron energy. However, if particles are confined on a lattice rather than a continuum, the situation is quite different. The Hamiltonian of a system on a square lattice subject to a perpendicular magnetic field in a tight-binding limit can be written as,

$$H = -J\sum_{x,y} \hat{a}^{\dagger}_{x+1,y}\hat{a}_{x,y}e^{-i\pi\alpha y} + \hat{a}^{\dagger}_{x,y+1}\hat{a}_{x,y}e^{i\pi\alpha x} + h.c., \tag{2.1}$$

where $2\pi\alpha$ is the phase that is acquired by the wave function of a particle due to the magnetic field once it hops around a plaquette. Hosftadter showed that the energy

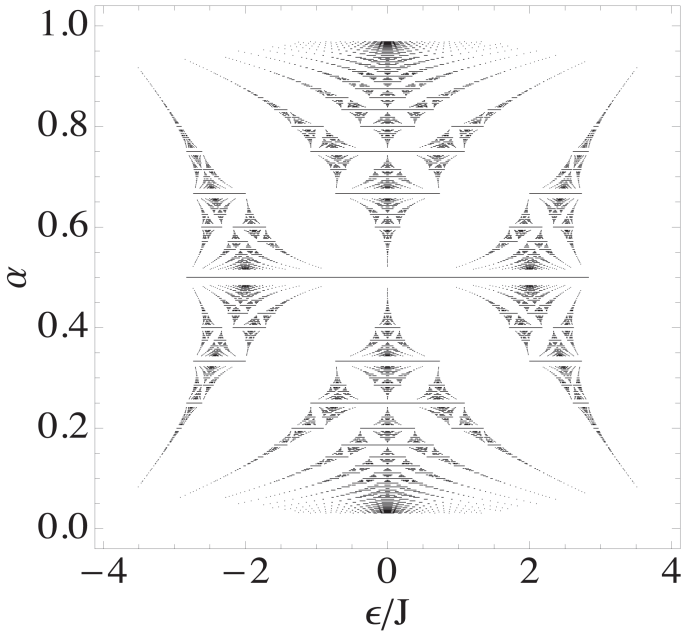

Figure 2.1: Hofstadter's Butterfly: The energy spectrum for different values of the magnetic field characterized by α. The energy band splits into q subbands for $\alpha = p/q$.

spectrum of a single electron on a lattice with perpendicular magnetic field takes a fractal form [81]. In particular, if $\alpha = p/q$ with p and q integers (i.e. α being a rational number), the energy spectrum splits into a finite number of exactly q bands. While if α is irrational, the energy spectrum breaks into many bands and therefore, the spectrum takes a form shown in Fig. 2.1.

2.2.2 Model

The fractional quantum Hall effect occurs for electrons confined in a two dimensional plane under the presences of a perpendicular strong magnetic field. If N is the number of electrons in the system and N_ϕ is the number of magnetic fluxes measured

in units of the quantum magnetic flux $\Phi_0 = h/e$, then depending on the filling factor $\nu = N/N_\phi$ the ground state of the system can form highly entangled states exhibiting a rich behaviors, such as incompressibility, charge density waves, and anyonic excitations with fractional statistics. In particular, when $\nu = 1/m$, where m is an integer, the ground state of the system is an incompressible quantum liquid which is protected by an energy gap from all other states, and in the Landau gauge is well described by the Laughlin wave function [108]:

$$\Psi(z_1, z_2, ..., z_N) = \prod_{j>k}^{N} (z_j - z_k)^m \prod_{j=1}^{N} e^{-y_j^2/2}, \tag{2.2}$$

where the integer m should be odd in order to meet the antisymmetrization requirement for fermions.

Although the fractional quantum Hall effect occurs for fermions (electrons), bosonic systems with repulsive interactions can exhibit similar behaviors. In particular, the Laughlin states with even m correspond to bosons. In this article, we study bosons since the experimental implementation are more advanced for the ultracold bosonic systems. We study a system of atoms confined in a 2D lattice which can be described by the Bose-Hubbard model [87] with the Peierls substitution [81, 129],

$$\begin{aligned} H &= -J \sum_{x,y} \hat{a}^\dagger_{x+1,y} \hat{a}_{x,y} e^{-i\pi\alpha y} + \hat{a}^\dagger_{x,y+1} \hat{a}_{x,y} e^{i\pi\alpha x} + h.c. \\ &+ U \sum_{x,y} \hat{n}_{x,y}(\hat{n}_{x,y} - 1), \end{aligned} \tag{2.3}$$

where J is the hopping energy between two neighboring sites, U is the onsite interaction energy, and $2\pi\alpha$ is the phase acquired by a particle going around a plaquette.

This Hamiltonian is equivalent to the Hamiltonian of a U(1) gauge field (transverse magnetic field) on a square lattice. More precisely, the non-interacting part can be written as

$$- J \sum_{<ij>} a_i^\dagger a_j \exp\left(\frac{2\pi i}{\Phi_0} \int_i^j \vec{A} \cdot \vec{dl}\right) \tag{2.4}$$

where $\vec{A}$ is the vector potential for a uniform magnetic field and the path of the integral is chosen to be a straight line between two neighboring sites. In the symmetric gauge, the vector potential is written as $\vec{A} = \frac{B}{2}(-y, x, 0)$. Hence, α will be the amount of magnetic flux going through one plaquette.

While the Hamiltonian in Eq. (2.3) occurs naturally for charged particles in a magnetic field, the realization of a similar Hamiltonian for neutral particles is not straightforward. As we discuss in Sec. 2.6 this may be achieved in a rotating harmonic trap, and this have been very successfully used in a number of experiments in magnetic traps [28, 148], but the situation is more complicated for an optical lattice. However, there has been a number of proposals for lattice realization of a magnetic field [153, 88, 119], and recently it has been realized experimentally [163]. Popp *et al.* [132] have studied the realization of fractional Hall states for a few particles in individual lattice sites. A new approach for rotating the entire optical lattice is discussed in Sec. 2.6. The essence of the above Hamiltonian is a non-zero phase that a particle should acquire when it goes around a plaquette. This phase can be obtained for example by alternating the tunneling and adding a quadratic superlattice potential [153] or by simply rotating the lattice (Sec.2.6). The advantage of confining ultracold gases in an optical lattice is to enhance the interaction between atoms which consequently result in a higher energy gap comparing to harmonic trap proposals (e.g., Ref. [176]). This

enhancement in the energy gap of the excitation spectrum can alleviate some of the challenges for experimental realization of the quantum Hall state for ultracold atoms.

2.2.3 Energy spectrum and overlap calculations

In order to approximate a large system, we study the system with periodic boundary condition, i.e. on a torus, where the topological properties of the system is best manifested.

There are two energy scales for the system: the first is the magnetic tunneling term, $J\alpha$, which is related to the cyclotron energy in the continuum limit $\hbar\omega_c = 4\pi J\alpha$ and the second is the onsite interaction energy U. Experimentally, the ratio between these two energy scales can be varied by varying the lattice potential height [71, 87] or by Feshbach resonances [45, 52, 177]. Let us first assume that we are in the continuum limit where $\alpha \ll 1$, i.e. the flux through each plaquette is a small fraction of a flux quantum. A determining factor for describing the system is the filling factor $\nu = N/N_\Phi$, and in this study we mainly focus on the case of $\nu = 1/2$, since this will be the most experimentally accessible regime.

We restrict ourself to the simplest boundary conditions for the single particle states $t_s(\vec{L})\psi(x_s, y_s) = \psi(x_s, y_s)$, where $t_s(\vec{L})$ is the magnetic translation operator which translates the single particle states $\psi(x_s, y_s)$ around the torus. The definition and detailed discussion of the boundary conditions will be elaborated in Section 2.3. The discussed quantities in this section, such as energy spectrum, gap and overlap, do not depend on the boundary condition angles (this is also verified by our numerical calculation).

In the continuum case, for the filling fraction $\nu = 1/2$, the Laughlin state in Landau gauge ($\vec{A} = -By\hat{x}$) is given by Eq. (2.2) with $m = 2$. The generalization of the Laughlin wave function to a torus takes the form [136]

$$\Psi(z_1, z_2, ..., z_N) = f_{rel}(z_1, z_2, ..., z_N) F_{cm}(Z) e^{-\sum_i y_i^2/2}, \tag{2.5}$$

where f_{rel} is the relative part of the wave function and is invariant under collective shifts of all z_i's by the same amount, and $F_{cm}(Z)$ is related to the motion of the center of mass and is only a function of $Z = \sum_i z_i$. For a system on a torus of the size $(L_x \times L_y)$, we write the wave function with the help of theta functions, which are the proper oscillatory periodic functions and are defined as $\vartheta \begin{bmatrix} a \\ b \end{bmatrix} (z|\tau) = \sum_n e^{i\pi\tau(n+a)^2 + 2\pi i(n+a)(z+b)}$ where the sum is over all integers. For the relative part we have,

$$f_{rel} = \prod_{i<j} \vartheta \begin{bmatrix} \frac{1}{2} \\ \frac{1}{2} \end{bmatrix} \left(\frac{z_i - z_j}{L_x} | i\frac{L_y}{L_x} \right)^2. \tag{2.6}$$

According to a general symmetry argument by Haldane [77], the center of mass wave function $F_{cm}(Z)$ is two-fold degenerate for the case of $\nu = 1/2$, and is given by

$$F_{cm}(Z) = \vartheta \begin{bmatrix} l/2 + (N_\phi - 2)/4 \\ -(N_\phi - 2)/2 \end{bmatrix} \left(\frac{2\sum_i z_i}{L_x} | 2i\frac{L_y}{L_x} \right) \tag{2.7}$$

where $l = 0, 1$ refers to the two degenerate ground states. This degeneracy in the continuum limit is due to the translational symmetry of the ground state on the torus, and the same argument can be applied to a lattice system when the magnetic length is much larger than the lattice spacing $\alpha \ll 1$. For higher magnetic filed, the lattice structure becomes more pronounced. However, in our numerical calculation for a

moderate magnetic field $\alpha \lesssim 0.4$, we observe a two-fold degeneracy ground state well separated from the excited state by an energy gap. We return to the discussion of the ground state degeneracy in Sec. 2.3.

In the continuum limit $\alpha \ll 1$, the Laughlin wave function is the exact ground state of the many body system with a short range interaction [76, 176, 128]. The reason is that the ground state is composed entirely of states in the lowest Landau level which minimizes the magnetic part of the Hamiltonian, the first term in Eq. (2.3). The expectation value of the interacting part of the Hamiltonian, i.e. the second term in Eq. (2.3), for the Laughlin state is zero regardless of the strength of the interaction, since it vanishes when the particles are at the same position.

To study the system with a non-vanishing α, we have performed a direct numerical diagonalization of the Hamiltonian for a small number of particles. Since we are dealing with identical particles, the states in the Hilbert space can be labeled by specifying the number of particles at each of the lattice sites. In the hard-core limit, only one particle is permitted on each lattice site, therefore for N particles on a lattice with the number of sites equal to $(N_x = L_x/a, N_y = L_y/a)$, where a is the unit lattice side, the Hilbert space size is given by the combination $\begin{pmatrix} N_x N_y \\ N \end{pmatrix} = \frac{N_x N_y!}{N!(N_x N_y - N)!}$. On the other hand, in case of finite onsite interaction, the particles can be on top of each other, so the Hilbert space is bigger and is given by the combination $\begin{pmatrix} N + N_x N_y - 1 \\ N \end{pmatrix}$. In our simulations the dimension of the Hilbert can be raised up to $\sim 4 \times 10^6$ and the Hamiltonian is constructed in the configuration space by taking into account the tunneling and interacting terms. The tunneling term is written in the symmetric gauge, and we make sure that the phase acquired around a plaquette is equal to $2\pi\alpha$,

and that the generalized magnetic boundary condition is satisfied when the particles tunnels over the edge of the lattice [to be discussed in Sec. 2.3, c.f. Eq. (2.12)]. By diagonalizing the Hamilton, we find the two-fold degenerate ground state energy which is separated by an energy gap from the excited states and the corresponding wave function in the configuration space. The Lauhglin wave function (2.5) can also be written in the configuration space by simply evaluating the Laughlin wave function at discrete points, and therefore we can compared the overlap of these two dimensional subspaces.

2.2.4 Results with the finite onsite interaction

The energy gap above the ground state and the ground state overlap with the Laughlin wave function for the case of $\nu = 1/2$ in a dilute lattice $\alpha \lesssim 0.2$, are depicted in figure. 2.2. The Laughlin wave function remains a good description of the ground state even if the strength of the repulsive interaction tends to zero (Fig. 2.2 a). Below, we discuss different limits:

First, we consider $U > 0$, $U \gg J\alpha$: If the interaction energy scale U is much larger than the magnetic one ($J\alpha$), all low energy states lie in a manifold, where the highest occupation number for each site is one, i.e. this corresponds to the hard-core limit. The ground state is the Laughlin state and the excited states are various mixtures of Landau states. The ground state is two-fold degenerate [77] and the gap reaches the value in for the hard-core limit at large $U \gtrsim 3J/\alpha$, as shown in Fig. 2.3 (a). In this limit the gap only depends on the tunneling J and flux α, and the gap is a fraction of J. These results are consistent with the previous work in Ref. [153].

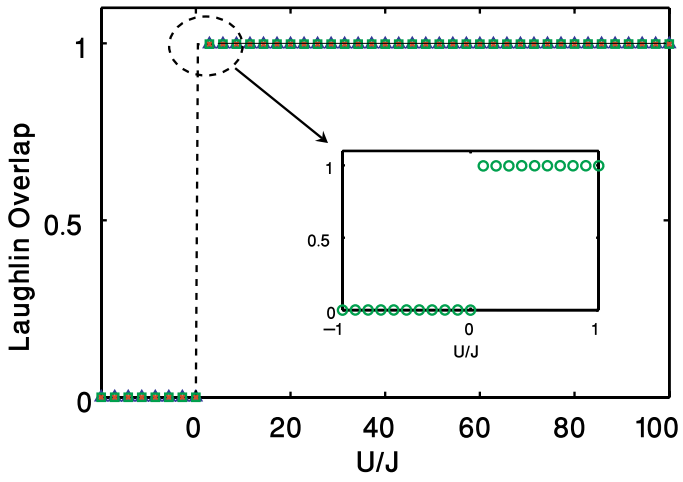

(a)

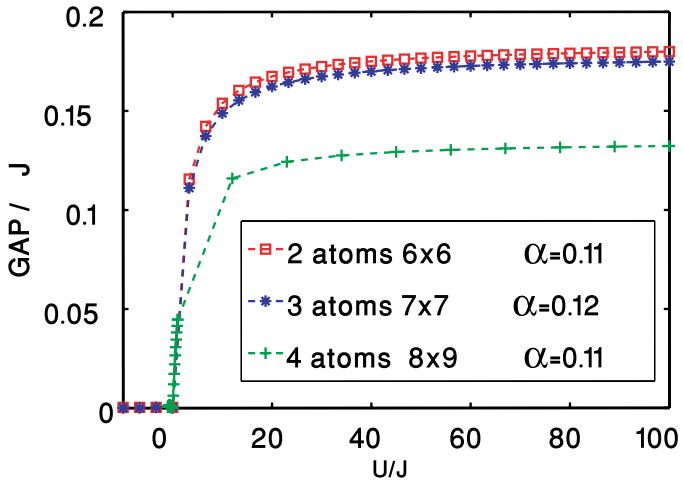

(b)

Figure 2.2: (a) The overlap of the ground state with the Laughlin wave function. For small α the Laughlin wave function is a good description of the ground state for positive interaction strengths. The inset shows the same result of small U. (b) The energy gap for $N/N_\phi = 1/2$ as a function of interaction U/J from attractive to repulsive. For a fixed α, the behavior does not depend on the number of atoms. The inset define the particle numbers, lattice sizes, and symbols for both parts (a) and (b).

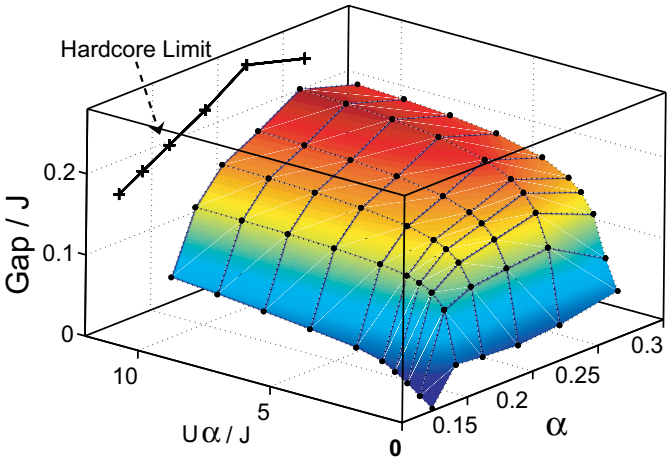

(a)

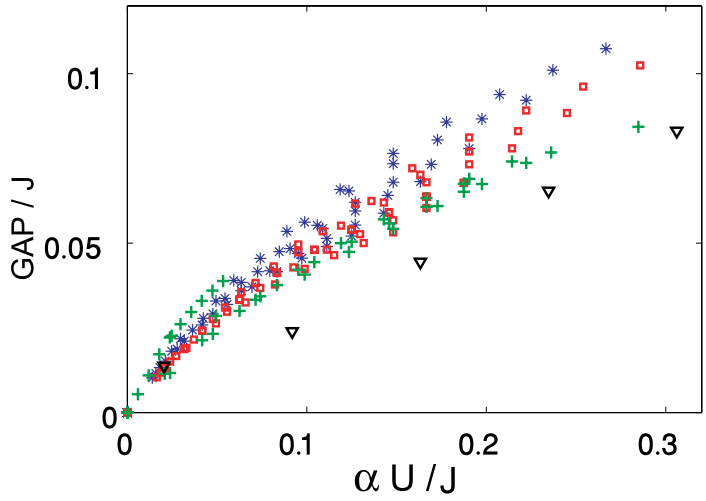

(b)

Figure 2.3: (a) The energy gap as a function of αU and α for a fixed number of atoms (N=4). The gap is calculated for the parameters marked with dots and the surface is an extrapolation between the points. (b) Linear scaling of the energy gap with αU for $U \ll J, \alpha \lesssim 0.2$. The results are shown for $N = 2(\square)$, $N = 3(*)$, $N = 4(+)$ and $N = 5(\triangledown)$. The gap disappears for non-interaction system, and increases with increasing interaction strength ($\propto \alpha U$) and eventually saturate to the value in the hardcore limit.

Secondly, we consider $|U| \ll J\alpha$. In this regime, the magnetic energy scale ($J\alpha$) is much larger than the interaction energy scale U. For repulsive regime ($U > 0$), the ground state is the Laughlin state and the gap increases linearly with αU, as shown in Fig. 2.3 b.

Thirdly, we study $U = 0$ where the interaction is absent and the ground state becomes highly degenerate. For a single particle on a lattice, the spectrum is the famous Hostadfer's butterfly [81], while in the continuum limit $\alpha \ll 1$, the ground state is the lowest Landau level (LLL). The single particle degeneracy of the LLL is the number of fluxes going through the surface, N_ϕ. So in the case of N bosons, the lowest energy is obtained by putting N bosons in N_ϕ levels. Therefore, the many-body ground state's degeneracy should be: $\begin{pmatrix} N+N_\phi-1 \\ N_\phi-1 \end{pmatrix}$. For example, 3 bosons and 6 fluxes gives a 336-fold degeneracy in the non-interacting ground state.

If we increase the amount of phase (flux) per plaquette (α) we are no longer in the continuum limit. The Landau level degeneracy will be replace by $\frac{L_1 L_2}{s}$ where $\alpha = r/s$ is the amount of flux per plaquette and r and s are coprime [58]. Then, the many-body degeneracy will be: $\begin{pmatrix} N+\frac{L_1L_2}{s}-1 \\ \frac{L_1L_2}{s}-1 \end{pmatrix}$.

Fourthly, we consider $U < 0$, $U \gg J\alpha$: when U is negative (i.e. attractive interaction) in the limit strong interaction regime, the ground state of the system will become a *pillar* state. In a pillar state, all bosons in the system condensate into a single site. Therefore, the degeneracy of the ground state is $N_x \times N_y$ and the ground state manifold can be spanned as,

$$\bigoplus_i \frac{1}{\sqrt{N!}}(a^\dagger)_i^N |vac\rangle. \tag{2.8}$$

These states will very fragile and susceptible to collapse [62].

In a lattice, it is also possible to realize the fractional quantum Hall states for attractive interaction in the limit when $|U| \gg J\alpha$. Assume that the occupation number of each site is either zero or one. Since the attraction energy U is very high and there is no channel into which the system can dissipate its energy, the probability for a boson to hop to a site where there is already a boson is infinitesimally small. Therefore, the high energy attraction will induce an effective hard-core constraint in the case of ultracold system. The energy of these state should be exactly equal to their hard-core ground state counterparts, since the interaction expectation value of the interaction energy is zero for the Laughlin state. The numerical simulation shows that these two degenerate states indeed have a good overlap with the Laughlin wave function similar to their repulsive hard-core counterparts and also their energies are equal to the hard-core ground state. These states are very similar to repulsively bound atom pairs in an optical lattice which have recently been experimentally observed [177].

So far we have mainly considered a dilute lattice $\alpha \lesssim 0.2$, where the difference between a lattice and the continuum is very limited. We shall now begin to investigate what happens for larger values of α, where the effect of the lattice plays a significant role. Fig. 2.4, shows the ground state overlap with the Laughlin wave function as a function of the strength of magnetic flux α and the strength of the onsite interaction U. As α increases the Laughlin overlap is no longer an exact description of the system since the lattice behavior of the system is more pronounced comparing to the continuum case. This behavior doesn't depend significantly on the number of particles for the limited number of particles that we have investigated $N \leq 5$. We

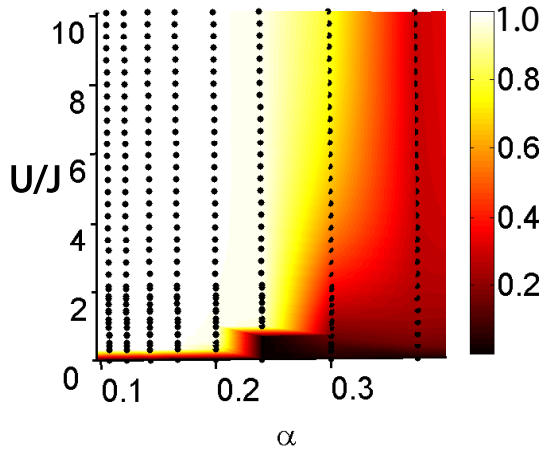

(a)

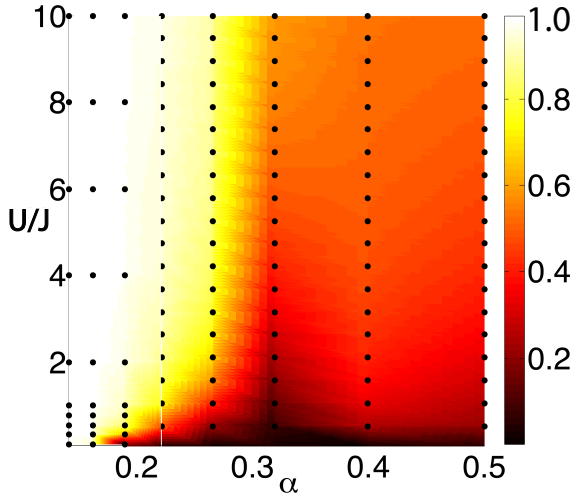

(b)

Figure 2.4: Ground state overlap with the Laughlin wave function. (a) and (b) are for 3 and 4 atoms on a lattice, respectively. α is varied by changing the size of the lattice (the size in the two orthogonal directions differ at most by unity). The Laughlin state ceases to be a good description of the system as the lattice nature of the system becomes more apparent $\alpha \gtrsim 0.25$. The overlap is only calculated at the positions shown with dots and the color coding is an extrapolation between the points.

have, however, not made any modification to the Laughlin wave function to take into account the underlying lattice, and from the calculations presented so far, it is unclear whether the decreasing wave function overlap represents a change in the nature of the ground state, or whether it is just caused by a modification to the Laughlin wave function due the difference between the continuum and the lattice. To investigate this, in the next Section, we provide a better characterization of the ground state in terms of Chern numbers, which shows that the same topological order is still present in the system for higher values of α.

As a summary, we observe that the Laughlin wave function is a good description for the case of dilute lattice ($\alpha \ll 1$), regardless of the strength of the onsite interaction. However, the protective gap of the ground state becomes smaller for weaker values of interaction and in the perturbative regime $U \ll J$ is proportional to αU for $\alpha \lesssim 0.2$.

2.3 Chern number and topological invariance

2.3.1 Introduction

Strong interaction in a many-body system can fundamentally change a physical system. Often such states can be characterized by an order parameter and spontaneous breaking of some global symmetries. The 'smoking gun' evidence of such states is the appearance of Goldstone modes of spontaneously broken symmetries. However, some types of quantum many-body phases can not be characterized by a local order parameter. Examples can be found in FQH systems[67], lattice gauge theories[110], and spin liquid states[5]. Such states can be characterized by the topo-

logical order[174] which encompasses global geometrical properties such as ground state degeneracies on non-trivial manifolds[175]. Topologically ordered states often exhibit fractional excitations[124] and have been proposed as a basis of a new approach to quantum computations[95]. However, in many cases, identifying a topologically ordered state is a challenging task even for theoretical analysis. Given an exact wave function of the ground state in a finite system, how can one tell whether it describes a FQH phase of a 2D electron gas or a spin liquid phase on a lattice? One promising direction to identifying topological order is based on the Chern number calculations[99, 80]. The idea of this approach is to relate the topological order to the geometrical phase of the many-body wave function under the change of the boundary conditions[122].

Chern classes are characteristic classes which emerge in topology, differential geometry, and algebraic geometry. These classes are topological invariants associated with vector bundles on a smooth manifold. Seminal work of Berry [21] and Simon [152] initiated the investigation on geometrical phase factors and since then the field has been extensively studied in different contexts – for a review see, for example, [26]. In quantum Hall (QH) systems, early works on the Chern number analysis is focused on the continuum regime and played an important role in demonstrating robustness of QH states against changes in the band structure[161] and the presence of disorder[175, 151]. Currently, there is also considerable interest in understanding FQH states in the presence of a strong periodic potential. Such systems are important in several contexts including anyonic spin states [96], vortex liquid states [13], and ultracold atoms in optical lattices [153, 75, 126, 119, 88] which are promising

candidates for an experimental realization.

2.3.2 Chern number and FQHE

In the theory of quantum Hall effect, it is well understood that the conductance quantization, is due to the existence of certain topological invariants, so called Chern numbers. The topological invariance was first introduced by Avron *et al.*[10] in the context of Thouless *et al.* (TKNdN)'s original theory [161] about quantization of the conductance. TKNdN in their seminal work, showed that the Hall conductance calculated from the Kubo formula can be expressed into an integral over the magnetic Brillouin zone, which shows the quantization explicitly. The original paper of TKNdN deals with the single-particle problem and Bloch waves which can not be generalized to topological invariance. The generalization to many-body systems has been done by Niu *et al.*[122] and also Tao *et al.*[158], by manipulating the phases describing the closed boundary conditions on a torus (i.e. twist angles), both for the integer and the fractional Hall systems. These twist angles come from natural generalization of the closed boundary condition.

To clarify the origin of these phases, we start with a single particle picture. A single particle with charge (q) on a torus of the size (L_x, L_y) in the presence of a magnetic field B perpendicular to the torus surface, is described by the Hamiltonian

$$H_s = \frac{1}{2m}\left[\left(-i\hbar\frac{\partial}{\partial x} - qA_x\right)^2 + \left(-i\hbar\frac{\partial}{\partial y} - qA_y\right)^2\right], \tag{2.9}$$

where $\vec{A}$ is the corresponding vector potential ($\frac{\partial A_y}{\partial x} - \frac{\partial A_x}{\partial y} = B$). This Hamiltonian is invariant under the magnetic translation,

$$t_s(\mathbf{a}) = e^{i\mathbf{a}\cdot\mathbf{k}^s/\hbar} \tag{2.10}$$

where $\mathbf{a}$ is a vector in the plane, and $\mathbf{k}^s$ is the pseudomomentum, defined by

$$\begin{aligned} k_x^s &= -i\hbar\frac{\partial}{\partial x} - qA_x - qBy \\ k_y^s &= -i\hbar\frac{\partial}{\partial y} - qA_y + qBx \end{aligned} \tag{2.11}$$

The generalized boundary condition on a torus is given by the single-particle translation

$$\begin{aligned} t_s(L_x\hat{x})\psi(x_s, y_s) &= e^{i\theta_1}\psi(x_s, y_s) \\ t_s(L_y\hat{y})\psi(x_s, y_s) &= e^{i\theta_2}\psi(x_s, y_s) \end{aligned} \tag{2.12}$$

where θ_1 and θ_2 are twist angles of the boundary. The origin of these phases can be understood by noting that the periodic boundary conditions corresponds to the torus in Fig. 2.5(a). The magnetic flux through the surface arises from the field perpendicular to the surface of the torus. However, in addition to this flux, there may also be fluxes due to a magnetic field residing inside the torus or passing through the torus hole, and it is these extra fluxes which give rise to the phases. The extra free angles are all the same for all particles and all states in the Hilbert space, and their time derivative can be related to the voltage drops across the Hall device in two dimensions.

The eigenstates of the Hamiltonian, including the ground state will be a function of these boundary angles $\Psi^{(\alpha)}(\theta_1, \theta_2)$. By defining some integral form of this eigenstate,

one can introduce quantities, that do not depend on the details of the system, but reveal general topological features of the eigenstates.

First we discuss the simplest situation, where the ground state is non-degenerate, and later we shall generalize this to our situation with a degenerate ground state. The Chern number is in the context of quantum Hall systems related to a measurable physical quantity, the Hall conductance. The boundary averaged Hall conductance for the (non-degenerate) αth many-body eigenstate of the Hamiltonian is [158, 122]: $\sigma_H^\alpha = C(\alpha)e^2/h$, where the Chern number $C(\alpha)$ is given by

$$C(\alpha) = \frac{1}{2\pi}\int_0^{2\pi} d\theta_1 \int_0^{2\pi} d\theta_2 (\partial_1 \mathcal{A}_2^{(\alpha)} - \partial_2 \mathcal{A}_1^{(\alpha)}), \tag{2.13}$$

where $\mathcal{A}_j^{(\alpha)}(\theta_1, \theta_2)$ is defined as a vector field based on the eigenstate $\Psi^{(\alpha)}(\theta_1, \theta_2)$ on the boundary torus $S_1 \times S_1$ by

$$\mathcal{A}_j^{(\alpha)}(\theta_1, \theta_2) \doteq i\langle \Psi^{(\alpha)} | \frac{\partial}{\partial \theta_j} | \Psi^{(\alpha)} \rangle. \tag{2.14}$$

It should be noted that the wave function $\Psi^{(\alpha)}(\theta_1, \theta_2)$ is defined up to a phase factor on the boundary-phase space. Therefore, $\Psi^{(\alpha)}(\theta_1, \theta_2)$ and $e^{if(\theta_1,\theta_2)}\Psi^{(\alpha)}(\theta_1, \theta_2)$ are physically equivalent for any smooth function $f(\theta_1, \theta_2)$. Under this phase change, $\mathcal{A}_j^{(\alpha)}(\theta_1, \theta_2)$ transforms like a gauge:

$$\begin{aligned} \mathcal{A}_j^{(\alpha)}(\theta_1, \theta_2) &\rightarrow \mathcal{A}_j^{(\alpha)}(\theta_1, \theta_2) - \partial_j f(\theta_1, \theta_2) \\ \Psi^{(\alpha)}(\theta_1, \theta_2) &\rightarrow e^{if(\theta_1,\theta_2)}\Psi^{(\alpha)}(\theta_1, \theta_2). \end{aligned} \tag{2.15}$$

Hence, the Chern number integral is conserved under this gauge transformation and it encapsulates general properties of the system. Chern numbers has been used

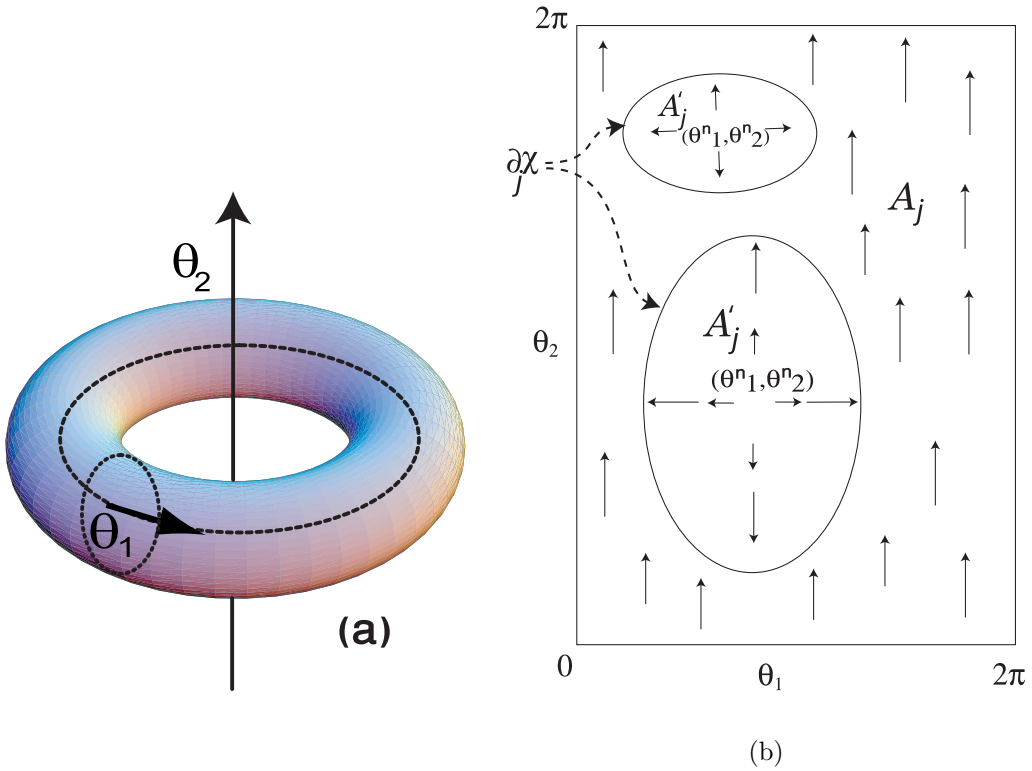

Figure 2.5: (a) Twist angles of the toroidal boundary condition. In addition to the flux going through the surface there may also be a flux inside the torus or going through the hole in the middle. When encircling these fluxes the wave function acquire an extra phase represented by the boundary conditions in Eq. (2.12) (b) Redefining the vector potential around the singularities: $\mathcal{A}_j$ is not well-defined everywhere on the torus of the boundary condition. Therefore, another vector field $\mathcal{A}'_j$ with different definition should be introduced around each singularity (θ_1^n, θ_2^n) of $\mathcal{A}_j$. $\mathcal{A}_j$ and $\mathcal{A}'_j$ are related to each other by a gauge transformation χ and the Chern number depends only on the loop integrals of χ around those singularities regions, c.f., Eq.(2.17).

extensively in the quantum Hall literature, for characterization of the localized and extended states (Ref. [151] and refs. therein). In this chapter, we use the Chern number as an indicator of order in the system. Moreover, it enables us to characterize the ground state in different regimes, especially where the calculation of the overlap with the Laughlin wave function fails to give a conclusive answer.

Before explaining the method for calculating the Chern number, we clarify some issues related to the degeneracy of the ground state. In some systems, the ground state can be degenerate, this can be intrinsic or it can be as a result of the topology of the system. If the ground state is degenerate, we should generalize the simple integral form of Eq. (2.13) to take into account the redundancy inside the ground state manifold. For example, in the case of a two-fold degenerate ground state, an extra gauge freedom related to the relative phase between two ground states, and this freedom should be fixed. In other words, as we change the twist angles, we can not keep track of the evolution of both states, since one can not distinguish them from each other. Therefore, to uniquely determine the Chern number of the ground state(s), we should resolve this gauge invariance, which is treated in Section 2.3.3 and 2.3.4.

It important to note that the degeneracy in the non-interacting regime is fundamentally different from the degeneracy in the interacting case. In the non-interacting limit, the degeneracy can be lifted by a local perturbation e.g., impurity, while in the hardcore case, the degeneracy remains in the thermodynamic limit [175]. The latter degeneracy in the ground state is a consequence of the global non-trivial properties of the manifold on which the particles move rather than related to a symmetry breaking

which happens in conventional models e.g., Ising model. The topological degeneracy is not a consequence of breaking of any symmetry only in the ground state, instead it is the entire Hilbert space which is split into disconnected pieces not related by any symmetry transformation. With a general argument, Wen [173] showed that if the degeneracy of a chiral spin system moving on a simple torus is k, then it should be k^g on a torus with g handles (Riemann surface with genus g), therefore the topological detergency is an intrinsic feature of the system. In particular, in the context of quantum Hall effect, this multicomponent feature of the ground state on a torus has a physical significance, while the single component ground state on a sphere boundary condition gives zero conductance, the torus geometry with multicomponent ground state results in a correct conductance measured in the experiment, since the torus boundary condition is more relevant to the experiment. Changing twists angles of the boundary will rotate these components into each other and gives an overall non-zero conductance [122].

As studied in a recent work by M. Oshikawa and T. Senthil [124], as a universal feature, it has been shown that in presence of a gap, there is a direct connection between the fractionalization and the topological order. More precisely, once a system has some quasiparticles with fractional statistics, a topological degeneracy should occur, which indicates the presence of a topological order. Therefore, the amount of the degeneracy is related to the statistics of the fractionalized quasiparticles e.g., in the case of $\nu = 1/2$, the two-fold degeneracy is related to $1/2$ anyonic statistics of the corresponding quasiparticles. Chern number has been also studies for spin $1/2$ system on a honeycomb lattice [96] for identifying Abelian and non-Abelian anyons.

Bellissard *et al.* [17] studies Chern number for disordered Fermi system using a non-commutative geometry.

To resolve the extra gauge freedom related to the two degenerate ground states, we consider two possibilities: I. lifting the degeneracy by adding some impurities, II. fixing the relative phase between the two states in the ground state. Below, we explore both cases. In the first case, we introduce some fixed impurities to lift the degeneracy in the ground state for all values of the twist angles. This is an artifact of the finite size of the system which we take advantage of. In the presence of perturbation, we show that the system has a topological order in spite of poor overlap with the Laughlin state. In the second approach, we use a scheme recently proposed by Hatsugai [165, 80] which is a generalized form for degenerate manifolds.

2.3.3 Resolving the degeneracy by adding impurities

In this section, we introduce some perturbation in the finite system in form of local potentials (similar to local impurities in electronic systems) to split the degeneracy of the ground state and resolve the corresponding gauge invariance, which allows us to compute the Chern number. Furthermore, the fact that we can still uniquely determine the Chern number in the presence of impurities, shows that the system retains its topological order, even when the impurities distort its ground state wave function away from the Laughlin wave function.

In the context of the quantum Hall effect, the conventional numerical calculation of various physical quantities such as the energy spectrum, screening charge density profile, wave functions overlaps, and the density-density correlation functions, can

not be used for understanding the transport properties of electrons in the presence of impurities (although useful for studying of isolated impurities [139, 179]). Recently, D. N. Sheng *et al.* [151] calculated the Chern number as an unambiguous way to distinguish insulating and current carrying states in the $\nu = 1/3$ quantum Hall regime which correspond to zero and non-zero Chern number, respectively. In this work, a weak random disorder was used to lift the degeneracy of the ground state (three-fold for $\nu = 1/3$) for a finite number of electrons. The energy splitting between the lowest three states then decreased with increasing number of particles, which indicates the recovery of the degeneracy in the thermodynamic limit. Moreover, the mobility gap can be determined by looking at the energy at which the Chern number drops towards zero. This energy gap is comparable to the energy gap obtained from the experiment and it is not necessarily equal to the spectrum gap which separates the degenerate ground state from the excited states This shows the significance of Chern number calculations for understanding these systems.

In a finite system, the coupling to a single-body interaction, e.g., impurities, can lift the degeneracy and one can uniquely determine the Chern number for the individual states by direct integration of Eq. (2.13). On one hand, the impurity should be strong enough to split the energy in the ground state (in this case E_2, E_1, where E_j denotes the energy of the jth energy level) for all values of the twist angles. On the other hand, these impurities should be weak enough so that the energy splitting in the ground state remains smaller than the thermodynamic gap (in this case $E_2 - E_1 \ll E_3 - E_2$).

To calculate the Chern number of individual level, as mentioned in the pervious

section, we have to fix the phase of the wave function. The method that we explore in this section can be considered as a simplified version of the general method developed by Hatsugai [80] which we will explore in the next section. Following Kohmoto's procedure [99], we assume that the ground state $\Psi(\theta_1, \theta_2)$ may be expanded for all twist angles on a $\mathbf{s}$-dimensional Hilbert discrete space $\Psi(\theta_1, \theta_2) = (c_1, c_2, ..., c_s)$. If $\mathcal{A}_j(\theta_1, \theta_2)$ in Eq. (2.13) is a periodic function on the torus of the boundary condition, then by application of Stoke's theorem, the Chern number will be always zeros. The non-triviality (non-zero conductance in the case of quantum Hall system) occurs because of the zeros of the wave function, where the phase is not well-defined. Therefore, $\mathcal{A}(\theta_1, \theta_2)$ is not well defined everywhere and its flux integral can be non-zero. To uniquely determine the Chern number, we assume that the wave function and the vector field are not defined for certain points (θ_1^n, θ_2^n) in S_n regions on the torus of the boundary condition. For simplicity, we first discuss this procedure, in the case of a non-degenerate ground state. For calculating the integral, we should acquire another gauge convention for the wave function inside these S_n regions, e.g., in a discrete system, we may require an arbitrary element of the wave function to be always real, and thereby we can define a new vector field $\mathcal{A}'^{(\alpha)}_j(\theta_1, \theta_2)$, which is well defined inside these regions. These two vector fields differ from each other by a gauge transformation (Fig. 2.5):

$$\mathcal{A}^{(\alpha)}_j(\theta_1, \theta_2) - \mathcal{A}'^{(\alpha)}_j(\theta_1, \theta_2) = \partial_j \chi(\theta_1, \theta_2), \tag{2.16}$$

and the Chern number reduces to the winding number of the gauge transformation $\chi(\theta_1, \theta_2)$ over small loops encircling (θ_1^n, θ_2^n), i.e. ∂S_n,

$$C(\alpha) = \sum_n \frac{1}{2\pi} \oint_{\partial S_n} \overrightarrow{\nabla} \chi \cdot d\overrightarrow{\theta}. \tag{2.17}$$

The one-dimensional gauge Eq. (2.16) should be resolved by making two conventions. For example, in one convention the first element and in the other the second element of the wave function in the Hilbert space should be real i.e. transforming the ground state Ψ into $\Psi_\Phi = P\Phi = \Psi\Psi^\dagger\Phi$ where $\Phi = (1, 0, ..., 0)^\dagger$ is a $\mathbf{s}$-dimensional vector and P is a projection into the ground state and similarly with the other reference vector $\Phi' = (0, 1, ..., 0)^\dagger$. Since the gauge that relates two vector fields is the same as the one that relates the corresponding wave functions (similar to Eq.(2.16)), we can uniquely determine the gauge transformation function χ by evaluating $\Omega(\theta_1, \theta_2) = e^{i\chi} = \Phi^\dagger P \Phi'$. Therefore, the Chern number will be equal to the number of windings of χ around regions where $\Lambda_\phi = \Phi^\dagger P \Phi = |c_1|^2$ is zero. Counting the vorticities has a vigorous computational advantage over the conventional method of direct integration of Eq. (2.13). In the direct integration, we need to choose a large number of mesh points for the boundary angles, because of the discrete approximation of derivatives in Eq. (2.13), and this makes the calculation computationally heavy. We note that for the system on a lattice, we should exactly diagonalize the Hamiltonian which is a sparse matrix as opposed to the continuum case where the Hamiltonian is a dense matrix residing on a smaller projected Hilbert space (lowest Landau level).

For removing the degeneracy, in our numerical simulations, we add a small amount of impurity which is modeled as delta function potentials located at random sites with a random strength, of the order of the tunneling energy J. This is described by a

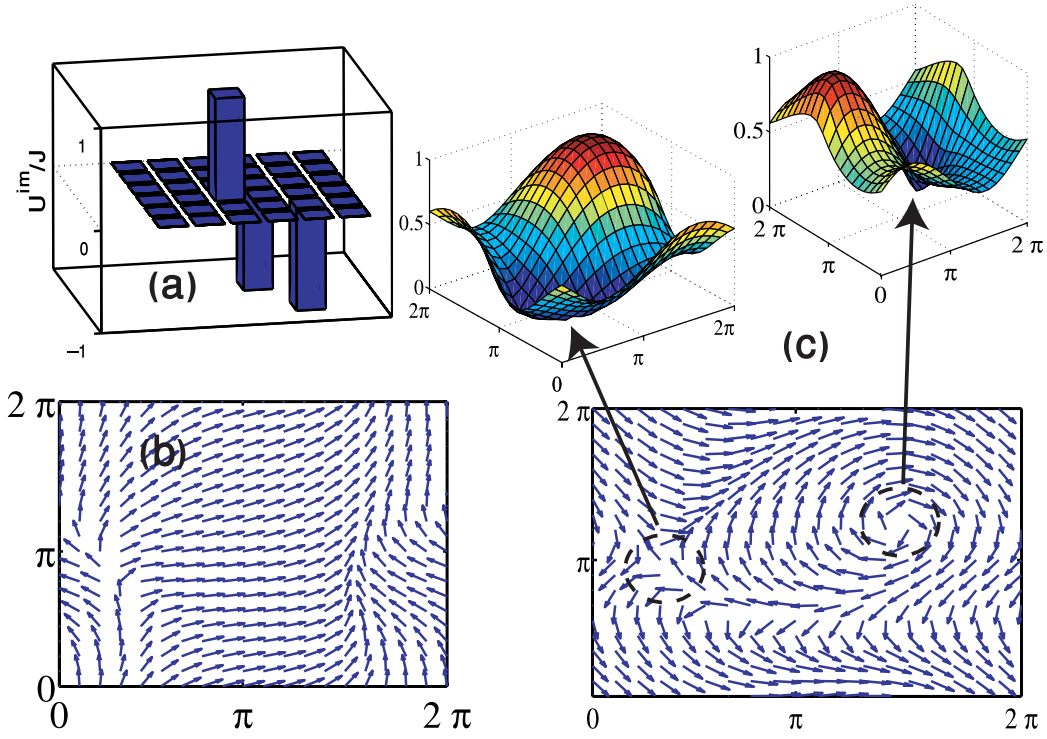

Figure 2.6: Chern number associated to low-lying energy states, in the presences of impurities. Due to the impurity potential (a), two-fold degenerate ground state splits and the wave function overlap with the Laughlin state drops to 52% and 65%, for the first and the second energy state, respectively. The results are for 3 atoms on a 6x6 lattice ($\alpha = 0.17$) in the hard-core limit. (b) $\Omega(\theta_1, \theta_2)$ for the first level has no vorticity. However, for the second level, as shown in (c), $\Omega(\theta_1, \theta_2)$ has vorticity equal to one associated with regions where either Λ_ϕ or Λ'_ϕ vanishes.

Hamiltonian of the form $H = \sum_i U_i^{im} \hat{n}_i$, where i numerates the lattice site, $\hat{n}_i$ is the atom number operator and U_i^{im} is the strength of the impurity at site i.

We choose reference states Φ and Φ' to be eigenvectors of the numerically diagonalized Hamiltonian at two different twist angles. In Fig. 2.6, vorticities of $e^{i\chi}$ associated with the first and the second energy level is depicted. It is easy to see that the Chern number associated to the two ground states is one. Number of vortices may vary for the first and second ground states, but their sum is always equal to one. The hard-core limit ($U \gg J$) is very similar to the case of fractional quantum Hall effect, which in the context of Hall systems, means a share of 1/2 (in e^2/h unit) for each ground state [158]. When the onsite interaction strength is small ($U < J$), the thermodynamic gap becomes comparable to the ground state energy splitting $E_2 - E_1 \sim E_3 - E_2$, the Chern number can not be uniquely determined, and the system doesn't have topological order. On the other hand, in the limit of strong interaction ($U \gg J$), the total Chern number associated to the ground states is equal to one, regardless of the impurity configuration. Moreover, in the hard-core limit, although the ground state is not described by the Laughlin wave function, since it is distorted by the impurity (in our model it can be as low as 50%), the Chern number is unique and robust. This is an indication that the topological order is not related to the symmetries of the Hamiltonian and it is robust against arbitrary local perturbations [175]. These results indicate the existence of a topological order in the system and robustness of the ground states against local perturbations.

2.3.4 Gauge fixing

The method developed in the previous section has the graphical vortex representation for the Chern number which makes it computationally advantageous compared to the direct integration of Eq. (2.13). It can not, however, be applied directly to a degenerate ground state, and therefore we had to introduce an impurity potential which lifted the degeneracy. On the other hand, a significant amount of impurity in the system may distort the energy spectrum, so that the underlying physical properties of the lattice and fluxes could be confounded by the artifacts due to the impurities, especially for large α. To address this issues, in this section, we explore a generalized method of the previous section based on Refs. [165] and [80], which works for a degenerate ground state.

By generalizing the Chern number formalism for a degenerate ground state manifold, instead of having a single vector field $\mathcal{A}_j^{(\alpha)}(\theta_1, \theta_2)$, a tensor field $\mathcal{A}_j^{(\alpha,\beta)}(\theta_1, \theta_2)$ should be defined, where $\alpha, \beta = 1, 2, ..., q$ for a $\mathbf{q}$-fold degenerate ground state

$$\mathcal{A}_j^{(\alpha,\beta)}(\theta_1, \theta_2) \doteq i\langle\Psi^{(\alpha)}|\frac{\partial}{\partial\theta_j}|\Psi^{(\beta)}\rangle \tag{2.18}$$

Similar to the non-degenerate case, when $\mathcal{A}_j^{(\alpha,\beta)}$ is not defined, a new gauge convention should be acquired for the regions with singularities. This gives rise to a tensor gauge transformation $\chi^{(\alpha,\beta)}(\theta_1, \theta_2)$ on the border of these regions

$$\mathcal{A}_j^{(\alpha,\beta)}(\theta_1, \theta_2) - \mathcal{A}'^{(\alpha,\beta)}_j(\theta_1, \theta_2) = \partial_j\chi^{(\alpha,\beta)}(\theta_1, \theta_2). \tag{2.19}$$

Following Hatsugai's proposal[80] for fixing the ground state manifold gauge, we take two reference multiplets Φ and Φ' which are two arbitrary $\mathbf{s} \times \mathbf{q}$ matrices; q is

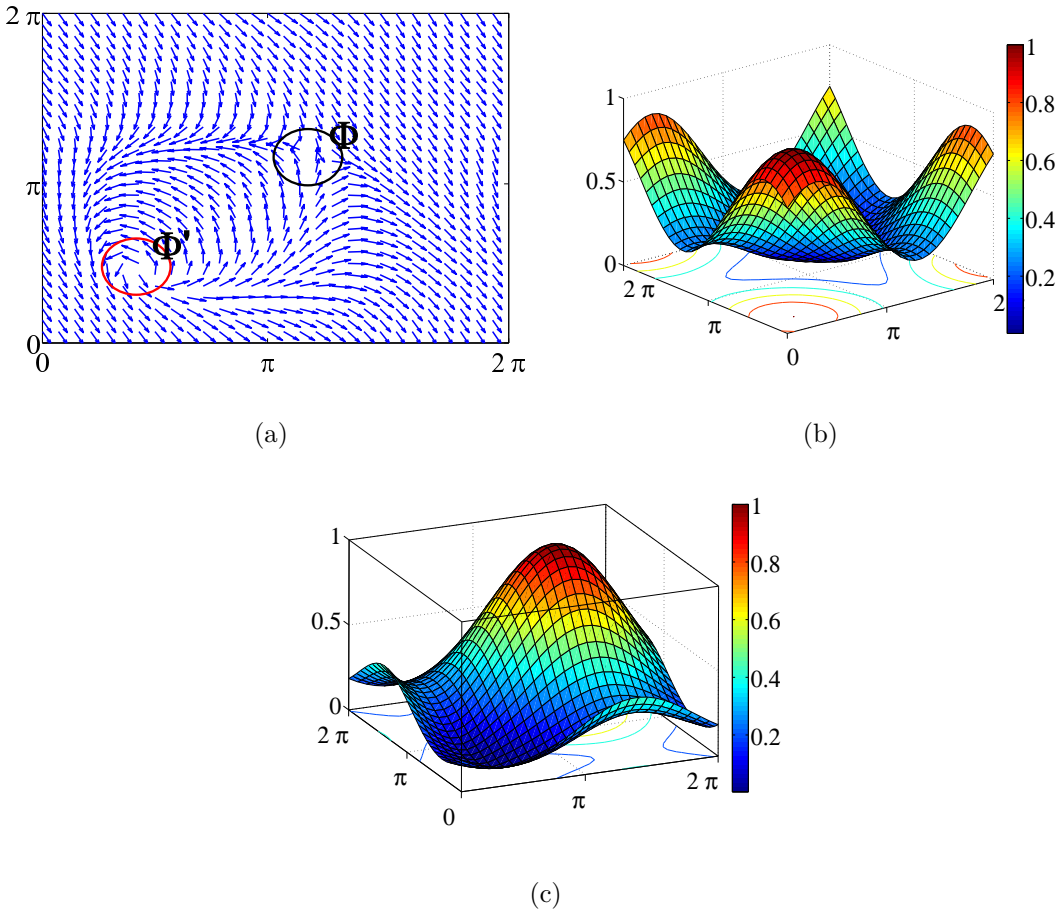

Figure 2.7: (a) shows the argument of $\Omega(\theta_1, \theta_2)$ as arrows for fixed Φ and Φ'. (b) and (c): surface plots of $\det\Lambda_\Phi$ and $\det\Lambda'_\Phi$ (blue is lower than red). θ_1 and θ_2 changes from zero to 2π. These plots have been produced for 3 atoms with $N_\phi = 6$ ($\alpha = 0.24$) in the hard-core limit on a 5x5 lattice. The total vorticity corresponding to each of the reference wave functions (Φ or Φ') indicates a Chern number equal to one.

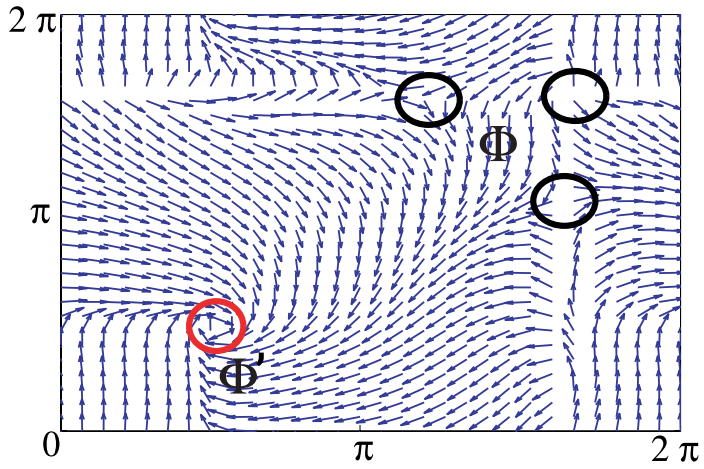

Figure 2.8: $\Omega(\theta_1, \theta_2)$ for fixed Φ and Φ'. θ_1 and θ_2 changes from zero to 2π. This plot has been produced for 4 atoms with $N\phi = 8$ in the hard-core limit on a 5x5 lattice ($\alpha = 0.32$). Although, there are more vortices here compared to Fig. 2.7, the total vorticity corresponding to each of the trial functions (Φ or Φ') indicates a Chern number equal to one.

the ground state degeneracy (equal to 2 in our case). In our numerical simulation, we choose the multiplets to be two sets of ground state at two different twist angles far from each other, e.g., $(0, 0)$ and (π, π). We define an overlap matrix as $\Lambda_\phi = \Phi^\dagger P \Phi$ where $P = \Psi\Psi^\dagger$ is again the projection into the ground state multiplet, and consider the regions where $\det\Lambda_\Phi$ or $\det\Lambda_{\Phi'}$ vanishes (similar to zeros of the wave function in the non-degenerate case). Hence, the Chern number for $\mathbf{q}$ degenerate states, will be equal to the total winding number of Tr $\chi^{(\alpha,\beta)}$ for small neighborhoods, S_n, in which $\det\Lambda_\Phi$ vanishes

$$C(1, 2, ..., q) \;=\; \sum_n \frac{1}{2\pi} \oint_{\partial S_n} \overrightarrow{\nabla} \mathrm{Tr}\ \chi^{(\alpha,\beta)} \cdot d\overrightarrow{\theta} \tag{2.20}$$

which is the same as the number of vortices of $\Omega(\Phi, \Phi') = \det(\Phi^\dagger P \Phi')$. It should be noted that the zeros of det Λ_Φ and $\det\Lambda'_\Phi$ should not coincide in order to uniquely

Atoms	*Lattice*	α	*Chern/state*	Overlap
3	6x6	.17	1/2	0.99
4	6x6	.22	1/2	0.98
3	5x5	.24	1/2	0.98
3	4x5	.3	1/2	0.91
4	5x5	.32	1/2	0.78
3	4x4	.375	1/2	0.29

Table 2.1: Chern Number for different configurations in the hard-core limit for fixed filling factor $\nu = 1/2$. The Laughlin state overlap is shown in the last column. although it deviates from the Laughlin state. Although the ground state deviates from the Laughlin state, the Chern number remains equal to one half per state before reaching some critical $\alpha_c \simeq 0.4$ where the energy gap vanishes.

determine the total vorticity. In Fig. 2.7, we have plotted Ω, $\det\Lambda_\Phi$, and $\det\Lambda_{\Phi'}$, found by numerical diagonalization of the Hamiltonian for a mesh (30×30) of winding angles θ_1 and θ_2. In this figure, the Chern number can be determined be counting the number of vortices and it is readily seen that the winding number is equal to one for the corresponding zeros of $\det\Lambda_\Phi$ (or $\det\Lambda_{\Phi'}$).

We have calculated the Chern number for fixed $\nu = 1/2$ and different α's by the approach described above. The result is shown in Table 2.1. For low $\alpha \ll 1$, we know from Sec. 2.2 that the ground state is the Laughlin state and we expect to get a Chern number equal to one. For higher α, the lattice structure becomes more apparent and the overlap with the Laughlin state decreases. However, in our calculation, the ground state remains two-fold degenerate and it turns out that the ground state Chern number tends to remain equal to one before reaching some critical $\alpha_c \simeq 0.4$. Hence, also in this regime we expect to have similar topological order and fractional statistics of the excitations above these states on the lattice.

For the arguments above to be applicable, it is essential that we can uniquely

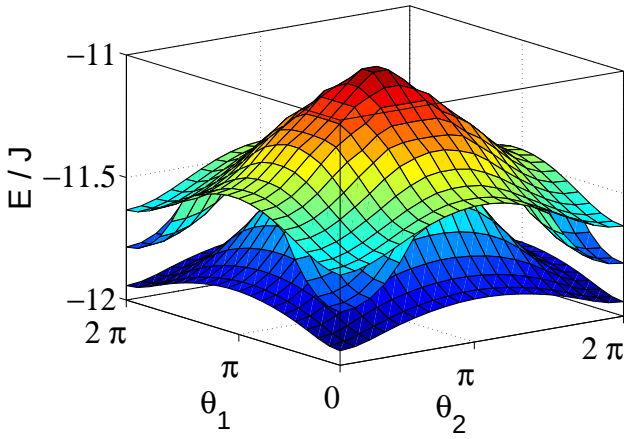

(a)

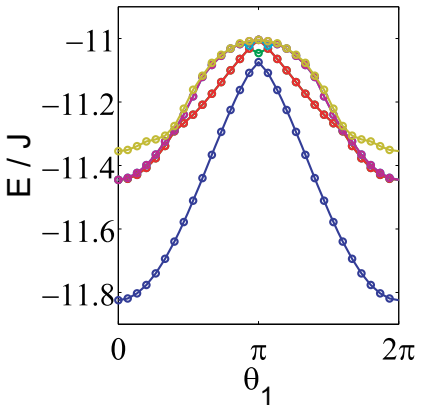

(b)

Figure 2.9: Low-lying energy levels as a function of twist angles. For high α the degeneracy of the ground state is a function of twist angles. The shown results are for 5 atoms on a 5x5 lattice i.e. $\alpha = 0.4$ (a) shows first three energy manifolds as a function of the toroidal boundary condition angles, (b) shows a cross section of (a) at $\theta_2 = \pi$ for seven lowest energy levels. The first and the second energy levels get close to each other at $\theta_1 = \theta_2 = \pi$.

identify a two-fold degenerate ground state which is well separated from all higher lying states. For higher flux densities, $\alpha > \alpha_c$, the two-fold ground state degeneracy is no longer valid everywhere on the torus of the boundary condition. In this regime, the issue of degeneracy is more subtle, and the finite size effect becomes significant. The translational symmetry argument [77], which was used in the Section 2.2, is not applicable on a lattice and as pointed out by Kol *et al.* [101] the degeneracy of the ground state may vary periodically with the system size. Some of the gaps which appear in the calculation may be due to the finite size and vanish in the thermodynamic limit, whereas others may represent real energy gaps which are still present in the thermodynamic limit. To investigate this, we study the ground state degeneracy as a function of boundary angles (θ_1, θ_2) which are not physical observable and therefore the degeneracy in thermodynamic limit should not depend on their value. In particular, Fig. 2.9 shows the energy levels of five particles at $\alpha = 0.4$ for different values of the twist angles. The first and the second level are split at $(\theta_1 = \theta_2 = 0)$, while they touch each other at $(\theta_1 = \theta_2 = \pi)$. We have observed similar behavior for different number of particles and lattice sizes e.g., 3 and 4 atoms at $\alpha = 0.5$. In this case, the system seems to not have a two-fold degeneracy. Therefore, the ground state enters a different regime which is a subject for further investigation.

For having the topological order, it is not necessary to be in the hard-core limit. Even at finite interaction strength $U \sim J\alpha$, we have observed the same topological order with the help of the Chern number calculation. If U gets further smaller, the energy gap above the ground state diminishes (as seen in Sec. 2.2) and the topological order disappears.

We conclude that the Chern number can be unambiguously calculated for the ground state of the system in a regime where Laughlin's description is not appropriate for the lattice. The non-zero Chern number of a two-fold degenerate ground state, in this case equal to one half per state, is a direct indication of the topological order of the system.

2.4 Extension of the Model

In Sections 2.2 and 2.3 above, we have investigated the conditions under which the fractional quantum Hall effect may be realized for particles on a lattice. The motivation for this study is the possibility to generate the quantum Hall effect with ultra cold atoms in an optical lattice but the results of these sections are applicable regardless of the method used to attain this situation. In this and the following sections, we investigate some questions which are of particular relevance to ultra cold atoms in an optical lattice. First, we introduce a long range, e.g., dipole-dipole, interaction which turn out to increase the energy gap and thereby stabilizes the quantum Hall states. We then turn to the case of $\nu = 1/4$ and show that in order to realize this state, it is essential to have some kind of long range interaction.

2.4.1 Effect of the long-range interaction

In an experimental realization of the quantum Hall effect on a lattice, it is desirable to have as large an energy gap as possible in order to be insensitive to external perturbations. So far, we have studied effect of the short range interaction, and we have shown that the gap increases with increasing interaction strength, but the value

of the gap saturates when the short range interaction becomes comparable to the tunneling energy J.

In this section, we explore the possibility of increasing the gap by adding a long-range repulsive dipole-dipole interaction to the system. Previously, such dipole-dipole interaction has also been studied in Ref.[141] as a method to achieve Read-Rezayi states [137] of rapidly rotating cold trapped atoms for $\nu = 3/2$ and as a means to realize fractional Quantum Hall physics with Fermi gases [14]. The dipole-dipole (magnetic or electric) interaction is described by the Hamiltonian:

$$H_{\mathrm{d-d}} = U_{dipole} \sum_{1 \le i < j \le N} \frac{\mathbf{p}_i \cdot \mathbf{p}_j - 3(\mathbf{n}_{ij} \cdot \mathbf{p}_i)(\mathbf{n}_{ij} \cdot \mathbf{p}_j)}{|\mathbf{r}_i - \mathbf{r_j}|^3} \tag{2.21}$$

where $\mathbf{n}_{ij} = (\mathbf{r}_i - \mathbf{r}_j)/|\mathbf{r}_i - \mathbf{r}_j|$. $\mathbf{p}_i$ are unit vectors representing the permanent dipole moments and the position vectors $\mathbf{r}_i$ are in units of the lattice spacing $\mathbf{a}$. For simplicity, we assume that all dipoles are polarized in the direction perpendicular to the plane. With time independent dipoles, the strength of the interaction is given by $U_{dipole} = \frac{\mu_0 \mu^2}{4\pi a^3}$ (or $\frac{\wp^2}{4\pi\epsilon_0 a^3}$) where μ's ($\wp$'s) are the permanent magnetic (electric) dipole moment. Static dipoles will thus give repulsive interaction $U_{dipole} > 0$, but experimentally time varying fields may be introduced which effectively change the sign of the interaction[65]. For completeness, we shall therefore both investigate positive and negative U_{dipole}, but the repulsive interaction corresponding to static dipoles will be the most desirable situation since it stabilizes the quantum Hall states.

Experimentally the dipole-dipole interaction will naturally be present in the recently realized Bose-Einstein condensation of Chromium[72] which has a large magnetic moment. However, for a lattice realization, polar molecules which have strong permanent electric dipole moments is a more promising candidate. For typical polar

molecules with the electric moment $\wp \sim 1$ Debye, on a lattice with spacing $\mathbf{a} \sim 0.5\mu$m, U_{dipole} can be up to few kHz, an order of magnitude greater than the typical tunneling $J/2\pi\hbar$ which can be few hundreds of Hz [71].

To study the effect of the dipole-dipole interaction, we again numerically diagonalize the Hamiltonian for a few hardcore bosons ($U \gg J$), in the dilute regime $\alpha \leqslant 0.3$, while varying strength of the dipole-dipole interaction. The results of this simulation is shown in Fig. 2.10 (a). After adding the dipole interaction, the ground state in a dilute lattice remains two-fold degenerate, since the interaction only depends on the relative distance of the particles and keeps the center of mass motion intact. If the dipole interaction becomes too strong ($\mathbf{U}_{dipole} \gg J$), the ground state wave function deviates from the Laughlin wave function, but the topological order remains the same as for the system without dipole interaction. We verified this by calculating the Chern number as explained in Sec. 2.3 for different values of the dipole-dipole interaction strength $\mathbf{U}_{dipole}$ and observed that the total Chern number of the two-fold degenerate ground state is equal to one. Moreover, as it is shown in Fig. 2.10 (b) adding such an interaction can increase the gap: the lower curve corresponds to the hard-core limit discussed in the previous work [153] and the upper curve corresponds to the system including the dipole-dipole interaction. This enhancement varies linearly with the flux density α in a dilute lattice and doesn't depend on the number of particles and consequently, it is expected to behave similarly in the thermodynamic limit.

One of the impediment of the experimental realization of Quantum Hall state is the smallness of the gap which can be improved by adding dipole-dipole interaction. In this section, we showed that this improvement is possible and moreover, by Chern

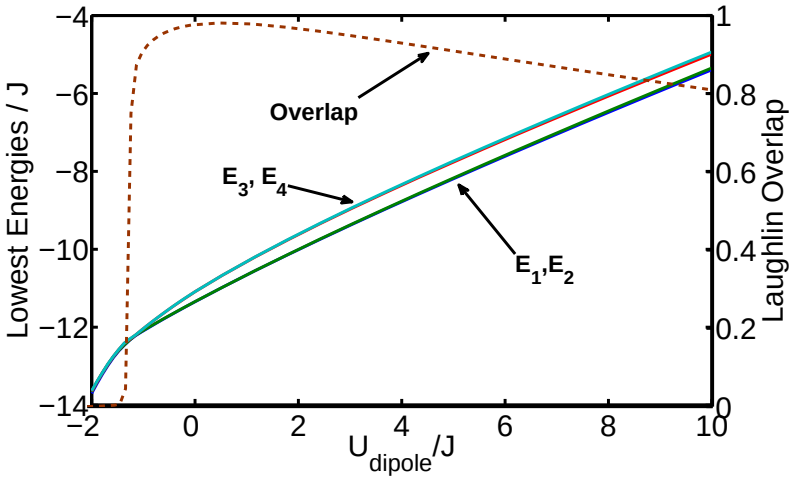

(a)

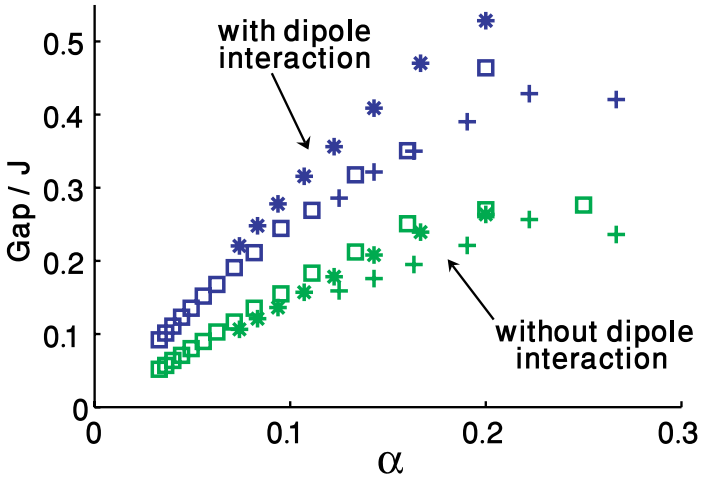

(b)

Figure 2.10: (a) The overlap of the ground state with the Laughlin wave function (dashed lines) and four low lying energies of the system (solid lines) versus the dipole-dipole interaction for four atoms on a 6x6 lattice. (b) Gap enhancement for a fixed repulsive dipole-dipole interaction strength $U_{dipole} = 5J$ versus α. The results are shown for $N = 2(\square)$, $N = 3(*)$, $N = 4(+)$

number evaluation, we verified that adding dipole interaction doesn't change the topological behavior of the ground state manifold.

2.4.2 Case of $\nu = 1/4$

So far we have concentrated on the case of $\nu = 1/2$. In this section, we briefly investigate the case of $\nu = 1/4$. It is expected that the Laughlin wave function remains a good description for the ground state of a bosonic system for any even q, where $\nu = 1/q$. Following Haldane's argument[77], due to the center of mass motion, the degeneracy of the ground state is expected to be q-fold on a torus. Similar to the case of $\nu = 1/2$, the Laughlin wave function should be a suitable description for any q provided that the magnetic field is weak so that we are close to the continuum limit, i.e. $\alpha \ll 1$. Also the Chern number is expected to be equal to one for the q-fold degenerate ground state, which in the context of quantum Hall effect means a share of $1/q$ of the conduction quantum e^2/h for each state in the q-fold degenerate ground state manifold.

We have done both overlap and the Chern number calculation to check those premises. In the case of $\nu = 1/4$, significant overlap occurs at low $\alpha \lesssim 0.1$. The average wave function overlap of four lowest energy eigenstates with the Laughlin wave function is depicted in figure 2.11, where we have used a generalization of the Laughlin wave function for periodic boundary conditions similar to Eq. (2.5) [136].

We observe that the Laughlin wave function is a reliable description of the system with $\nu = 1/4$ but only for much more dilute lattices ($\alpha \lesssim 0.1$) compared to $\nu = 1/2$ where significant overlap occurs for $\alpha \lesssim 0.3$. Contrary to $\nu = 1/2$, where the gap is a

fraction of the tunneling energy J, the gap for $\nu = 1/4$ between the 4-fold degenerate ground state and the next energy level is infinitesimal. The reason for the vanishing gap can be understood in the continuum limit from the argument put forward in Ref. [126]: as noted previously the Laughlin wave function is an exact eigenstate of the Hamiltonian with an energy per particle equal to the lowest Landau level energy. The energy of the $m = 4$ state is thus equal to the $m = 2$ state. It thus costs a negligible energy to compress the $\nu = 1/4$ state to the $\nu = 1/2$ state, and therefore there is no gap. In an external trap the system will always choose the highest density state which is the $\nu = 1/2$ state. Note, however that this argument only applies to short range interactions. For long range interactions, we expect to see a non vanishing gap.

Even though that with short range interactions, the gap is very small in our numerical calculations, it is still sufficiently large that it allows us to unambiguously determine the Chern number for the ground state manifold as described in Sec. 2.3.4. As expected the calculation shows that the Chern number is equal to one corresponding to a four-fold degenerate ground state consistent with the generalization of the fermionic case in the fractional quantum Hall theory [122, 158]. In Fig. 2.11, the overlap of the first four lowest energy state with the Laughlin wave function is depicted. In the absence of the dipole interaction, the ground state overlap is significant only for $\alpha \lesssim 0.1$, however, by adding a moderate dipole interaction ($U_{dipole} = 5J$), the overlap becomes more significant for a larger interval of the flux density, i.e. $\alpha \lesssim 0.25$. This is due to the fact that state with lower density become more favorable in the presence of a long-range repulsive interaction.

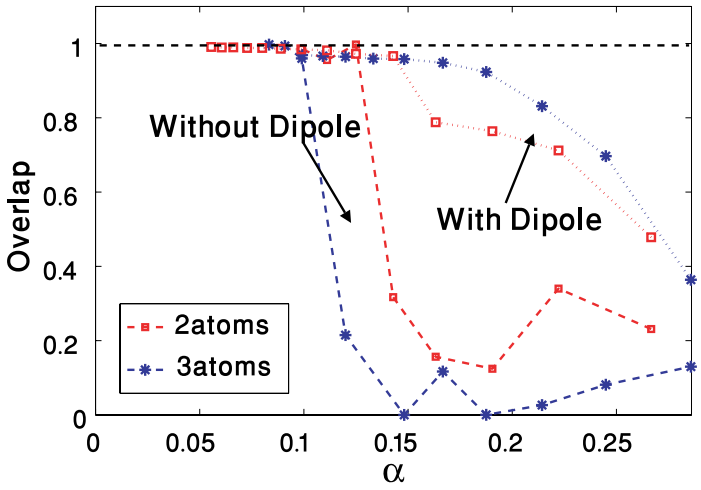

Figure 2.11: The overlap of the first four low-lying energy states with the Laughlin wave function for the case of $\nu = 1/4$ on a torus. The dashed (dotted) line shows the overlap for the system without (with) dipole interaction ($U_{dipole} = 5J$). The Laughlin state is only a good description for a more dilute lattice $\alpha \lesssim 0.1$ compared to $\nu = 1/2$. The dipole interaction stabilizes the system and the overlap is more significant for higher values of $\alpha \lesssim 0.2$.

We observed that adding a dipole interaction would lead to an improvement of the gap for $\nu = 1/2$ and make the Laughlin overlap more significant for larger interval of magnetic field strength α in the case of $\nu = 1/4$. Therefore this long-range interaction can be used as an tool for stabilizing the ground state and make the realization of these quantum states, experimentally more feasible.

2.5 Detection of the Quantum Hall state

In an experimental realization of the quantum Hall states, it is essential to have an experimental probe which can verify that the desired states were produced. In most experiments with cold trapped atoms, the state of the system is probed by releasing the atoms from the trap and imaging the momentum distribution. In Ref. [153],

it was shown that this technique provide some indication of the dynamics in the system. This measurement technique, however, only provides limited information, since it only measures the single particle density matrix, and provides no information about the correlations between the particles. In Refs. [126] and [4] a more advanced measurement techniques were proposed, where the particle correlation is obtained by looking at the correlations in the expansion images. In this section, we study Bragg scattering as an alternative measurement strategy which reveals the excitation spectrum of the quantum system. In Ref. [22] bosonic quantum Hall system responses to a perturbative potential is studied. We focus on Bragg scattering where two momentum states of the same internal ground state are connected by a stimulated two-photon process [156]. By setting up two laser beams with frequencies ω_1 and ω_2 and wave vectors $\vec{k_1}$ and $\vec{k_2}$ in the plane of the original lattice, a running optical superlattice will be produced with frequency $\omega_1 - \omega_2$ and wave vector $\vec{k_1} - \vec{k_2}$. (Both frequencies ω_1 and ω_2 should be close to an internal electronic dipole transition in the atoms). The beams should be weak and sufficiently detuned so that direct photon transitions are negligible, i.e. $\mathcal{E}_1,\ \mathcal{E}_2,\ \gamma \ll \omega_1 - \omega_0,\ \omega_2 - \omega_0$, where ω_0 is the frequency of the transition, γ is the corresponding spontaneous decay rate and $\mathcal{E}_1, \mathcal{E}_2$ are the Rabi frequencies related to the laser-atom coupling. In this perturbative regime, the inelastic scattering of photons will be suppressed; the atom starts from the internal ground state, absorbs one photon from e.g., beam 1 by going to a virtual excited state and then emits another photon into beam 2 by returning to its internal ground state. After this process, the system has acquired an energy equal to $\hbar\omega = \hbar(\omega_1 - \omega_2)$ and a momentum kick equal to $\vec{q} = \vec{k_1} - \vec{k_2}$. Therefore, the overall effect of the

recoil process is a moving AC Stark shift as a perturbing moving potential, and the effective Hamiltonian represents the exchange of the two-photon recoil momentum and the energy difference to the system and is proportional to the local density i.e. $H \propto \rho(r)e^{-i(\omega_1-\omega_2)t+i(\vec{k_1}-\vec{k_2}).\vec{r}} + c.c.$.

This process can be used to probe density fluctuations of the system and thus to measure directly the dynamic structure factor $S(q,\omega)$ and static structure factor $S(q)$. This kind of spectroscopy has been studied for a BEC in a trap by Blakie *et al.* [24] and Zambelli *et al.* [29] and has been realized experimentally in Refs. [154, 171, 125, 155, 91, 120].

Also, Bragg spectroscopy in an optical lattice is discussed in Ref. [117] in a mean-field approach and also in Ref. [138] as a probe of the Mott-insulator excitation spectrum. On the other hand, in the context of quantum Hall effect, the static structure factor has been studied for probing the magnetoroton excitations [68] and charge density waves [140]. The dynamic and static structure factors are given respectively as

$$S(\vec{q},\omega) = \sum_{n,0} |\langle n|\rho^\dagger(\vec{q})|0\rangle|^2 \delta(\omega - E_n + E_0), \tag{2.22}$$

$$S(\vec{q}) = \sum_{n,0} |\langle n|\rho^\dagger(\vec{q})|0\rangle|^2 = \sum_{n,0} |\langle n| \sum_{\vec{r_i}} e^{i\vec{q}\cdot\vec{r_i}}|0\rangle|^2, \tag{2.23}$$

where the density fluctuation operator is defined as $\rho^\dagger(\vec{q}) = \sum_{m,n} \mathcal{A}_{\vec{q}}(m,n) c_m^\dagger c_n$ and the coefficient are defined as Fourier transforms of the Wannier functions: $\mathcal{A}_{\vec{q}}(m,n) = \int d^2\vec{r}\, e^{i\vec{q}\cdot\vec{r}} \phi^*(\vec{r}-\vec{r}_m)\phi(\vec{r}-\vec{r}_n)$, where the Wannier function $\phi(\vec{r}-\vec{r}_n)$ is the wave function of an atom localized on a site centered at $\vec{r}_n$. Below, we focus on deep optical lattices,

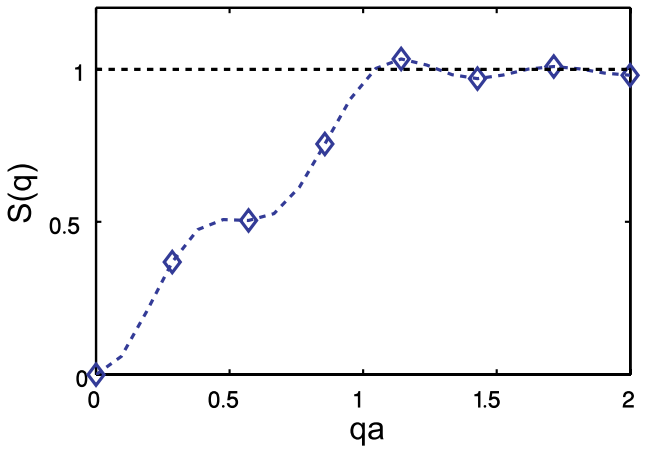

(a)

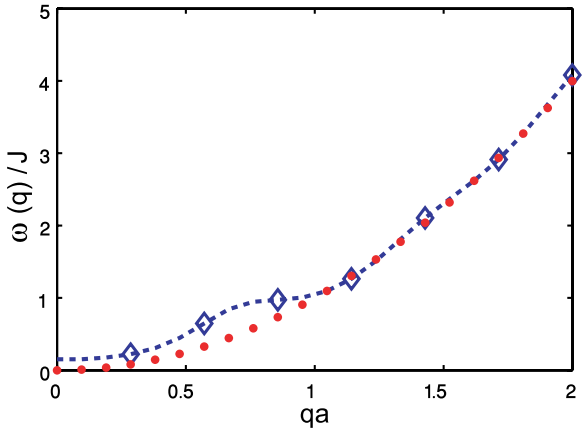

(b)

Figure 2.12: (a) Structure factor and (b) energy spectrum for a 11x11 lattice with 3 atoms on a torus. Points shows the momentums allowed by the boundary conditions. The dotted line in (b) shows for comparison the low energy spectrum of a free particle which equals $J(qa)^2$.

where $\mathcal{A}_{\vec{q}}(m,n) = e^{i\vec{q}\cdot\vec{r}_m}\delta_{m,n}$.

In the structure factor, there is a sum over the excited states $|n\rangle$ and ground states $|0\rangle$ and the self-term is thus excluded. The ground state on a torus is two-fold degenerate and therefore in our numerics, we add the contribution of both.

Since we are working on a discrete lattice, there will be a cut-off in the allowed momentum given by the lattice spacing $q_{\max} = \pi/a$, where a is the distance between lattice sites. Fig. 2.12(a) shows the structure factor for the case $\nu = 1/2$ for a small α calculated from our numerical diagonalizations. In the data presented here, we have chosen $\overrightarrow{q} = q\hat{x}$ and but the result should be similar in other directions in the lattice plane. We see that $S(q)$ is modulated at a momentum corresponding to the magnetic length. For the parameters that we have investigated, the general features of the structure factor is independent of the size of the system.

We obtain the excitation spectrum shown in Fig. 2.12 (b) similar to Ref. [68] by the Feynman-Bijl approximation. In the continuum limit ($\alpha \ll 1$), we assume that the low-lying excitations are long-wavelength density oscillations and their wave functions can be approximated to have the form $\propto \rho_k|0\rangle$. Therefore, the variational estimate for the excitation energy is $\omega(q) \simeq \hbar^2 q^2 /\ 2mS(q)$. At zero momentum and at the momentum corresponding to the magnetic length, there are gaps, and we also observe a deviation from the free particle spectrum similar to the magneoroton case as a reminiscent of the Wigner crystal. It should be noted that the deviation does not depend on the size or the number of particles in the system. As clearly seen in the Fig. 2.12 the energy spectrum and structure factor deviate from those of free particles, therefore, it could be used as an experimental probe of the system.

The structure factor and excitation spectrum imply some general features that are very different from that of the Mott-insulator and superfluid states, and can be used a powerful experimental indication of the quantum Hall states.

2.6 Generating Magnetic Hamiltonian for neutral atoms on a lattice

Recently, there has been several proposals for producing artificial magnetic field for neutral atoms in optical lattices [88, 119, 153], however, the implementation of each of them is still experimentally demanding. Recently, there has been an experimental demonstration of a rotating optical lattice [163] which is equivalent to an effective magnetic field (see below). The technique used in this experiment, however, generates a lattice with a large lattice spacing, because it uses laser beam which are not exactly counter propagating. This longer spacing reduces the energy scale in the lattice and thereby also reduces quantities such as energy gaps. Here, we shall now introduce an alternative method for generating a rotating optical lattice, which does not result in an increased lattice spacing. This method consists of rotating the optical lattice by manipulating laser beams.

In a frame of reference rotating with angular velocity ω around the $z - axis$, the Hamiltonian for a particle of mass m in an (planar) harmonic trap of natural frequency ω_0 is

$$H = \frac{p^2}{2m} + \frac{1}{2}m\omega_0(x^2 + y^2) - \omega\hat{z}.r \times p$$

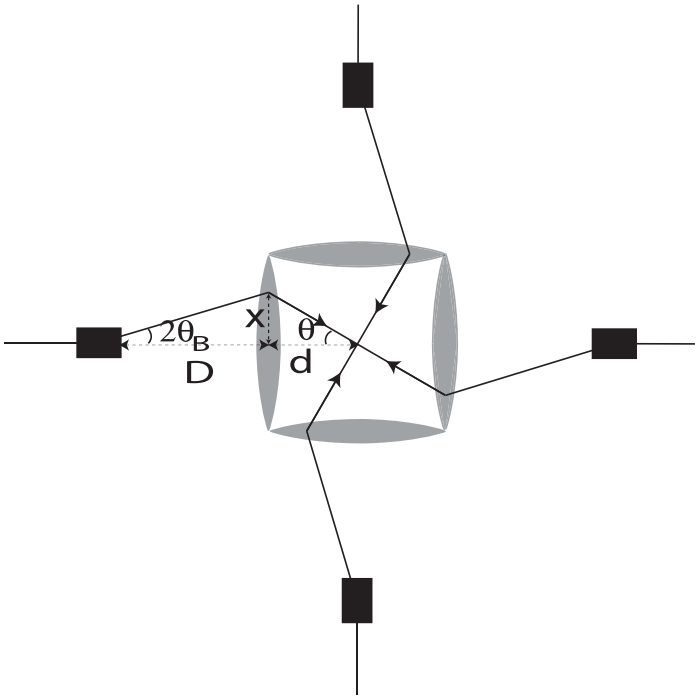

Figure 2.13: Proposal for realizing a rotating optical lattice. Four AOMs (black boxes) changes the direction of the lattice beam, which are subsequently focussed in the middle of the setup by four lenses (grey). Simultaneously varying the four diffraction angles in the AOMs will generate a rotating optical lattice.

$$= \frac{(p - m\omega\hat{z} \times r)^2}{2m} + \frac{1}{2}m(\omega_0^2 - \omega^2)(x^2 + y^2) \tag{2.24}$$

At resonance $\omega_0 = \omega$ the form is equivalent to the Hamiltonian of a particle of charge q experiencing an effective magnetic field $B = \bigtriangledown \times (m\omega\hat{z} \times r/q) = (2m\omega/q)\hat{z}$. Therefore, by simply rotating the optical lattice, we can mimic the magnetic field for neutral atoms.

To rotate the optical lattice, we propose to set up four acousto-optic modulators (AOM) and four focusing composite lenses as shown in the Fig. 2.13. By sweeping the acoustic wave frequency, the beams can be focused and make a rotating optical lattice.

In an AOM, for the first order diffracted light we have $\sin\theta_B = \frac{\lambda}{2\Lambda}$, where Λ is the wavelength of sound in the medium, λ is the light wavelength and θ_B is half of the angle between a diffracted beam and the non-diffracted beam (Fig. 2.13). By increasing the frequency of the acoustic wave, the diffraction angle increases. However, the beam should be focused by a large aperture lens so that it always passes the region where we want to make the optical lattice. By focusing a similar but counter-propagating beam, we can make a rotating standing wave (Fig. 2.13). By repeating the same configuration in the transverse direction, we can make a rotating optical lattice. In particular, if the AOM is far from the composite lenses, $D \gg d$, then $x/D = \lambda/\Lambda$ and $x/d = \tan\theta$ where $-\pi/4 \leq (\theta = \omega t) \leq \pi/4$, where the parameters are defined in Fig. 2.13. If we consider a square lattice with dimensions $N_x = N_y = \mathcal{N}$, the number of magnetic flux given by rotation is

$$N_\phi = \frac{BA}{\Phi_0} = \frac{\pi}{2}\frac{\mathcal{N}^2\omega}{\omega_r} \tag{2.25}$$

where $\omega_r = \hbar k^2/2M$ is the atomic recoil frequency.

On the other hand, the upper limit for the magnetic field comes from the single Bloch band approximation which we made in writing the Hamiltonian for the optical lattice. In order for the particles to remain in the first band, the traveling lattice beams should move them adiabatically. From Ref. [41], the adiabaticity condition for a moving lattice with an acceleration η equal to $\omega^2\mathcal{N}\lambda/4$ at the edge, is $m\eta\lambda \ll \hbar\frac{\omega_p^4}{\omega_r^3}$, where ω_p is the frequency difference between the first and the second band in the lattice. This puts a limit on how large the lattice can become $\mathcal{N} \ll \frac{\omega_p^4}{\omega^2\omega_r^2}$.

Hence, for $\nu = 1/2$ with a lattice filling fraction $\frac{N}{\mathcal{N}^2} \sim \frac{1}{8}$ and a typical recoil frequency $\omega_r = (2\pi)4$ kHz, one can enter the regime of fractional quantum Hall effect

by rotating the lattice at $\omega \sim (2\pi)650$ Hz. If a deep optical lattice is used e.g., $\omega_p \sim 10\omega_r$, the adiabaticity condition is easily satisfied for a lattice of size $\mathcal{N} \sim 1000$. The experimentally challenging part will, however, likely be to mitigate the instability of the lattice caused by the thickness of the beam and aberration of the lenses at the turning points i.e. near $\theta = \pi/4$.

2.7 Conclusions

An extended study of the realization of the fractional quantum Hall states in optical lattices has been presented. We showed that a Hamiltonian similar to that of a magnetic field for charged particles can be constructed for neutral ultra cold atoms and molecules confined in an optical lattice. By adding an onsite interaction for the case of $\nu = 1/2$, an energy gap develops between the ground state and the first excited state, which increases linearly as αU and saturates to its value in the hardcore limit $U \gg J$. We learned that the Laughlin wave function is a reliable description of the system for low flux densities $\alpha \lesssim 0.25$. However, for higher α's, the lattice structure becomes more pronounced and a better description of the system can be carried out by investigating the Chern number associated to the ground state manifold. The Chern number indicates that the system has topological order up to some critical flux density $\alpha_c \simeq 0.4$, where the properties of the ground state manifold starts to change. We have also studied $\nu = 1/4$, where compared to $\nu = 1/2$, the Laughlin wave function only describes the ground state for lower values of the flux $\alpha \lesssim 0.1$. We showed that a dipole-dipole interaction can enhance the gap and stabilize the system, and therefore make the ground state more experimentally realizable. Bragg

spectroscopy has been studied as a potential experimental tool to diagnose theses incompressible states.

Characterization of the ground state by evaluating the Chern number, developed in Sec. 2.3.4, can be generalized to other interesting many-body systems where the conventional overlap calculation fails to work. In particular, this method can be applied to ground states with non-Abelian statistics which are appealing candidates for fault-tolerant quantum computation.

Chapter 3

Photonic quantum transport in a nonlinear optical fiber

3.1 Introduction

Physical systems that enable single photons to interact strongly with each other are extremely valuable for many emerging applications. Such systems are expected to facilitate the construction of single-photon switches and transistors [23, 147, 37], networks for quantum information processing, and the realization of strongly correlated quantum systems using light [79, 70, 36]. One potential approach involves the use of high-finesse optical microcavities containing a small number of resonant atoms that mediate the interaction between photons [134, 23]. Their nonlinear properties are relatively straightforward to analyze or simulate because they involve very few degrees of freedom (*i.e.*, a single optical mode) [84, 69, 85]. Recently, an alternative approach has been suggested, involving the use of an ensemble of atoms coupled to propa-

gating photons in one-dimensional, tightly-confining optical waveguides [63, 93, 3]. Here, the nonlinearities are enhanced due to the transverse confinement of photons near the diffraction limit and the subsequent increase in the atom-photon interaction strength. The propagation of an optical field inside such a nonlinear medium (*e.g.*, systems obeying the quantum nonlinear Schrödinger equation) is expected to yield much richer effects than the case of an optical cavity due to the large number of spatial degrees of freedom available. Simultaneously, however, these degrees of freedom make analysis much more difficult and in part cause these systems to remain relatively unexplored [106, 90, 49, 150, 36]. We show that the multi-mode, quantum nature of the system plays an important role and results in phenomena that have no analogue in either single-mode cavities or classical nonlinear optics. It is interesting to note that similar low-dimensional, strongly interacting condensed matter systems are an active area of research, but most of this work is focused on closed systems close to the ground state or in thermal equilibrium [111, 103, 94, 127, 31]. On the other hand, as will be seen here, the relevant regime for photons often involves open systems and driven dynamics.

In this chapter, we develop a technique to study the quantum transport of a few photons inside a finite-length, strongly nonlinear waveguide where the light propagation is governed by the quantum nonlinear Schrödinger equation (NLSE), and apply this technique to study the operation of this system as a single-photon switch. In particular, we study the transmission and reflection properties of multi-photon fields from the system as well as higher-order correlation functions of these fields. We find that these correlations not only reflect the switching behavior, but reveal some aspects

of the rich structure associated with the spatial degrees of freedom inside the system, which allow photons to "organize" themselves. In the regime where an effectively repulsive interaction between photons is achieved, anti-bunching in the transmitted field is observed because of the switching effect, and is further reinforced by the tendency of photons to repel each other. In the attractive regime, either anti-bunching (due to switching) or bunching can occur. We show that the latter phenomenon is a clear signature of the creation of photonic bound states in the medium. Although we focus on a particular realization involving the propagation of light, our conclusions on quantum transport properties are quite general and valid for any bosonic system obeying the NLSE.

This chapter is organized as follows. In Sec. 3.2, we describe an atomic system whose interactions with an optical field can be manipulated using quantum optical techniques such that the light propagation obeys the quantum NLSE. This method relies upon electromagnetically induced transparency (EIT) to achieve resonantly enhanced optical nonlinearities with low propagation losses and the trapping of stationary light pulses using spatially modulated control fields. Before treating the nonlinear properties of the system, we first consider the linear case in Sec. 3.3, where it is shown that the light trapping technique leads to a field build-up inside the medium and a set of discrete transmission resonances, much like an optical cavity. In Sec. 3.4, we then investigate the nonlinear transport properties of the system such as reflectivity and transmittivity in the semi-classical limit, where the NLSE is treated as a simple complex differential equation. Here we find that the presence of the nonlinearity causes the transmission resonances to shift in an intensity-dependent way – the system be-

haves as a low-power, nonlinear optical switch, whose behavior does not depend on the sign of the nonlinear interaction. In Sec. 3.5, we present a full quantum formalism to treat the NLSE transport problem in the few-photon limit. Sec. 3.6 is dedicated to analytical solutions of the NLSE with open boundary conditions when the system is not driven. In particular, we generalize the Bethe ansatz technique to find the resonant modes of the system, which help to elucidate the dynamics in the case of the driven system. The driven system is studied in Sec. 3.7, where numerical solutions are presented along with a detailed study of the different regimes of behavior. In particular, we find that the correlation functions for the transmitted light do depend on the sign of the nonlinear interaction, in contrast to what the semi-classical calculations would suggest. We conclude in Sec. 3.8.

3.2 Model: Photonic NLSE in 1D waveguide

In this section, we consider the propagation of light inside an finite-length atomic medium under EIT conditions and with a Kerr nonlinearity. We also describe a technique that allows for these pulses of light to be trapped within the medium using an effective Bragg grating formed by additional counter-propagating optical control fields. We show that in the limit of large optical depth the evolution of the system can be described by a nonlinear Schrödinger equation.

Following Ref. [36], we consider an ensemble of atoms with the four-level internal structure shown in Fig. 3.1, which interact with counter-propagating quantum fields with slowly-varying envelopes $\hat{\mathcal{E}}_{\pm}$ inside an optical waveguide. These fields are coupled to a spin coherence between states $|a\rangle$ and $|c\rangle$ via two classical, counter-propagating

control fields with Rabi frequencies $\Omega_\pm$ largely detuned from the $|b\rangle \rightarrow |c\rangle$ transition. The case where the fields propagate only in one direction (say in the "+" direction) and where the detuning is zero corresponds to the usual EIT system, where the atomic medium becomes transparent to $\hat{\mathcal{E}}_+$ and the group velocity can be dramatically slowed due to coupling between the light and spin wave (so-called "dark-state polaritons") [54]. On the other hand, the presence of counter-propagating control fields creates an effective Bragg grating that causes the fields $\hat{\mathcal{E}}_\pm$ to scatter into each other. This can modify the photonic density of states and create a bandgap for the quantum fields. This photonic bandgap prevents a pulse of light from propagating and can be used to effectively trap the light inside the waveguide [8, 12]. The trapping phenomenon is crucial because it increases the time over which photons can interact inside the medium. The presence of an additional, far-detuned transition $|c\rangle \rightarrow |d\rangle$ that is coupled to $\hat{\mathcal{E}}_\pm$ leads to an intensity-dependent energy shift of level $|c\rangle$, which translates into a Kerr-type optical nonlinearity [144].

We now derive the evolution equations for the quantum fields. We assume that all atoms are initially in their ground states $|a\rangle$. To describe the quantum properties of the atomic polarization, we define collective, slowly-varying atomic operators, averaged over small but macroscopic volumes containing $N_z \gg 1$ particles at position z,

$$\hat{\sigma}_{\alpha\beta}(z,t) = \frac{1}{N_z}\sum_{i=1}^{N_z} |\alpha_i\rangle\langle\beta_i|. \tag{3.1}$$

The collective atomic operators obey the following commutation relations,

$$[\hat{\sigma}_{\alpha\beta}(z), \hat{\sigma}_{\mu\nu}(z')] = \frac{L}{N}\delta(z-z')(\delta_{\beta\mu}\hat{\sigma}_{\alpha\nu}(z) - \delta_{\alpha\nu}\hat{\sigma}_{\mu\beta}(z)), \tag{3.2}$$

while the forward and backward quantized probe fields in the z direction obey bosonic commutation relations (at equal time),

$$[\hat{\mathcal{E}}_+(z), \hat{\mathcal{E}}_+^\dagger(z')] = \delta(z - z'). \tag{3.3}$$

The Hamiltonian for this system in the rotating frame can be written as

$$\begin{aligned}
\hat{H} &= -\frac{N}{L}\int \Delta_1\hat{\sigma}_{bb}(z) + \Delta_3\hat{\sigma}_{cc}(z) + (\Delta_2+\Delta_3)\hat{\sigma}_{dd}(z) && (3.4)\\
&+ g\sqrt{2\pi}[(\hat{\sigma}_{ba}(z) + \hat{\sigma}_{dc}(z))(\hat{\mathcal{E}}_+ e^{ik_0 z} + \hat{\mathcal{E}}_- e^{-ik_0 z}) + H.c.] && (3.5)\\
&+ [\hat{\sigma}_{bc}(z)(\Omega_+ e^{ik_c z} + \Omega_- e^{-ik_c z}) + H.c.]dz, && (3.6)
\end{aligned}$$

where $g = \mu\sqrt{\frac{\omega_{ab}}{4\pi\hbar\epsilon_0 A}}$ is the atom-field coupling strength, μ is the atomic dipole matrix element, and A is the effective area of the waveguide modes. For simplicity, we have assumed that the transitions a-b and c-d have identical coupling strengths g and have ignored transverse variation in the fields. The terms Δ_i denote the light field-atomic transition detunings as shown in Fig. 3.1(a). k_c is the wavevector of the control fields, while $k_0 = n_b\omega_{ab}/c$ characterizes the fast-varying component of the quantum field and n_b is the background refractive index. We also define $n_0 = N/L$ as the linear density of atoms in the z direction, and $v_g = c\Omega^2/2\pi g^2 n_0$ as the group velocity that the quantum fields would have if they were not trapped by the Bragg grating (we will specifically be interested in the situation where $\Omega_+ = \Omega_- = \Omega$). Following Ref. [54], we can define dark-state polariton operators that describe the collective excitation of field and atomic spin wave, which in the limit of slow group velocity $\eta = \frac{c}{2v_g} \gg 1$ are given by $\hat{\Psi}_\pm = \frac{g\sqrt{2\pi n_0}}{\Omega_\pm}\hat{\mathcal{E}}_\pm$. These operators obey bosonic commutation relations $[\hat{\Psi}_\pm(z), \hat{\Psi}_\pm^\dagger(z')] = \delta(z-z')$. The definition of the polariton operators specifies that the

photon flux entering the system at its boundary is equal to the rate that polaritons are created at the boundary inside the system – *i.e.*, $c\langle\hat{\mathcal{E}}_+^\dagger\hat{\mathcal{E}}_+\rangle = v_g\langle\hat{\Psi}_+^\dagger\hat{\Psi}_+\rangle$. In other words, excitations enter (and leave) the system as photons with velocity c, but inside the waveguide they are immediately converted into polariton excitations with group velocity v_g. Field correlations will also be mapped in a similar fashion – in particular, correlation functions that we calculate for polaritons at the end of the waveguide $z = L$ will also hold for the photons transmitted from the system. The total number of polaritons in the system is given by $\mathcal{N}_{pol.} = \int\langle\hat{\Psi}_+^\dagger\hat{\Psi}_+\rangle + \langle\hat{\Psi}_-^\dagger\hat{\Psi}_-\rangle dz$. The optical fields coupled to the atomic coherences of both the $a-b$ and $c-d$ transitions are governed by Maxwell-Bloch evolution equations,

$$\left(\frac{\partial}{\partial t} \pm c\frac{\partial}{\partial z}\right)\hat{\mathcal{E}}_\pm(z,t) = ig\sqrt{2\pi}n_0(\hat{\sigma}_{ab} + \hat{\sigma}_{cd}). \tag{3.7}$$

Similar to the photonic operators, the atomic coherences can also be written in terms of slowly-varying components,

$$\hat{\sigma}_{ab} = \hat{\sigma}_{ab}^+ e^{ik_0 z} + \hat{\sigma}_{ab}^- e^{-ik_0 z}, \tag{3.8}$$

$$\hat{\sigma}_{cd} = \hat{\sigma}_{cd}^+ e^{ik_0 z} + \hat{\sigma}_{cd}^- e^{-ik_0 z}. \tag{3.9}$$

We note that higher spatial orders of the coherence are thus neglected. In practice, these higher orders are destroyed due to atomic motion and collisions as atoms travel distances greater than an optical wavelength during the typical time of the experiment [183]. Alternatively, one can use dual-V atomic systems that do not require this approximation [182] (see also Chapter 4).

In the weak excitation limit ($\hat{\sigma}_{aa} \simeq 1$), the population in the excited state $|b\rangle$ can

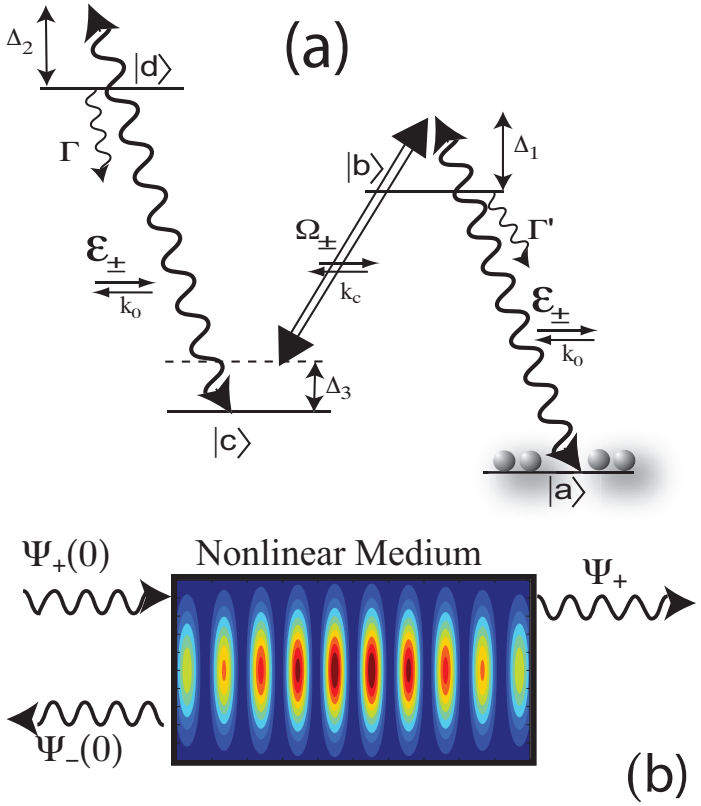

Figure 3.1: (a) Four-level atomic system for creating strong nonlinearity. Counter-propagating control fields modulate the EIT for the forward- and backward-propagating probe, and $|c\rangle \rightarrow |d\rangle$ transition gives rise to a Kerr-type nonlinearity. (b) The light is confined in the transverse direction due to the presence of the waveguide and experiences an effective Bragg grating due to the presence of the counter-propagating light.

be neglected, $\langle\hat{\sigma}_{bb}\rangle\approx 0$. In this limit, the evolution of the atomic coherence is given by

$$\dot{\hat{\sigma}}_{ab}^{\pm} = (i\Delta_1 - \Gamma/2)\hat{\sigma}_{ab}^{\pm} + ig\sqrt{2\pi}\hat{\mathcal{E}}_{\pm} + i\Omega_{\pm}\hat{\sigma}_{ac}e^{\pm i\Delta kz} \tag{3.10}$$

where $\Delta k = k_c - k_0$ and Γ is the total spontaneous emission rate of state b (for simplicity we also assume that state d has an equal spontaneous emission rate). In the adiabatic limit where $g\sqrt{2\pi}\langle\hat{\sigma}_{ac}\hat{\mathcal{E}}_{\pm}\rangle \ll \Gamma$, the coherence $\hat{\sigma}_{ad}$ can be approximated by

$$\hat{\sigma}_{ad} \simeq \frac{g\sqrt{2\pi}\hat{\sigma}_{ac}}{-\Delta_2 - \Delta_3 - i\frac{\Gamma}{2}}(\hat{\mathcal{E}}_{+}e^{+ik_0z} + \hat{\mathcal{E}}_{-}e^{-ik_0z}). \tag{3.11}$$

Therefore, the spin wave evolution can be written as,

$$\dot{\hat{\sigma}}_{ac} = i\Delta_3\hat{\sigma}_{ac} + \frac{2\pi ig^2}{-\Delta_2 - \Delta_3 - i\frac{\Gamma}{2}}(\hat{\mathcal{E}}_{+}^{\dagger}\hat{\mathcal{E}}_{+} + \hat{\mathcal{E}}_{-}^{\dagger}\hat{\mathcal{E}}_{-})\hat{\sigma}_{ac} \tag{3.12}$$

$$+ i(\hat{\sigma}_{ab}^{+}\Omega_{+}^{*}e^{-i\Delta kz} + \hat{\sigma}_{ab}^{-}\Omega_{-}^{*}e^{i\Delta kz}) \tag{3.13}$$

We now consider the situation where $\Omega_+ = \Omega_- = \Omega$, such that the counter-propagating control fields form a standing wave. In the adiabatic limit [54], and keeping all terms up to third order in the quantum fields, substituting these results into Eq. (3.7) and simplifying yields the following evolution equations for the dark-state polariton operators,

$$(c\partial_z + \partial_t)\hat{\Psi}_{+} = -\frac{\xi}{2}(\hat{\Psi}_{+} - \hat{\Psi}_{-}) - \frac{\eta}{2}\partial_t(\hat{\Psi}_{+} + \hat{\Psi}_{-}) \tag{3.14}$$

$$- i\Delta_n\left[(\hat{\Psi}_{+}^{\dagger}\hat{\Psi}_{+} + \hat{\Psi}_{-}^{\dagger}\hat{\Psi}_{-})(\hat{\Psi}_{+} + \hat{\Psi}_{-}) + (\hat{\Psi}_{+}^{\dagger} + \hat{\Psi}_{-}^{\dagger})(\hat{\Psi}_{+} + \hat{\Psi}_{-})\hat{\Psi}_{+}\right]$$

$$(-c\partial_z + \partial_t)\hat{\Psi}_{-} = +\frac{\xi}{2}(\hat{\Psi}_{+} - \hat{\Psi}_{-}) - \frac{\eta}{2}\partial_t(\hat{\Psi}_{+} + \hat{\Psi}_{-}) \tag{3.15}$$

$$- i\Delta_n\left[(\hat{\Psi}_{+}^{\dagger}\hat{\Psi}_{+} + \hat{\Psi}_{-}^{\dagger}\hat{\Psi}_{-})(\hat{\Psi}_{+} + \hat{\Psi}_{-}) + (\hat{\Psi}_{+}^{\dagger} + \hat{\Psi}_{-}^{\dagger})(\hat{\Psi}_{+} + \hat{\Psi}_{-})\hat{\Psi}_{-}\right],$$

where the linear dispersion is characterized by $\xi = \frac{2\pi g^2 n_0}{-i\Delta_1+\Gamma/2}$. The nonlinearity coefficient is given by the single photon AC-Stark shift: $\Delta_n = \frac{\pi g^2}{2(\Delta_2+i\Gamma/2)}$. We note that the wave-vector mismatch Δk has been compensated for by a small extra two-photon detuning equal to $(-\Delta k c/\eta)$.

The above equations describe the evolution of two coupled modes. It is convenient to re-write these equations in terms of the anti-symmetric and symmetric combinations $A = (\Psi_+ - \Psi_-)/\sqrt{2}$ and $S = (\Psi_+ + \Psi_-)/\sqrt{2}$. For large optical depths, we then find that the anti-symmetric mode adiabatically follows the symmetric mode, $A \simeq -(c/\xi)\partial_z S$. In this limit, the evolution of the whole system can be described by a single nonlinear Schrödinger equation,

$$\eta\frac{\partial}{\partial t}S - \frac{c^2}{\xi}\frac{\partial^2}{\partial z^2}S + 8i\Delta_n S^\dagger S^2 = 0. \tag{3.16}$$

Physically, the coupling between $\hat{\Psi}_\pm$ induced by the Bragg grating causes them to no longer behave independently, much like the two counter-propagating components of an optical cavity mode. We can write the above equation in dimensionless units by introducing a characteristic length scale $L_{coh} = c/|\mathrm{Im}[\xi]| = \mathrm{c}(\Delta_1^2 + \Gamma^2/4)/2\pi\mathrm{g}^2\mathrm{n}_0|\Delta_1|$ and time scale $t_{coh} = \eta/|\mathrm{Im}[\xi]| = (\Delta_1^2 + \Gamma^2/4)/2\Omega^2|\Delta_1|$. L_{coh} corresponds to the length over which the field acquires a π-phase in the propagation. The dimensionless NLSE then reads

$$i\frac{\partial\tilde{S}}{\partial\tau} = -\frac{1}{2m}\frac{\partial^2\tilde{S}}{\partial\tilde{z}^2} + 2\kappa\tilde{S}^\dagger\tilde{S}^2, \tag{3.17}$$

where for $\Delta_1 < 0$, the effective mass is $m = \frac{1}{2}(1 + i\frac{\Gamma}{2|\Delta_1|})$ and the nonlinearity coefficient is $\kappa = \frac{2\Delta_n}{c} = \frac{\pi g^2/c}{\Delta_2+i\Gamma/2}$. Note that $\tilde{\Psi}_\pm(z,t)$ and $\tilde{S}(z,t)$ are also in units of

$\sqrt{L_{coh}^{-1}}$, such that $[\tilde{S}(\tilde{z}), \tilde{S}^{\dagger}(\tilde{z}')] = \delta(\tilde{z} - \tilde{z}')$. For simplicity, we omit tilde superscripts in the following. We can also write the nonlinear coefficient as $\kappa = \frac{\Gamma_{1D}}{4(\Delta_2 + i\Gamma/2)}$, where we have identified $\Gamma_{1D} = 4\pi g^2/c$ as the spontaneous emission rate into the guided modes ($\Gamma_{1D} \leq \Gamma$). Note that in this notation, the anti-symmetric combination of forward and backward polaritons is given by $A \simeq -i/2m\partial_z S \simeq -i\partial_z S$.

3.3 Linear case: Stationary light enhancement

In this section, we investigate the linear transmission properties of the signal field as a function of its frequency. The control field leads to a Bragg grating that couples the forward and backward components of the signal field together. We show that the system therefore acts as an effective cavity whose *finesse* is determined by the optical density of the atomic medium.

For the linear case ($\kappa = 0$), it is sufficient to treat the forward and backward field operators as two complex numbers. In the slow light regime ($\eta \gg 1$), the coupled mode equations (Eqs. 3.16) can be written in the Fourier domain, with our dimensionless units, as

$$\partial_z \Phi_+ = \frac{i}{2}\delta(\Phi_+ + \Phi_-) + im(\Phi_+ - \Phi_-) \tag{3.18}$$

$$-\partial_z \Phi_- = \frac{i}{2}\delta(\Phi_+ + \Phi_-) - im(\Phi_+ - \Phi_-), \tag{3.19}$$

where $\Psi_+(z,\tau) = \Phi_+(z,\delta)e^{-i\delta\tau}$ and $\Psi_-(z,\tau) = \Phi_-(z,\delta)e^{-i\delta\tau}$and δ is the dimensionless two-photon detuning $\delta = \Delta_3 t_{coh}$. We specify that a classical field $\Phi_+(z=0,\delta) = \alpha$ enters the system at $z = 0$ with no input at the other end of the system ($z = d$), $\Phi_-(z = d, \delta) = 0$, as shown in Fig. 3.1(b). We note that $d = L/L_{coh}$ is the length

of the system in units of the coherence length introduced earlier. For negligible losses ($|\Delta_1| \gg \Gamma$) and $\Delta_1 < 0$, $m \simeq 1/2$ and the profile of forward-going polaritons inside the system will look like:

$$\frac{\Phi_+(z,\delta)}{\alpha} = \frac{2i\sqrt{\delta}\cos[(d-z)\sqrt{\delta}] + (1+\delta)\sin[(d-z)\sqrt{\delta}]}{2i\sqrt{\delta}\cos[d\sqrt{\delta}] + (1+\delta)\sin[d\sqrt{\delta}]}. \tag{3.20}$$

Therefore, for a system with fixed length d, the transmission coefficient varies with the frequency of the incident field, with transmission resonances occurring at the values $\sqrt{\delta_0}d = n\pi$ (n is an integer). At these resonances, the system transmittance is equal to one ($|\Phi(d,\delta)| = |\Phi(0,\delta)|$) and a field build-up occurs inside the medium with a bell-shaped profile, similar to a cavity mode (see Fig. 3.2). The positions of these resonances (quadratic in n) reflect the quadratic dispersion in Eq. (3.17). Note that in real units, the positions of the resonances will depend on the amplitude of the control field, since $\Delta_3 = \delta\frac{|\Delta_1|}{2|\Omega|^2}$. In the limit of a coherent optically large system ($d \gg 1$), the intensity amplification in the middle of the system is equal to $(d/2\pi)^2$ for the first resonance. In other words, the Bragg scattering creates a cavity with an effective finesse proportional to the square of the coherent length of the system ($\mathcal{F} \propto d^2$).

We now derive the width of the first transmission resonance. For small variations $\delta_0 \pm \delta_b$ around the resonance frequency, we can write

$$\frac{\Phi_+(d)}{\Phi_+(0)} = -1 - \frac{i\pi}{4\delta_0^{3/2}}\delta_b + \frac{\pi^2}{16\delta_0^3}\delta_b^2 + O(\delta_b^3). \tag{3.21}$$

Therefore, the width of the resonances (say where it drops by half) is given by

$$2\delta_b \simeq \delta_0^{3/2} = (\frac{\pi}{d})^3. \tag{3.22}$$

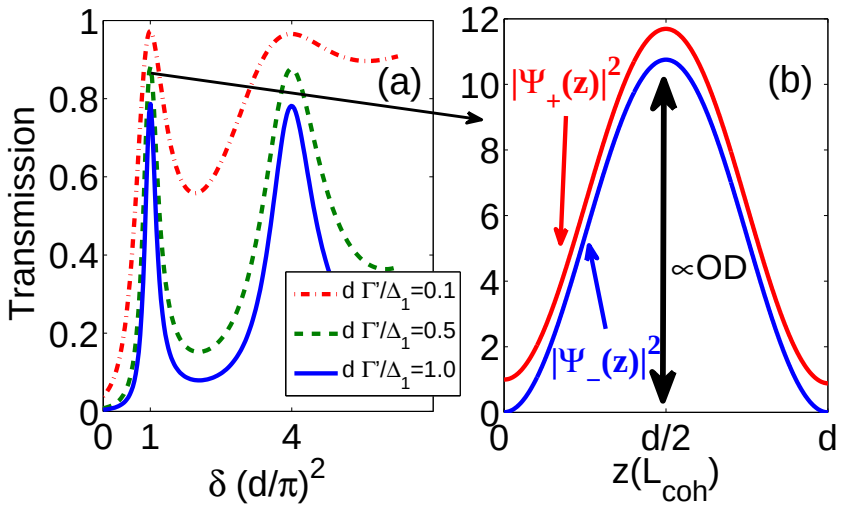

Figure 3.2: Linear case: (a) Transmittivtiy as a function of two-photon detuning. Transmission peaks are attenuated because of linear loss on $|a\rangle \rightarrow |b\rangle$ transition which are plotted for three different loss rates $\beta = d\,\Gamma/\Delta_1$. (b) When the system is tuned on a transmission resonance ($\sqrt{\delta_0}d = n\pi$), the field inside the medium is amplified.

We have kept terms up to second order in δ_b, since the first order term does not give a decreasing correction to the transmittance. While we have previously ignored absorption (as determined by the real part of ξ), we can estimate that its effect is to attenuate the probe beam transmission by a factor $\beta = d\,\Gamma/|\Delta_1|$. As it is shown in Fig. 3.3, for large optical densities, β can fully characterize the transmission coefficient on resonance ($\delta = \delta_0$). In particular, for a fixed β, the resonant transmission is constant for any large optical density. In other words, since the optical depth of the system is given by $OD = d\frac{|\Delta_1|}{\Gamma}$, the transmittivity of the system remains constant for any OD with the choice $|\Delta_1| = \Gamma\sqrt{OD/\beta}$. In this case the effective cavity finesse for the system becomes proportional to the optical density, *i.e.*, $\mathcal{F} \propto OD$.

The total number of polaritons in the system can be estimated by,

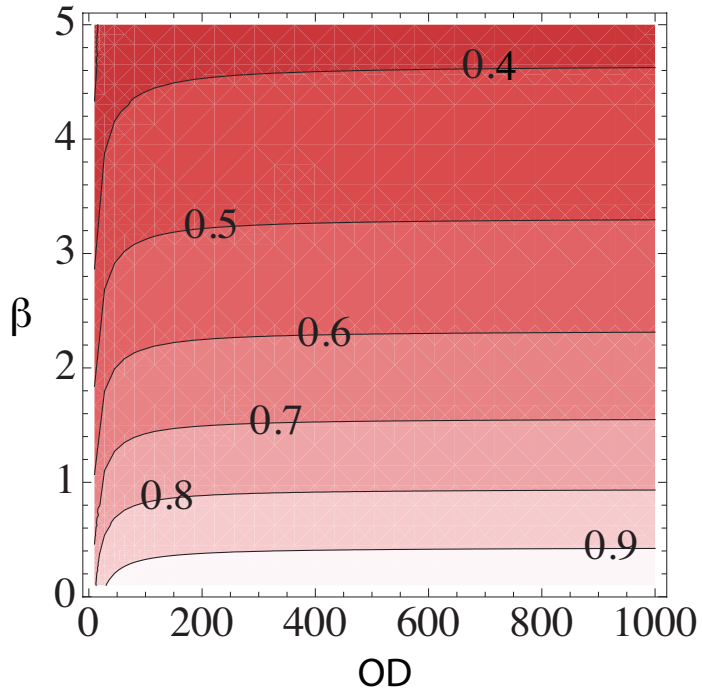

Figure 3.3: For large optical densities, the transmission on resonance ($\delta = \delta_0$), only depends on $\beta = OD\left(\frac{\Gamma}{\Delta_1|}\right)^2$.

$$\mathcal{N}_{pol} = \int_0^d |\Phi_+(z)|^2 + |\Phi_-(z)|^2 dz = \frac{(d^2+\pi^2)^2}{4d\pi^2}|\Phi_+(0)|^2 \simeq \frac{d^3}{4\pi^2}|\Phi_+(0)|^2. \quad (3.23)$$

This again shows that the polaritons experience many round trips inside the system before exiting. In particular, if we define the average intensity inside the medium as $|\Phi_+^{ave}|^2 = \mathcal{N}_{pol}/d$, then we readily observe that the intensity of the polariton field is amplified inside the medium by the square of the system size ($|\Phi_+^{ave}|^2/|\Phi_+(0)|^2 = (d/2\pi)^2$) – *i.e.* the finesse is proportional to the optical density (OD).

The original proposal for observing an enhanced Kerr nonlinearity with a four-level atomic system using EIT makes use of an optical cavity to enhance the nonlinearity [84]. However, as pointed out in Ref. [69], the scheme suffers from some inaccuracies in the effective Hamiltonian. More specifically, in Ref. [84], the effective Hamiltonian was evaluated at the center of the EIT transparency window. However, in practice, EIT dramatically decreases the cavity linewidth because of the large dispersion that accompanies the vanishing absorption [115]; this causes photons at frequencies slightly shifted from the central frequency to be switched out of the cavity. This leads to an extremely small allowable bandwidth for the incoming photons [69] and was neglected in the original analysis. We emphasize that the analysis presented here takes into account the dispersive properties of the medium, as we have included the field dynamics up to second order in the detuning from resonance (this accounts for the effective mass of the photons in our system). We verify the consistency of this derivation in Appendix A by solving the linear system including full susceptibilities. It is shown that the results are consistent near the two-photon resonance (*i.e.*, frequencies around $\delta = 0$).

3.4 Semi-classical nonlinear case

3.4.1 Dispersive regime

In this section, in contrast to the previous section, we include the nonlinear term in the evolution equations to investigate its effect in the semi-classical limit (where the fields are still treated as complex numbers). In this picture, the effect of nonlinearity causes the transmission peaks to shift in frequency in an intensity-dependent way to the left or right depending on the sign of the nonlinearity coefficient κ. We show that when $|\kappa|OD \gg 1$, the magnitude of the shift is large even at intensities corresponding to that of a single photon. In this regime, we expect that the system can act as a single-photon switch and that signatures of quantum transport will become apparent (the quantum treatment is described in Sec.3.5).

Because of the self-phase modulation term in the evolution equations (Eqs. 3.16), the forward and backward fields acquire a phase shift proportional to their intensity. Moreover, due to the conjugate-phase modulation terms, each field undergo an extra phase shift proportional the intensity of the other field. Classically, this yields a frequency shift in the transmission spectrum when the nonlinearity is small. The shift in the transmission peak can be approximated by $\Delta\delta \simeq 2\kappa|\Phi_+^{ave}|^2$ where $|\Phi_+^{ave}|^2 \simeq \frac{d^2}{4\pi^2}|\Phi_+(0)|^2$ is the average intensity of polaritons in the system. Suppose that we want the nonlinearity to be strong enough to shift the transmission peaks at least by half of their widths, $\Delta\delta \simeq \frac{1}{2}\delta^{3/2}$. Then, from Eq.(3.22) this condition can be written as

$$|\Phi_+^{\mathrm{cr}}(0)|^2 = \left(\frac{\pi}{d}\right)^5 \frac{1}{|\kappa|} \tag{3.24}$$

On the other hand, according to Eq.(3.23), we can write this condition in terms of the critical number of polaritons inside the system,

$$\mathcal{N}_{pol}^{\mathrm{cr}} = \frac{\pi^3}{4d^2\kappa}. \tag{3.25}$$

Since the nonlinearity coefficient is given by the light shift on the $|c\rangle \rightarrow |d\rangle$ transition, in the dispersive regime ($\Delta_2 \gg \Gamma$), we have $\kappa = \frac{1}{4}\frac{\Gamma_{1D}}{\Gamma}\frac{\Gamma}{\Delta_2}$. Thus, we expect to have substantial nonlinearities at the level of one polariton (*i.e.*, one incoming photon), $\mathcal{N}_{pol.}^{\mathrm{cr.}} = 1$, if

$$d^2 = \pi^3 \frac{\Gamma}{\Gamma_{1D}}\frac{\Delta_2}{\Gamma} \tag{3.26}$$

where Γ_{1D} is the rate of spontaneous emission rate into the guided modes. Strictly speaking, note that a single photon cannot actually have a nonlinear phase shift (as correctly derived later using a fully quantum picture); however, we can still use the results of this semiclassical calculation to qualitatively understand the relevant physics.

We can also rewrite the above condition in term of the optical density ($OD = d\frac{\Delta_1}{\Gamma}$) needed in the system. From the linear case, we know that an optimal detuning, for a transmission of 90%, should satisfy $d\frac{\Gamma}{\Delta_1} \sim 0.5$. Then, Eq. (3.26) can be written as

$$OD = 2\pi^3 \frac{\Gamma}{\Gamma_{1D}}\frac{\Delta_2}{\Gamma}. \tag{3.27}$$

Taking for example a system where $\Delta_2 \sim 5\Gamma$ and $\frac{\Gamma_{1D}}{\Gamma} \sim 0.1$, nonlinearities at a few-photon level can be observed for an optical density OD $\simeq 6200$.

First, let us consider the case of positive κ. In Fig. 3.4, we observe that at large enough optical density, the system can have very different transmission spectra for

low and *high* intensities that classically correspond to having one and two polaritons (photons) inside the system, respectively. Although we have ignored the quantization of photons in this section, we can develop some insight into the transmission properties of one- and two-photon states. Loosely speaking, if we fix the input field frequency to lie at the one-photon (linear) transmission peak (δ_0), the system would block the transmission of incident two-photon states. More realistically, suppose we drive the system with a weak classical field (coherent state), which can be well-approximated as containing only zero, one, and two-photon components. We then expect that the one-photon component will be transmitted through the system, while the two-photon component will be reflected, leading to anti-bunching of the transmitted light. We note that the general spirit of this conclusion is sound; however, the correct description of the system is achieved by taking into account the quantization of photons which is presented in the next sections.

A similar analysis holds for the case of negative κ. Note that the sign of κ depends on the detuning of the photonic field from the atomic transition $|c\rangle \rightarrow |d\rangle$, which can easily be adjusted in an experiment. This is in contrast to conventional nonlinear optical fibers and nonlinear crystals, where the nonlinearity coefficient is fixed both in magnitude and sign. We find that a negative nonlinearity simply shifts the transmission spectrum in the opposite direction as for the positive case, as shown in Fig. 3.5, but all other conclusions remain the same. In particular, we would expect anti-bunching to occur for this case as well, when a weak coherent field is incident with its frequency fixed to the linear transmission resonance. Surprisingly, the quantum treatment (Sec.3.7), shows that the above conclusion is wrong and system behaves

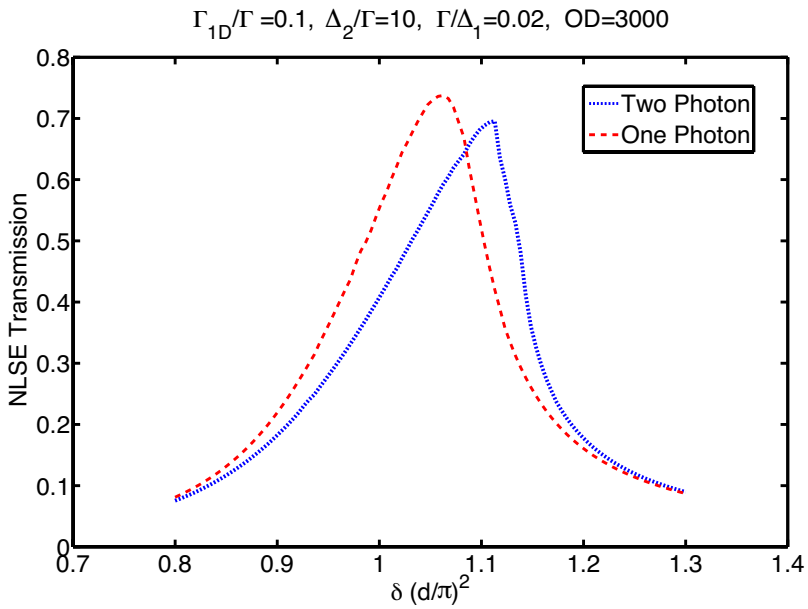

Figure 3.4: Due to nonlinearity, in the perturbative limit, the transmission spectrum shifts for different intensities. The integrated intensities inside the system is related to the number of present field quanta. OD=3000

very differently for negative nonlinearity. We show that this difference in behavior can be attributed to the presence of additional eigenstates (photonic bound states) in the medium and their excitation by the incident field.

For even larger nonlinearities or intensities, the transmission spectrum can become even more skewed and exhibit bistable behavior, as similarly found in Ref. [135] in the context of transport of Bose-Einstein condensates in one dimension. There, the classical NLSE (Gross-Pitaevskii equation) was solved to find the mean-field transport properties of a condensate scattering off a potential barrier.

Instead of considering the switching effect as a function of number of photons inside the medium, we can also consider the number of photons that need to be sent into the system. Clearly, to have a well-defined transmission amplitude without substantial pulse distortion, the incident pulse must be long enough so that it fits

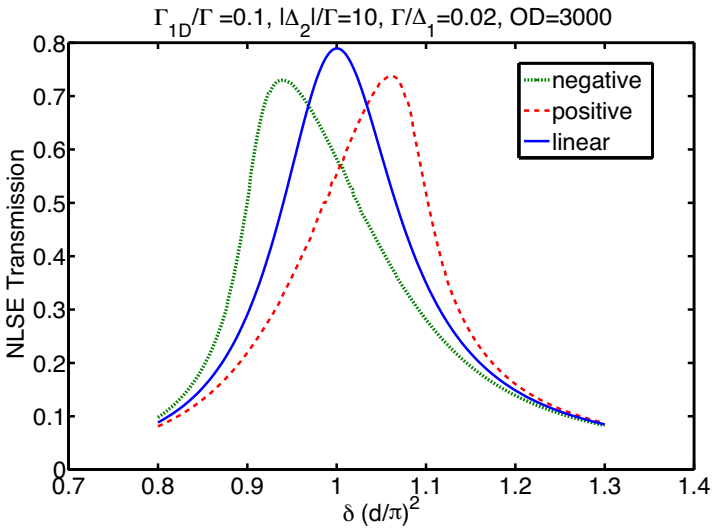

Figure 3.5: For positive (negative) nonlinearity, in the perturbative limit, the transmission spectrum shifts to the right (left) of linear transmission spectrum (solid line), which is shown in dotted line (dashed line). The incoming intensity corresponds to one-photon in the system.

within the bandwidth of the system resonance, as given in Eq. (3.22). To be specific, we consider an input pulse whose duration is equal to the inverse of the bandwidth, $t_b = (\frac{d}{\pi})^3 t_{coh}$. We can relate the number of incoming photons to an average incident intensity:

$$|\Phi_+(0)|^2 = \mathcal{N}_{pol.} \frac{t_b}{t_{coh}} = \frac{\mathcal{N}_{pol.}}{(d/\pi)^3} \tag{3.28}$$

Now, since the number of incident photons and incoming polaritons are the same, we can assign an average amplitude to any incoming photons number by Eq. (3.28), and evaluate the transmission. Hence, we can evaluate the number of incident photons needed to observe a significant nonlinearity and saturate the system. Fig. 3.6 shows the transmittivity of the nonlinear system as a function of number of photons in the incoming wavepacket. We observe that for high optical densities ($OD > 1000$), the

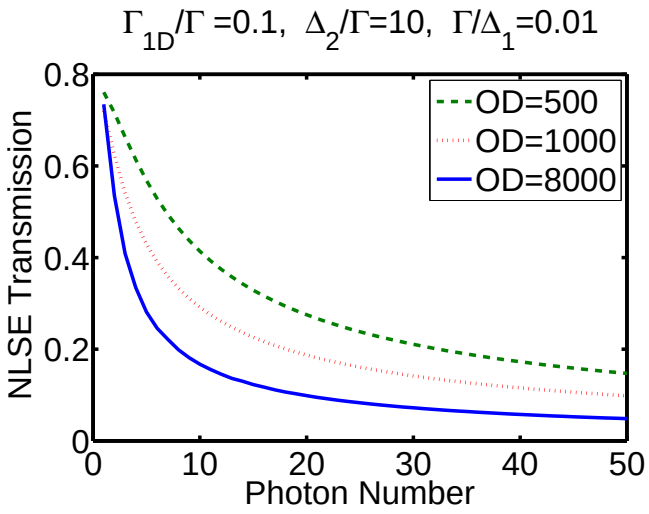

Figure 3.6: Transmission vs. the number of incident photons. For each OD, Γ/Δ_1 is chosen so that the system exhibit a similar transmission for one photon.

transmittivity drops as the number of incoming photons increases and the system gets saturated for even few photons.

3.4.2 Dissipative Regime

In this section, we investigate the system in the presence of nonlinear absorption, where κ is imaginary. The nonlinear dispersion of the previous case can simply be turned into nonlinear absorption by setting the nonlinear detuning to zero ($\Delta_2 = 0,\ \kappa = \frac{\Gamma_{1D}}{2i\Gamma}$). In the quantum picture, this term does not affect the one-photon state, while two-photon states can be absorbed by experiencing three atomic transitions, $|a\rangle \rightarrow |b\rangle \rightarrow |c \rightarrow |d\rangle$, and subsequently being scattered from excited state $|d\rangle$ [78]. We consider the quantum treatment of absorption later and first study the semiclassical limit here.

The presence of nonlinear absorption suppresses the transmission of multi-photon

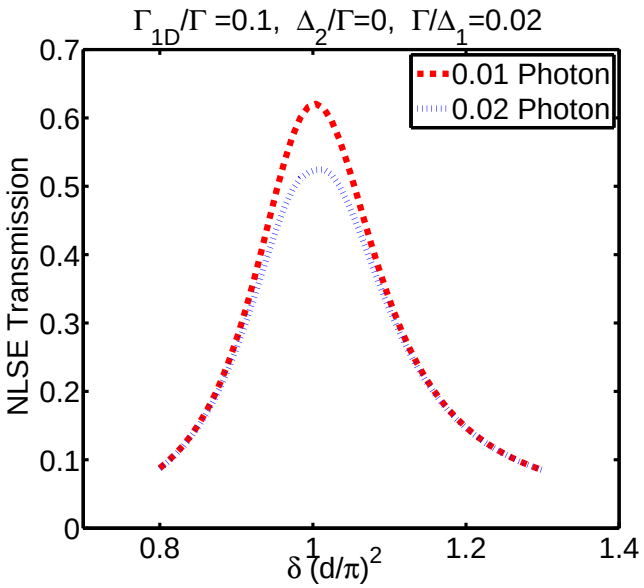

Figure 3.7: Due to nonlinearity absorption, the transmission is suppressed for higher intensities. The integrated intensities inside the system is related to the number of present field quanta. OD=3000

states through the medium by causing them to decay. This suppression becomes stronger for higher intensities as shown in Fig. 3.7. We have used the same optical density (OD) and 1D confinement (Γ_{1D}/Γ) as in Fig. 3.4. We observe that the effects of nonlinear absorption are stronger than that of nonlinear dispersion studied in Sec.3.4.1, since it occurs at resonance ($\Delta_2 = 0$) where the atomic response is strongest. It is thus possible to observe its effect at even lower intensities, corresponding to effective photon numbers two orders of magnitude smaller than the dispersive case. Much like the dispersive case, the suppression of transmission of multi-photon components should yield anti-bunching in the transmitted field. In this case, however, these components are simply lost from the system (as opposed to showing up as a bunched reflected field).

3.5 Quantum nonlinear formalism: Few-photon limit

In this section, we describe a quantum mechanical approach that enables one to solve the problem of quantum transport of a small number of photons through the finite, nonlinear system described in Sec.3.2. This few-photon number limit is of particular interest since it captures the physics of single-photon switching.

We find it convenient to study the dynamics of the system of photons in the Schrödinger picture, where one can explicitly solve for the few-body wave functions. This approach is made possible by truncating the Hilbert space so that only subspaces with n_{max} photons are less are present. In the following, we will consider the case where $n_{max} = 2$, although our analysis can be easily extended to cover any other value. This truncation is justified when the incident coherent field is sufficiently weak that the average photon number is much smaller than one inside the system ($|\alpha_0|^2 d^3 \ll 1$, where α_0 is the amplitude of the incoming field). Thus, we can write the general state of the system as:

$$|\psi(t)\rangle \simeq \int dz_1 dz_2 \phi(z_1, z_2, t) S^\dagger(z_1) S^\dagger(z_2)|0\rangle + \int dz \theta(z, t) S^\dagger(z)|0\rangle + \epsilon|0\rangle. \quad (3.29)$$

The first, the second and the third term correspond to two-photon, one-photon and vacuum state, respectively. Note that because of bosonic symmetrization, $\phi(z_1, z_2, t)$ should be symmetric in z_1 and z_2. This formalism allows us to capture any non-trivial spatial order between photons in our system (*e.g.*, the de-localization of two photons as represented by the off-diagonal terms in $\phi(z_1, z_2)$). Since the NLSE Hamiltonian

commutes with the field number operator $\hat{S}^\dagger \hat{S}$, manifolds with different field quanta are decoupled from each other inside the medium. Therefore, the evolution for the one-photon and two-photon manifolds under the NLSE Hamiltonian can be written as,

$$i\frac{\partial}{\partial t}\phi(z_1, z_2, t) = -\frac{1}{2m}\left(\frac{\partial^2}{\partial z_1^2} + \frac{\partial^2}{\partial z_2^2}\right)\phi(z_1, z_2, t) + 2\kappa\phi(z_1, z_2, t)\delta(z_1 - z_2) \tag{3.30}$$

$$i\frac{\partial}{\partial t}\theta(z, t) = -\frac{1}{2m}\frac{\partial^2}{\partial z^2}\theta(z, t). \tag{3.31}$$

However, the system is driven with an input field at $z = 0$, which allows different manifolds to be coupled at the boundaries. This is analogous to fiber soliton experiments where a classical input field mixes quantum solitons with different photon numbers [48]. In particular, for a classical input field,

$$\hat{\Psi}_+(z = 0)|\psi(t)\rangle = \alpha(t)|\psi(t)\rangle \tag{3.32}$$

$$\hat{\Psi}_-(z = d)|\psi(t)\rangle = 0|\psi(t)\rangle, \tag{3.33}$$

which corresponds to a coherent state with (possibly time-dependent) amplitude $\alpha(t)$ as an input at $z = 0$, and no input (*i.e.*, vacuum) at $z = d$. Since we specify that the input coherent field is weak ($\alpha \ll 1$), the amplitude of the vacuum state is almost equal to one ($\epsilon \simeq 1$). The annihilation operator in these equations reduces the photon number on the left-hand side by one. Thus, such boundary conditions relate different photon subspaces whose photon number differ by one, *e.g.* the two-photon and one-photon wavefunctions. In the adiabatic limit where the anti-symmetric part of the field ($A = (\hat{\Psi}_+ - \hat{\Psi}_-)/\sqrt{2}$) follows the symmetric part ($S = (\hat{\Psi}_+ + \hat{\Psi}_-)/\sqrt{2}$),

we have

$$\Psi_+ = \frac{1}{\sqrt{2}}(S - \frac{i}{2m}\partial_z S) \quad , \quad \Psi_- = \frac{1}{\sqrt{2}}(S + \frac{i}{2m}\partial_z S). \tag{3.34}$$

Therefore the boundary conditions at $z = 0$ can be re-written as

$$\frac{1}{\sqrt{2}}\int dz_1 dz_2 \, [S - \frac{i}{2m}\partial_z S]_{z=0} S^\dagger(z_1) S^\dagger(z_2)\phi(z_1, z_2, t)|0\rangle = \alpha \int dz \theta(z,t) S^\dagger|0\rangle, \tag{3.35}$$

$$\frac{1}{\sqrt{2}}\int dz \, [S - \frac{i}{2m}\partial_z S]_{z=0} S^\dagger(z)\theta(z,t)|0\rangle = \alpha|0\rangle. \tag{3.36}$$

Using the identity $\int [\partial_z S(z), S^\dagger(z')] f(z') dz' = \partial_z f(z)$, the boundary conditions on the one-photon and two-photon wave functions can be written as:

$$\phi(z_1 = 0, z_2, t) - \frac{i}{2m}\partial^{(1)}\phi(z_1, z_2, t)|_{z_1=0} = \frac{1}{\sqrt{2}}\alpha\theta(z_2, t) \tag{3.37}$$

$$\theta(z = 0, t) - \frac{i}{2m}\partial_z\theta(z = 0, t) = \sqrt{2}\alpha, \tag{3.38}$$

where $\partial^{(1)}$ acts on the first parameter. This type of open boundary condition is known as a Robin or mixed boundary condition, which involves a combination of both the function and its derivative. In the present case, the open boundary conditions allow particles to freely *enter* and *leave* the system. We emphasize that this process is noise-less, in that the loss of population from the interior of our system is related by our boundary condition equations to the flow of particle current through the system boundaries. This is in contrast to an optical cavity, for instance, where photons inside the cavity leak *dissipatively* into the environment [60]. Similarly the boundary condition at $z = d$ reads

$$\phi(d, z, t) + \frac{i}{2m}\partial^{(1)}\phi(d, z, t) = 0 \quad , \quad \theta(d, t) + \frac{i}{2m}\partial_z\theta(d, t) = 0. \tag{3.39}$$

Given the boundary conditions and the equations of motion in the interior, we can completely solve for the photon wavefunctions.

Once the wavefunctions are determined, it is possible to determine the intensity profile as well as any other correlation function for the photons. For example, the intensity of the forward-going polariton is

$$I(z,t) = \langle\psi(t)|\hat{\Psi}_+^\dagger(z)\hat{\Psi}_+(z)|\psi(t)\rangle = \langle 1|\hat{\Psi}_+^\dagger(z)\hat{\Psi}_+(z)|1\rangle + \langle 2|\hat{\Psi}_+^\dagger(z)\hat{\Psi}_+(z)|2\rangle, \quad (3.40)$$

where $|j\rangle$ denotes the component of the total wavefunction $|\psi(t)\rangle$ containing j photons. The first and second terms on the right thus correspond to the one- and two-photon contributions to the intensity. By re-writing expressions in terms of S instead of $(\hat{\Psi}_+, \hat{\Psi}_-)$, we obtain:

$$I(z,t) = \frac{1}{2}\left|\theta(z) - \frac{i}{2m}\partial_z\theta(z)\right|^2 + 2\int dz' \left|\phi(z',z) - \frac{i}{2m}\partial^{(2)}\phi(z',z)\right|^2 \quad (3.41)$$

Similarly, the second-order correlation function for the forward field is

$$\langle\psi|\hat{\Psi}_+^{\dagger 2}(z)\hat{\Psi}_+^2(z)|\psi\rangle = \left|\phi(z,z) - \frac{i}{m}\partial^{(1)}\phi(z,z) - \frac{1}{4m^2}\partial^{(1)}\partial^{(2)}\phi(z,z)\right|^2 \quad (3.42)$$

which in our truncated space only depends on the two-photon wave function. Now, we evaluate the normalized second-order correlation function $g_2(z)$, which characterizes the photon statistics of an arbitrary field. This function takes the form

$$g_2(z) = \frac{\langle\psi|\hat{\Psi}_+^{\dagger 2}(z)\hat{\Psi}_+^2(z)|\psi\rangle}{\left|\langle\psi|\hat{\Psi}_+^\dagger(z)\hat{\Psi}_+(z)|\psi\rangle\right|^2}, \quad (3.43)$$

and physically characterizes the relative probability of detecting two consecutive photons at the same position z. If this quantity is less (greater) than one, the photonic

field is anti-bunched (bunched). In particular, if $g_2(z) = 0$, the field is perfectly anti-bunched and there is no probability for two photons to overlap in position. In our truncated Hilbert space, $g_2(z)$ of the transmitted field is given by

$$g_2(z=d) \simeq \frac{\langle 2|\Psi_+^{\dagger 2}(d)\Psi_+^2(d)|2\rangle}{\left|\langle 1|\Psi_+^\dagger(d)\Psi_+(d)|1\rangle + \langle 2|\Psi_+^\dagger(d)\Psi_+(d)|2\rangle\right|^2} \tag{3.44}$$

$$= \frac{4\left|\phi(d,d) - \frac{i}{m}\partial^{(1)}\phi(d,d) - \frac{1}{4m^2}\partial^{(1)}\partial^{(2)}\phi(d,d)\right|^2}{\left(\left|\theta(d) - \frac{i}{2m}\partial_z\theta(d)\right|^2 + 4\int dz' \left|\phi(z',d) - \frac{i}{2m}\partial^{(2)}\phi(z',d)\right|^2\right)^2} \tag{3.45}$$

We note that this expression can be simplified, since at $z = d$, we have $\Psi_- = \frac{1}{\sqrt{2}}(S + \frac{i}{2m}\partial_z S) = 0$ and $\Psi_+ = \sqrt{2}S$. Therefore,

$$g_2(d) = \frac{4|\phi(d,d)|^2}{\left(|\theta(d)|^2 + 4\int dz' \,|\phi(z',d)|^2\right)^2}. \tag{3.46}$$

We can also evaluate the stationary two-time correlation, which is defined in the Heisenberg picture as:

$$g_2(z,\tau) = \frac{\langle\psi|\Psi_+^\dagger(z,0)\Psi_+^\dagger(z,\tau)\Psi_+(z,\tau)\Psi_+(z,0)|\psi\rangle}{\left|\langle\psi|\Psi_+^\dagger(z,0)\Psi_+(z,0)|\psi\rangle\right|^2}, \tag{3.47}$$

where the denominator is simplified in the stationary steady-state regime. This correlation function characterizes the probability of detecting two photons at position z but separated by time τ. We can re-write $g_2(z,\tau)$ in terms of wavefunctions in the Schrödinger picture in the following way. We first note that the expression $|\tilde{\psi}(0)\rangle = \hat{\Psi}_+(z,0)|\psi\rangle$ appearing in the equation above can be thought of as a new wavefunction, which describes the state of the system after a photon is initially detected at time $t = 0$ and position z. This new state naturally has one less photon

than the original state, and by simplifying the expressions, it can be written as:

$$|\tilde{\psi}(0)\rangle = \int \theta^{\text{new}}(z')S^{\dagger}(z')|0\rangle + \epsilon^{\text{new}}|0\rangle \tag{3.48}$$

where the new one-photon and vacuum amplitudes are given by

$$\theta^{\text{new}} = \sqrt{2}\left(\phi(d,z',t=0) - \frac{i}{2m}\partial^{(1)}\phi(d,z',t=0)\right) \tag{3.49}$$

$$\epsilon^{\text{new}} = \frac{1}{\sqrt{2}}\left(\theta(d,t=0) - i\partial\theta(d,t=0)\right). \tag{3.50}$$

Here we have assumed that $z = d$, since we are interested in the transmitted field. Now, Eq. (3.47) can be written as

$$g_2(d,\tau) = \langle\tilde{\psi}(0)|\hat{\Psi}_+^{\dagger}(d,\tau)\hat{\Psi}_+(d,\tau)|\tilde{\psi}(0)\rangle / |\langle\tilde{\psi}(0)|\tilde{\psi}(0)\rangle|^2. \tag{3.51}$$

The numerator describes the expectation value for the intensity operator $\hat{I}(\tau) = \hat{\Psi}_+^{\dagger}(d,\tau)\hat{\Psi}_+(d,\tau)$ in the Heisenberg picture given an initial state $|\tilde{\psi}(0)\rangle$. However, we can easily convert this to the Schrödinger picture by moving the evolution from the operator to the state, *i.e.*, by evolving $|\tilde{\psi}(0)\rangle$ under the same evolution equations (Eqs. 3.30-3.31) and boundary conditions (Eq. 3.38) that we used earlier. Therefore, the correlation function $g_2(z,\tau)$ will be given by:

$$g_2(z,\tau) = \frac{\langle\tilde{\psi}(\tau)|\Psi_+^{\dagger}(z)\Psi_+(z)|\tilde{\psi}(\tau)\rangle}{\left|\langle\psi(0)|\Psi_+^{\dagger}(z)\Psi_+(z)|\psi(0)\rangle\right|^2}. \tag{3.52}$$

3.6 Analytical solution for NLSE with open boundaries

In this section, we show that a NLSE system with open boundary conditions yields analytical solutions in absence of an outside driving source ($\alpha_0 = 0$). To obtain the analytical solutions, we use the Bethe ansatz technique [111, 107]. This ansatz specifies that the eigenstates consist of a superposition of states in which colliding particles exchange their wavenumbers k_i. Unlike the typical formulation, the values of k_i here can be complex to reflect the *open* nature of our boundary conditions, which allow particles to freely enter or leave. In particular, we present the one-, two- and many-body eigenmodes of the system along with their energy spectra. Finding certain eigenmodes of the system (*e.g.*, bound states) helps us understand the correlation functions and also spatial wavefunctions which are numerically calculated later in Sec.3.7 for a driven system.

3.6.1 One-particle problem

First, we calculate the fundamental modes for the one-particle states. These modes are of particular interest when we later want to construct the many-body wavefunction of the interacting system in the absence of an input field.

Specifically, we want to find solutions of the Schrödinger equation for a single particle in a system of length d,

$$i\frac{\partial}{\partial t}\theta(z,t) = -\frac{1}{2m}\frac{\partial^2}{\partial z^2}\theta(z,t), \tag{3.53}$$

subject to open boundary conditions. The boundary condition for the undriven system at $z = 0$ is given by

$$\theta(0) - \frac{i}{2m}\partial_z\theta(0) = 0 \tag{3.54}$$

and similarly for $z = d$,

$$\theta(d) + \frac{i}{2m}\partial_z\theta(d) = 0. \tag{3.55}$$

We look for stationary solutions of the form $\theta(z,t) = e^{-i\delta t}\theta(z)$, where $\theta(z) = A\sin(kz) + B\cos(kz)$. For simplicity, we assume $m = 1/2$. Therefore, we recover the quadratic dispersion relation $\delta = k^2$. The values of k are allowed to be complex to reflect the open nature of our boundary conditions, which allows particles to freely enter or leave. By enforcing the boundary conditions we get a set of equations for the coefficients A, B,

$$B - iAk = 0 \quad , \quad (A - iBk)\sin(kd) + (B + iAk)\cos(kd) = 0, \tag{3.56}$$

which yields the characteristic equation for finding eigenmodes and eigen-energies of system,

$$e^{2ikd} = \left(\frac{k+1}{k-1}\right)^2. \tag{3.57}$$

Therefore the normalized corresponding wave function for each allowed k will be:

$$\theta(z) = A(\sin(kz) + ik\cos(kz)) \quad , \quad A^2 = \frac{4k}{2dk(1+k^2) + (k^2-1)\sin(2dk)} \tag{3.58}$$

We note that in the limit of large optical density $d \gg 1$, the lowest energy modes of the open system are very close to those of a system with closed boundary conditions,

whose characteristic equation is given by $kd = n\pi$. For example, at $d = 100$, the wave number corresponding to lowest energy is $k \simeq 0.0314 - i0.00063 \simeq \pi/100$. We note that the many-body solutions of the system in the presence of very strong interactions (large κ) can be constructed from these single-particle solutions and proper symmetrization, as we show in Sec.3.6.5.

3.6.2 Two-particle problem

In this section, we study the problem of two particles obeying the NLSE with mixed boundary conditions. We wish to solve

$$E\phi(z_1, z_2) = -\frac{1}{2m}\left(\frac{\partial^2}{\partial z_1^2} + \frac{\partial^2}{\partial z_2^2}\right)\phi(z_1, z_2) + 2\kappa\phi(z_1, z_2)\delta(z_1 - z_2), \tag{3.59}$$

where E is the energy of the system and can be complex. Again, we assume the mass is entirely real, $m = 1/2$.

We should note that the conventional method of separation of variables cannot be applied in this case. The reason for this can be understood in the following way. On one hand, if we ignore the delta interaction term in the evolution equation of the two particles, finding the eigenfunctions is essentially equivalent to solving the Laplace equation in a box with mixed boundary conditions. Therefore, for this problem the natural separation of variables involves solutions given by products of functions $f(z_1)$ and $g(z_2)$. On the other hand, if we neglect the boundaries, the problem of two particles interacting at short range can be solved by utilizing the center of mass and relative coordinates and invoking solutions involving products of functions $\tilde{f}(z_1 + z_2)$ and $\tilde{g}(z_1 - z_2)$. We immediately see that the two sets of solutions are irreconcilable and thus separation of variables is not applicable when both the boundary conditions

and interaction term are present.

We thus take a different approach, using a method similar to the Bethe ansatz method for continuous, one-dimensional systems [111]. Specifically, we solve the Schrödinger equation in the triangular region where $0 \leq z_1 < z_2 \leq d$, and we treat the interaction as a boundary condition at $z_1 = z_2$. In other words, when two particles collide with each other at $z_1 = z_2$, they can exchange momenta, which is manifested as a cusp in the wave function at $z_1 = z_2$. Hence, for the boundary conditions in this triangular region, we have

$$\phi(0, z_2) - i\partial_{z_1}\phi(0, z_2) = 0 \tag{3.60}$$

$$\phi(z_1, d) + i\partial_{z_2}\phi(z_1, d) = 0 \tag{3.61}$$

$$(\partial_{z_2} - \partial_{z_1})\,\phi(z_1, z_2)|_{z_2=z_1} = \kappa\phi(z_1, z_2)|_{z_2=z_1} \tag{3.62}$$

We note that the last boundary condition is deduced from integrating Eq. (3.59) across $z_1 = z_2$ and enforcing that the wavefunction is symmetric,

$$(\partial_{z_2} - \partial_{z_1})\,\phi(z_1, z_2)|_{z_2=z_1^+} - (\partial_{z_2} - \partial_{z_1})\,\phi(z_1, z_2)|_{z_2=z_1^-} = 2\kappa\phi(z_1, z_2)|_{z_1=z_2}. \tag{3.63}$$

Inside the triangle, the solution consists of superpositions of *free* particles with complex momenta. Since particles can exchange momenta when they collide at $z_1 = z_2$, we should consider solutions of the following form,

$$\phi(z_1, z_2) = \sum_{\{\epsilon\}} \mathcal{A}_\epsilon e^{i\epsilon_1 k_1 z_1 + i\epsilon_2 k_2 z_2} + \mathcal{B}_\epsilon e^{i\epsilon_1 k_2 z_1 + i\epsilon_2 k_1 z_2} \tag{3.64}$$

where the summation should be performed on all sets of signs $\epsilon = \pm 1$. Given the terms containing $\mathcal{A}_\epsilon$, the terms $\mathcal{B}_\epsilon$ then arise from the scattering of the particles off

each other. Let's first consider the portion of the wavefunction containing the terms $\mathcal{A}_\epsilon$, which we can write in the form:

$$\phi_{\mathcal{A}}(z_1, z_2) = e^{ik_1 z_1 + ik_2 z_2} + \alpha e^{-ik_1 z_1 + ik_2 z_2} + \beta e^{-ik_1 z_1 - ik_2 z_2} + \gamma e^{+ik_1 z_1 - ik_2 z_2}, \tag{3.65}$$

where the energy is equal to $E = k_1^2 + k_2^2$ and could be complex. Similar to the single-particle solutions, the presence of the imaginary part in the energy reflects the fact that the two-particle state stays a finite amount of time inside the system. Applying boundary conditions at $z = 0$ and $z = d$ subsequently generates four equations relating α, β, γ where one of them is redundant. Their solution reduces the wavefunction to

$$\phi_{\mathcal{A}}(z_1, z_2) = e^{ik_1 z_1 + ik_2 z_2} + \frac{k_1 + 1}{k_1 - 1} e^{-ik_1 z_1 + ik_2 z_2} + \frac{k_1 + 1}{k_1 - 1} \gamma e^{-ik_1 z_1 - ik_2 z_2} + \gamma e^{+ik_1 z_1 - ik_2 z_2} \tag{3.66}$$

where $\gamma = \frac{k_2 - 1}{k_2 + 1} e^{2ik_2 d}$. A similar expression results for the portion of $\phi(z_1, z_2)$ containing the $\mathcal{B}_\epsilon$ terms, once the boundary conditions at $z = 0$ and $z = d$ are applied:

$$\begin{aligned} \phi_{\mathcal{B}}(z_1, z_2) &= \frac{1}{t}\left(e^{ik_2 z_1 + ik_1 z_2} + \frac{k_2 + 1}{k_2 - 1} e^{-ik_2 z_1 + ik_1 z_2}\right) && (3.67) \\ &+ \frac{1}{t}\left(\frac{k_2 + 1}{k_2 - 1} \gamma' e^{-ik_2 z_1 - ik_1 z_2} + \gamma' e^{+ik_2 z_1 - ik_1 z_2}\right) && (3.68) \end{aligned}$$

where $\gamma' = \frac{k_1 - 1}{k_1 + 1} e^{2ik_1 d}$, and t is a coefficient to be determined from the boundary condition at $z_1 = z_2$. To find t, it is convenient to re-write each of ther terms in $\phi_{\mathcal{A},\mathcal{B}}$ as a product of relative coordinate ($r = z_2 - z_1$) and center-of-mass coordinate ($R = (z_1 + z_2)/2$) functions,

$$\tilde{\phi}_{\mathcal{A}}(R, r) = e^{ipR - iqr} + \frac{k_1 + 1}{k_1 - 1} e^{-iqR + ipr} + \gamma \frac{k_1 + 1}{k_1 - 1} e^{-ipR + iqr} + \gamma e^{iqR - ipr}, \tag{3.69}$$

$$\tilde{\phi}_{\mathcal{B}}(R,r) = t^{-1}\left(e^{ipR+iqr} + \frac{k_2+1}{k_2-1}e^{iqR+ipr} + \gamma'\frac{k_2+1}{k_2-1}e^{-ipR-iqr} + \gamma' e^{-iqR-ipr}\right), \tag{3.70}$$

where $p = (k_1+k_2)$ and $q = (k_1-k_2)/2$. The boundary condition at $z_1 = z_2$ leaves the center-of-mass parts of the wavefunction unaffected, but yields the following condition on the relative coordinates,

$$\partial_r \phi(R,r)|_{r=0^+} = \frac{\kappa}{\sqrt{2}}\phi(R,r)|_{r=0^+}. \tag{3.71}$$

where $\phi = \phi_{\mathcal{A}}+\phi_{\mathcal{B}}$ is the total wavefunction in the triangular region. We should satisfy this boundary condition separately for each of the center-of-mass momentum terms $e^{\pm ipR}, e^{\pm iqR}$ in the total wavefunction. This leads to three independent equations (one out of four is redundant). However, we introduce a new parameter (t') to simplify the equations, which turns them into four equations:

$$t = \frac{k_1-k_2+i\kappa}{k_1-k_2-i\kappa} \quad , \quad t' = \frac{k_1+k_2+i\kappa}{k_1+k_2-i\kappa} \tag{3.72}$$

$$t\ t'\left(\frac{k_1+1}{k_1-1}\right)^2 = e^{2ik_1 d} \tag{3.73}$$

$$t'\left(\frac{k_2+1}{k_2-1}\right)^2 = te^{2ik_2 d}, \tag{3.74}$$

which can be written in the following short form:

$$e^{2ik_i d} = \frac{(k_i+1)^2}{(k_i-1)^2}\prod_{j\neq i}\frac{(k_i-k_j+i\kappa)(k_i+k_j+i\kappa)}{(k_i-k_j-i\kappa)(k_i+k_j-i\kappa)} \tag{3.75}$$

where i, j can be (1,2). These are transcendental equations for (k_1, k_2), which generate the spectrum of two interacting particles. We can also write the wave functions ($\phi = \phi_{\mathcal{A}}(z_1,z_2) + \phi_{\mathcal{B}}(z_1,z_2)$) in the region ($0 \leq z_1 < z_2 \leq d$) in a more compact way, by using the single particle solutions $\eta_k(z) = \sin(kz) + ik\cos(kz)$:

$$\phi_{\mathcal{A}}(z_1, z_2) = \frac{4}{k_1 - 1}\frac{e^{ik_2 d}}{k_2 + 1}\eta_{k_1}(z_1)\eta_{k_2}(d - z_2) \tag{3.76}$$

$$\phi_{\mathcal{B}}(z_1, z_2) = \frac{4t^{-1}}{k_2 - 1}\frac{e^{ik_1 d}}{k_1 + 1}\eta_{k_2}(z_1)\eta_{k_1}(d - z_2). \tag{3.77}$$

It is interesting to note that in the limit of strong interaction (either for positive or negative κ), the solutions are very similar to the non-interacting case. The reason can be seen from the transcendental Eqs. (3.75), in the limit $\kappa \to \pm\infty$. We then recover the same characteristic equations $e^{2ikd} = (\frac{k+1}{k-1})^2$ for both wavevectors as the non-interacting case, Eq. (3.57). We should note that there are some trivial solutions to the transcendental Eqs. (3.75), which do not have any physical significance. For example, equal wave vectors $k_1 = k_2$. Although one can find such wave vectors, this solution is readily not a solution to Eq.(3.59), since it does not satisfy the interacting part (this solution only contains center of mass motion). One can also plug back the wave vectors into wave function and arrive at a wave function equal to zero everywhere. Another example is when one of the wave vectors is zero. In this case, one can also show that the wave function is zero everywhere. If (k_1, k_2) are solutions to the transcendental equations, then $(\pm k_1, \pm k_2)$ are also solutions with equal energies. In next two sections, we investigate non-trivial solutions to the transcendental equation for two particles and discuss the related physics.

3.6.3 Solutions close to non-interacting case

The transcendental equations allow a set of solutions with the wavevectors close to two different non-interacting modes say (m, n). In the non-interacting regime, any mode can be populated by an arbitrary number of photons. However, once

the interaction is present, photons can not occupy the same mode and therefore, the photons will *reorganize* themselves and each acquire different modes. Fig. 3.8 shows a normal mode wavefunction of a non-driven system in both non-interacting and strongly interacting regime ($\kappa d \gg 1$). The wave function has a cusp on its diagonal and diagonal elements are depleted for both repulsive and attractive strong interaction.

This is a manifestation of *fermionization* of bosons in one dimensional system in the presence of strong interaction [66, 111]. Such solutions can exist both for repulsive and attractive interactions. However, we note in the case of attractive interaction such solutions are not the ground state of the system and solutions with lower energies exist which will be discussed below. We later argue that indeed on the repulsive side, the anti-bunching behavior of a driven system is due to the repulsion of the photons inside the medium. We can also estimate the energy of such modes which is always positive. In the strong interacting regime, particles avoid each other and therefore, their energy of a strongly two interacting bosons $E(m, n)$ will be equal to the energy of a system which has two non-interacting bosons, one in state m and the other in state n. This is shown in Fig. 3.9, where by increasing the interaction strength the energy of interacting particles reaches that of the non-interacting particles. As we pointed out in the previous section (Sec.3.6.1), the energy of modes ($E(n)$) in an open box has an imaginary part which represents how fast the particle leave the system. However, for large systems ($d \gg 1$), this decay is very small compared to the energy of the mode and one can approximate the energy of an open system by that of a closed box (i.e. $E(n) \simeq (\frac{n\pi}{d})^2$). Therefore, the energy of two strongly interacting

photons ($\kappa d \gg 1$), in the limit of large system ($d \gg 1$), will be given by:

$$E(n,m) \simeq \left(\frac{n\pi}{d}\right)^2 + \left(\frac{m\pi}{d}\right)^2 \tag{3.78}$$

We note that our strongly interacting system is characterized by the parameter κd which is the same γ-parameter conventionally used for interacting 1D Bose gas. More precisely, the γ-parameter which is the ratio of the interaction to kinetic energy can be simplified in our case for two particles: $m\kappa d/2 = \kappa d/4$.

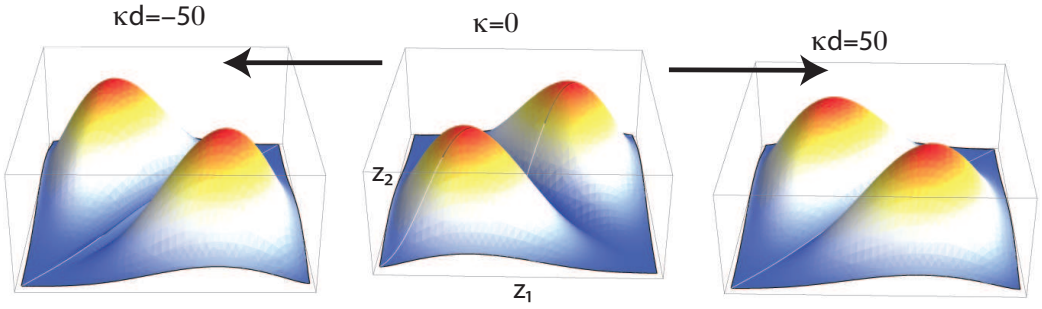

Figure 3.8: The amplitude of the two-photon wavefunction for (m=1, n=2) mode when the system is not driven. By increasing the interaction, photons self-organize inside the medium and exhibit anti-bunching (depletion of diagonal elements). For this plot: $d = 30$.

3.6.4 Bound States Solution

For attractive interaction ($\kappa < 0$), the mode equation (3.75) admits solutions which take the form of photonic bound states. Specifically, in the reference frame of the center of mass, two particles experience an attractive delta function interaction $-2|\kappa|\delta(z_2 - z_1) \rightarrow -\sqrt{2}|\kappa|\delta(r)$, which allows one bound state in the relative coordinate. Therefore, the part of the wavefunction describing the relative coordinate roughly takes the form $e^{iq|r|}$, where the relative momentum $q = (k_1 - k_2)/\sqrt{2} \simeq$

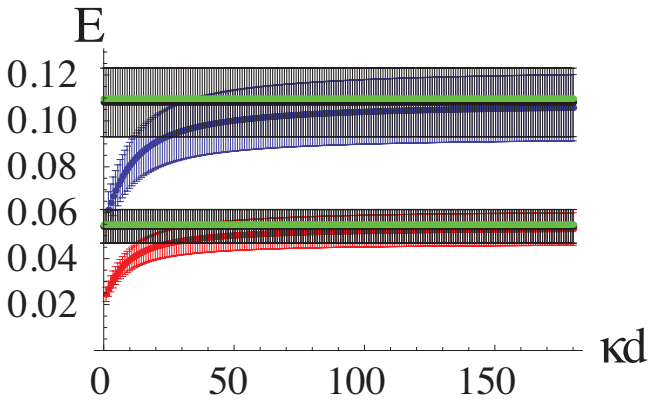

Figure 3.9: Energy of two-photon states: by increasing the interaction strength ($\kappa d \gg 1$) the energy of interacting particles (red:E(1,2) and blue:E(1,3)) reaches that of the non-interacting particles (black). For large system (in this case $d = 30 \gg 1$), the energy limit is equal to energy of particles in a closed box (green). The error bars show that imaginary part of the energies.

$i|\kappa|/\sqrt{2}$ is imaginary and its energy is about $-\kappa^2/2$. On the other hand, the center of mass momentum can take a discrete set of values that are determined by the system boundary conditions. We find that the center of mass solutions can be approximately described by two different types. The first type is where the real part of each photon wavevector roughly takes values allowed for a single particle in a box, such that $k_1 \simeq \left(\frac{n\pi}{d}\right) + i\frac{\kappa}{2}$ and $k_2 \simeq \left(\frac{n\pi}{d}\right) - i\frac{\kappa}{2}$. In this case the center of mass has wavevector $p = k_1 + k_2 \simeq 2(\frac{n\pi}{d})$. The corresponding energies for these states are

$$E_n^b \simeq 2\left(\frac{n\pi}{d}\right)^2 - \frac{\kappa^2}{2}. \tag{3.79}$$

Here, the first term on the right corresponds to the energy of the center of mass motion, and the second term corresponds to the bound-state energy of the relative motion. Fig. 3.12 shows that the energies estimated in this way agree very well with the exact values obtained by solving the transcendental Eqs. (3.75).

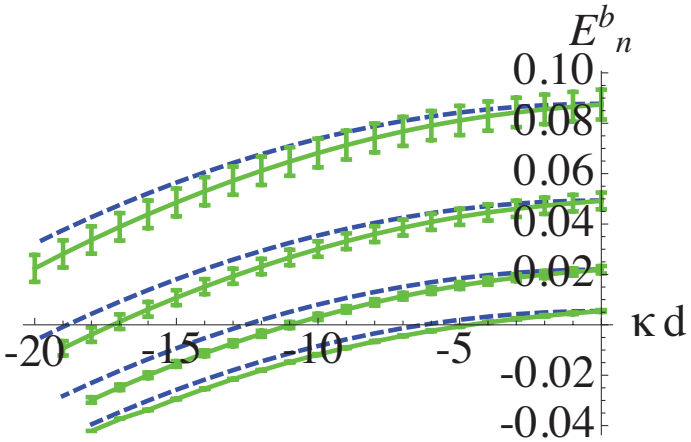

Figure 3.10: Energy of bound states versus strength of nonlinearity. Green (solid) curves are obtained by solving transcendental Eqs. (3.75). Blue (dashed) curves are estimated based on $E_n^b \simeq 2\left(\frac{n\pi}{d}\right)^2 - \frac{\kappa^2}{2}$. In this plot $d = 30$.

The second type of solution allowed for the center of mass motion is where its energy approximately takes a single-particle value, $\frac{p^2}{2(2m)} = (\frac{n\pi}{d})^2$ where $p = k_1 + k_2 \simeq \sqrt{2}(\frac{n\pi}{d})$. Therefore, the momentum of individual particles will be given by $k_1 \simeq \left(\frac{n\pi}{\sqrt{2}d}\right) + i\frac{\kappa}{2}$, $k_2 \simeq \left(\frac{n\pi}{\sqrt{2}d}\right) - i\frac{\kappa}{2}$ and the energy of this paired composite can be estimated as

$$E_n^b \simeq \left(\frac{n\pi}{d}\right)^2 - \frac{\kappa^2}{2}. \tag{3.80}$$

Again, the estimated energies agree well with exact solutions, as shown in Fig. 3.12. We note that some of the estimated allowed energies for the two types of center of mass solutions coincide (*e.g.*, the lowest lying energy level in Fig. 3.10 and Fig. 3.12).

The energies of this series of bound states decrease with increasing strength of nonlinearity $|\kappa|$. Now, suppose we drive the system with a coherent field of fixed frequency δ, while varying κ. The system is expected to display a set of resonances as $|\kappa|$ is increased, each time δ is equal to some particular bound state energy E_n^b. This effect in fact gives rise to oscillatory behavior in the correlation functions as a

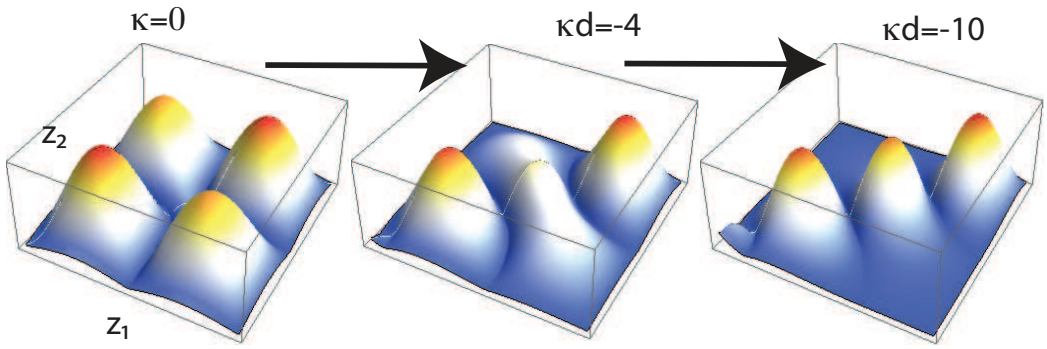

Figure 3.11: The amplitude of the two-photon wavefunction for a bound state when the system is not driven. By increasing interaction, photons becomes more bunched. $(k_1, k_2) \simeq \left(\frac{n\pi}{d}\right) \pm i\frac{\kappa}{2}$. For this plot: $d = 60, n = 3$.

function of κ, as we will see later (Fig. 3.18(a) and (b)).

The wavefunction amplitude of a typical bound state is shown in Fig. 3.13. Due to the attractive interaction, diagonal elements $z_1 = z_2$ become more prominent as $|\kappa|$ increases, indicating a stronger bunching effect for the photons, and these states become more tightly bound in the relative coordinate. The center of mass of the bound states can acquire a free momentum that is quantized due to the system boundary conditions (*e.g.*, $k \simeq n\pi/d$). Fig. 3.13 shows the wavefunction of the third bound state (n=3). The three peaks evident for large $|\kappa|$ reflect the quantum number of the center of mass motion.

3.6.5 Many-body problem

In this section, we obtain the general solution for the many-body case. For the many-body system, the Schrödinger equation takes the form

$$E\phi(z_1, ..., z_N) = -\frac{1}{2m}\sum_i \frac{\partial^2}{\partial z_i^2}\phi(z_1, ..., z_N) + \sum_{<i,j>} 2\kappa\phi(z_1, ..., z_N)\delta(z_i - z_j), \quad (3.81)$$

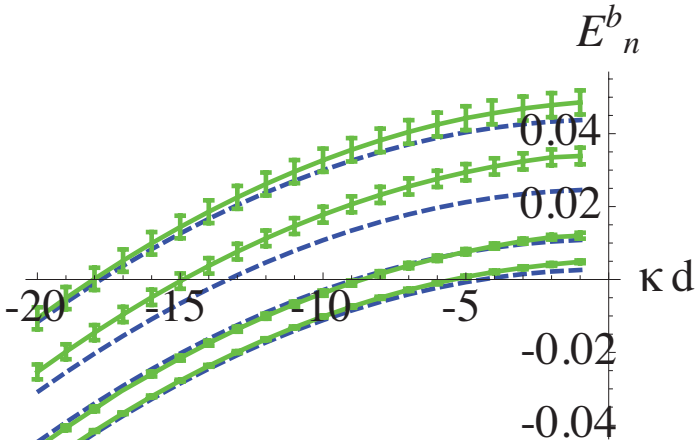

Figure 3.12: Energy of bound states versus strength of nonlinearity. Green (solid) curves are obtained by solving transcendental Eqs. (3.75). Blue (dashed) curve are estimated based on $E_n^b \simeq \left(\frac{n\pi}{d}\right)^2 - \frac{\kappa^2}{2}$. In this plot $d = 30$.

where $< i, j >$ indicates pairs of particles. The open boundary conditions for the many-body problem are given by

$$\left[\phi(z_1, ..., z_N) - i\frac{\partial}{\partial z_i}\phi(z_1, ..., z_N)\right]_{z_i=0} = 0 \tag{3.82}$$

$$\left[\phi(z_1, ..., z_N) + i\frac{\partial}{\partial z_i}\phi(z_1, .., z_N)\right]_{z_i=d} = 0. \tag{3.83}$$

Before presenting the general many-body solution, we first study the limit of very large interaction strength for two particles. In the limit of hardcore bosons where $\kappa \to \infty$, the expressions can be simplified since $t, t' = -1$ and $e^{ikd} = \frac{k+1}{k-1}$ for both $k = k_{1,2}$. Then, the two components of the wavefunction $\phi_{\mathcal{A}}$ and $\phi_{\mathcal{B}}$ take very similar forms,

$$\phi_{\mathcal{A}}(z_1, z_2) = \frac{4}{(k_1 - 1)(k_2 - 1)}\eta_{k_1}(z_1)\eta_{k_2}(z_2) \tag{3.84}$$

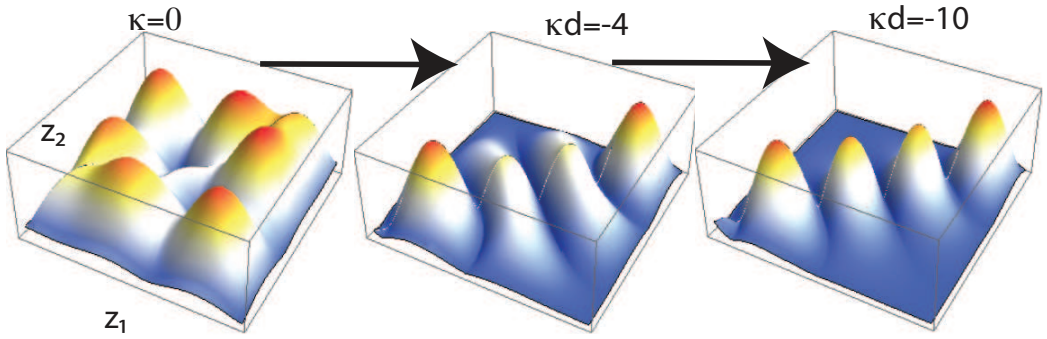

Figure 3.13: The amplitude of the two-photon wavefunction for a bound state for a non-driven system. By increasing interaction, photons becomes more bunched. $(k_1, k_2) \simeq \left(\frac{n\pi}{\sqrt{2}d}\right) \pm i\frac{\kappa}{2}$. For this plot: $d = 60, n = 3$.

$$\phi_{\mathcal{B}}(z_1, z_2) \quad = \quad \frac{-4}{(k_1 - 1)(k_2 - 1)} \eta_{k_2}(z_1)\eta_{k_1}(z_2). \tag{3.85}$$

The generalization to the many-body solution is straightforward for the hardcore boson case (also see Ref. [100]):

$$\phi(z_1, z_2, ..., z_N) = \left(\prod_{j=1}^{N} \frac{1}{(k_j - 1)}\right) \left| \det_{1 \le j,k \le N} \eta_j(z_k) \right| \tag{3.86}$$

Similar to two-body solution, we note that such solutions are present both for positive and negative κ. Since the system is one dimensional, strong interaction leads to fermionization of bosons (in this case photons)[66, 111].

We can also extend the many solution for an arbitrary interaction strength, following Refs.[111, 30]. Similar to the two-body case, we can construct the general many-body wave function of the form:

$$\phi(z_1, z_2, ..., z_N) = \sum_{\epsilon} A_{\epsilon} \sum_{P} B_P e^{i \sum_i \epsilon_{p_i} k_{p_i} z_i} \tag{3.87}$$

where the first sum is over forward and backward going waves ($\epsilon = \pm 1$) and the second sum is over different momentum permutations of the set $\{k\} = (k_1, k_2, ..., k_N)$, therefore there are $2^N N!$ terms. We can find B_P coefficient by requiring $\sum_P B_P \prod_{i<j} e^{i\epsilon_{p_i} k_{p_i} z_i}$

to be solution to the Schrödinger equation (Eq.3.81). We can write these coefficients in a compact way according to Gaudin [61, 47], $B_P = \prod_{i<j}\left(1+\frac{i\kappa}{\epsilon_{p_i}k_{p_i}-\epsilon_{p_j}k_{p_j}}\right)$ with the total energy $E=\sum_i k_i^2$. Now, we apply the boundary condition Eq.(3.82) which relates coefficient A_ϵ. For a given momentum permutation $P=(p_1,p_2,,...,p_N)$, by considering the terms corresponding to different signs of ϵ_{p_i}, the boundary condition requires A_ϵ to satisfy equations of the form

$$\begin{aligned}(1+\epsilon_{p_i}k_{p_i})A_{\epsilon_1,..\epsilon_{p_i}..\epsilon_N}\prod_{j(\neq p_i)}\left(1+\frac{i\kappa}{\epsilon_{p_i}k_{p_i}-\epsilon_j k_j}\right) \quad + \\ (1-\epsilon_{p_i}k_{p_i})A_{\epsilon_1,..(-\epsilon_{p_i})..\epsilon_N}\prod_{j(\neq p_i)}\left(1+\frac{i\kappa}{-\epsilon_{p_i}k_{p_i}-\epsilon_j k_j}\right) \quad = \quad 0\end{aligned}$$

The above equations can be satisfied by the following solution for A_ϵ

$$A_\epsilon=\prod_{i<j}\left(1-\frac{i\kappa}{\epsilon_i k_i+\epsilon_j k_j}\right)\prod_{m=1}^{N}\left(1-\frac{1}{\epsilon_m k_m}\right). \tag{3.88}$$

Therefore, the wavefunction can be written as:

$$\begin{aligned}\phi(z_1,z_2,...,z_N) &= \sum_\epsilon\sum_P\prod_{m=1}^{N}\left(1-\frac{1}{\epsilon_m k_m}\right)e^{[i(\epsilon_{p_1}k_{p_1}x_1+..+\epsilon_{p_N}k_{p_N}x_N)]} &(3.89)\\ &\times \prod_{i<j}\left[\left(1-\frac{i\kappa}{\epsilon_i k_i+\epsilon_j k_j}\right)\left(1+\frac{i\kappa}{\epsilon_{p_i}k_{p_i}-\epsilon_{p_j}k_{p_j}}\right)\right] &(3.90)\end{aligned}$$

Similar to two-body case, we have to subject this solution to the boundary condition at other end (i.e., $z=d$) to determine the momenta k_i's. This condition yields the transcendental equations for momenta:

$$e^{2ik_i d}=\frac{(k_i+1)^2}{(k_i-1)^2}\prod_{j\neq i}\frac{(k_i-k_j+i\kappa)(k_i+k_j+i\kappa)}{(k_i-k_j-i\kappa)(k_i+k_j-i\kappa)}. \tag{3.91}$$

If we assume only two particles in the system, one can easily verify the the above transcendental equations reduce to two-body transcendental equation derived in the previous section (Eq.(3.75)).

3.7 Quantum transport properties

In this section, we investigate transport properties of the photonic nonlinear one-dimensional system in the regimes of attractive, repulsive, and absorptive interactions between photons. We present numerical solutions for the transport of photons incident from one end of the waveguide (a driven system), while using the analytical solutions of the non-driven system (Sec. 3.6) to elucidate the various behaviors that emerge in the different regimes.

3.7.1 Repulsive Interaction ($\kappa > 0$)

We first study the quantum transport properties of the system in the dispersive regime where the nonlinearity coefficient is almost real and positive ($\kappa > 0$), such that photons effectively *repel* each other inside the system.

We assume that a weak coherent field is incident to the waveguide at one end, $z = 0$, with no input at the other end, $z = d$ [similar to Fig. 3.1(b)]. We fix the detuning of the input field to $\delta_0 = (\pi/d)^2$, which corresponds to the first transmission resonance in the linear regime (Sec. 3.3). Because we have assumed a weak input field, we can apply the techniques described in Sec. 3.5 to describe the transport. Our numerical techniques for solving these equations are given in Appendix B. While the numerical results presented in this and the following sections are evaluated for a specific set of parameters (system size, detuning, etc.), the conclusions are quite general. Numerically, we begin with no photons inside the medium, and evaluate quantities such as the transmission intensity and correlation functions only after the system reaches steady state in presence of the driving field. In Fig. 3.14, the transmission of

the single-photon intensity

$$T_1 = \frac{\langle 1|\Psi_+^\dagger(d)\Psi_+(d)|1\rangle}{\langle 1|\Psi_+^\dagger(0)\Psi_+(0)|1\rangle}, \tag{3.92}$$

the transmission of the two-photon intensity

$$T_2 = \frac{\langle 2|\Psi_+^\dagger(d)\Psi_+(d)|2\rangle}{\langle 2|\Psi_+^\dagger(0)\Psi_+(0)|2\rangle} \tag{3.93}$$

and the transmitted correlation function $g_2(z = d, \tau = 0)$ is shown as the system evolves in time. The system reaches its steady state after a time of the order of the inverse of the system bandwidth (Sec. 3.3). In fact, T_1 coincides with the linear transmission coefficient of the system in the absence of the nonlinearity.

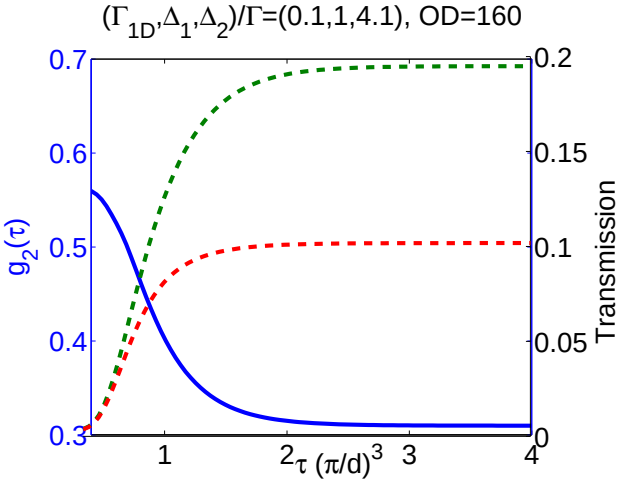

Figure 3.14: $g_2(\tau = 0)$ reaches the steady-state after a time interval which is set by the bandwidth of the system, one-photon state (green) is partially transmitted while the transmission of the two-photon state (red) is further suppressed due the nonlinear dispersion. This has been generated for a system with $\Gamma_{1D}/\Gamma = 10\%$ an OD=160.

First, we note that the single-photon wave function is not affected by the presence of the nonlinearity and will be perfectly transmitted in the absence of linear losses. Thus, in our truncated Hilbert space, the only subspace affected by κ is the

two-photon wave function, which is shown in Fig. 3.15. We clearly observe that the nonlinearity causes repulsion between two photons inside the system, as the wave function along the diagonal $z_1 = z_2$ becomes suppressed while the off-diagonal amplitudes become peaked (indicating the de-localization of the photons). This behavior closely resembles that of the natural modes of the system, as calculated in Sec. 3.6. A similar behavior involving the "self-organization" of photons in an NLSE system in equilibrium has been discussed in Ref. [36].

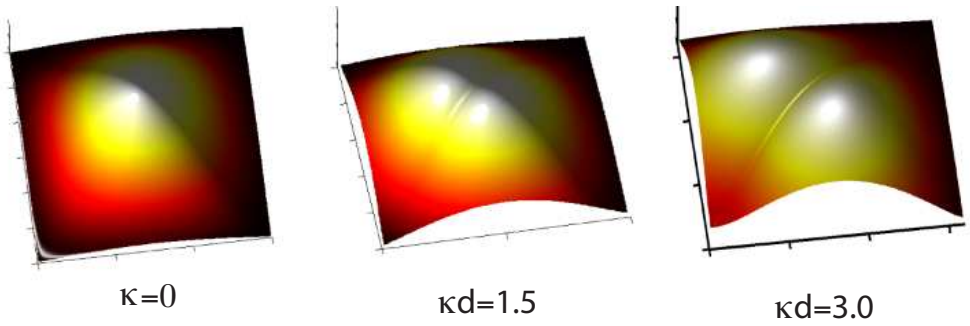

Figure 3.15: Two-photon wave function $|\phi(z_1, z_2)|$ exhibiting delocalization. We have assumed no dissipation ($\Gamma' = \Gamma = 0$) in this plot. $d = 30$ for different values of κ.

In the presence of linear absorption (discussed in Sec. 3.3), the system will not be perfectly transmitting even on resonance, and therefore in a realistic situation the transmittivity will be less than one ($T_1 < 1$). Note, however, that such absorption would result in a classical output given a classical input. Significantly, in the presence of a nonlinearity, we find that the output light can acquire non-classical character. Specifically, the transmitted light exhibits anti-bunching ($g_2(z = d, \tau = 0) < 1$), which becomes more pronounced with increasing κd^2 (Fig. 3.16). This effect partly arises from the suppression of transmission of two-photon components, due to an extra

nonlinear phase shift that shifts these components out of transmission resonance. In fact, these components are more likely to get reflected, which causes the reflected field to subsequently exhibit bunching behavior. We note that this effect is similar to photon blockade in a cavity (e.g., see Refs.[84, 69, 85]). In addition, additional anti-bunching occurs due to the fact that two-photon components inside the system tend to get repelled from each other. This effect arises due to the spatial degrees of freedom present in the system, which is fundamentally different than switching schemes proposed in optical cavities (e.g., Refs.[84, 69, 85]) or wave-guides coupled to a point-like emitter [150, 37]. In the limit where $\kappa \to \infty$, the transmitted field approaches perfect anti-bunching, $g_2(d, \tau = 0) = 0$.

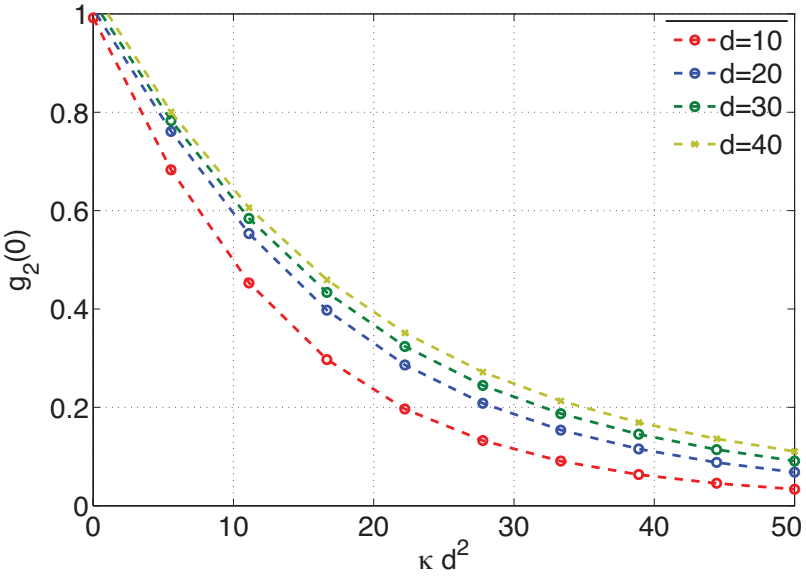

Figure 3.16: $g_2(\tau = 0)$ as a function of nonlinearity. For large system sizes $d \gg 1$, the anti-bunching of the system scales with κd^2.

In an experimental realization, the requirement to see the photon repulsion ($\kappa d^2 \geq 40$) for a system with $\Gamma_{1D}/\Gamma = 10\%$, would be a coherent optical length of $d \simeq 40$ when $\Delta_2/\Gamma = 1$. Therefore, at least an optical density of $OD \simeq 160$ is needed for

$T_1 \simeq 20\%$. The anti-bunching in the transmitted light is more pronounced as the optical density increases, which increases the effective system finesse (Fig. 3.17).

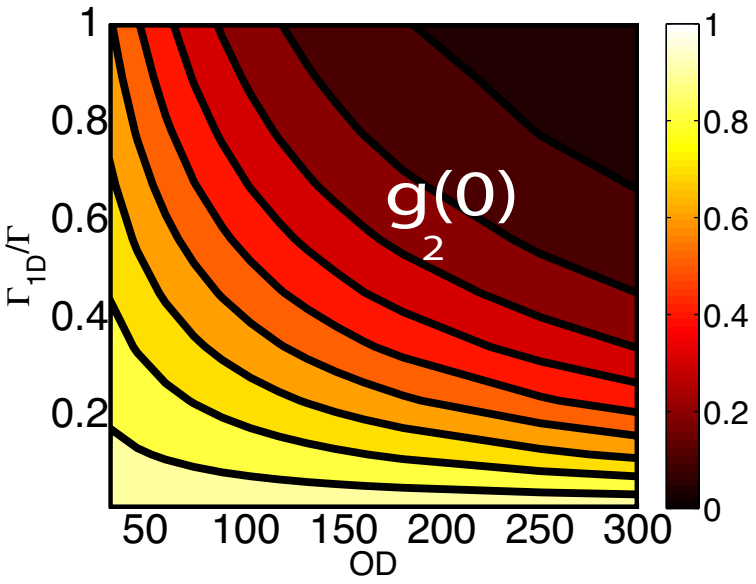

Figure 3.17: Repulsive photons: Correlation function $g_2(\tau = 0)$ of the transmitted light when the frequency is set to the single-photon transmission resonance with $T_1 \simeq 20\%$ and $\frac{\Delta_2}{\Gamma} = 5$.

3.7.2 Attractive Interaction ($\kappa < 0$)

In this section, we study the quantum transport properties of the system in the presence of dispersive nonlinearity with negative coefficient. Contrary to the semi-classical prediction, we show that the second-order correlation function of the transmitted field oscillates as function of nonlinear interaction strength and can exhibit both bunching and anti-bunching. We explain the origin of this behavior in terms of the analytical solutions obtained in Sec. 3.6.2.

In Fig. 3.18(a), we plot $g_2(\tau = 0)$ for the transmitted field versus κd. Initially, the system exhibits anti-bunching behavior for small values of $|\kappa|d$ which indicates that multi-photon components tend to switch themselves out of transmission resonance. However, as we increase $|\kappa|d$, oscillations develop in the correlation function, exhibiting strong bunching behavior at particular values of κd. Thus, unlike the repulsive case, a competing behavior arises between the photon switching effect and the resonant excitation of specific bound states within the system, as we describe below. In particular, the bound state energies E_n^b decrease quadratically with changing κ, according to Eq. (3.80) or Eq. (3.79), which is shown in Fig. 3.18(b). For a fixed detuning δ, the oscillation peaks (where g_2 is largest) correspond to situations where the energy of a bound state becomes equal to the energy of two incoming photons ($E_n^b = 2\delta$). This effect is further confirmed by examining the two-photon wave function at each of these oscillation peaks (Fig. 3.18a). We clearly observe that these wave functions correspond to the bound states calculated in Sec. 3.6.2. Similar to Fig. 3.11 and Fig. 3.13, it is readily seen that the wave functions at these peaks are localized along the diagonal, indicating a bound state in the relative coordinates

and leading to the bunching effect in transmission. On the other hand, an increasing number of nodes and anti-nodes develop along the diagonal for increasing $|\kappa|d$, which are associated with the higher momenta of the center-of-mass motion. We note that such resonances deviate significantly from the the semiclassical picture, where anti-bunching was predicted for both positive and negative nonlinearity. We also note that in cavity QED systems this effect is not present since these systems are single-mode.

The experimental requirement to see such behaviors is more stringent than the photon repulsion in the previous section. For example, if we want to observe the second photonic bound state ($\kappa d \geq 5$) for a system with $\Gamma_{1D}/\Gamma = 0.2$, the coherent optical length should be at least $d \simeq 200$ when $\Delta_2/\Gamma = -5$. To achieve a reasonable signal (linear transmission $T_1 = 1\%$) an optical density of $OD = 3500$ is needed. Importantly, however, we have shown that the presence of bound states inside the nonlinear medium can be probed with classical light, simply by examining higher-order correlation functions in the output field, rather than sending in complicated quantum inputs.

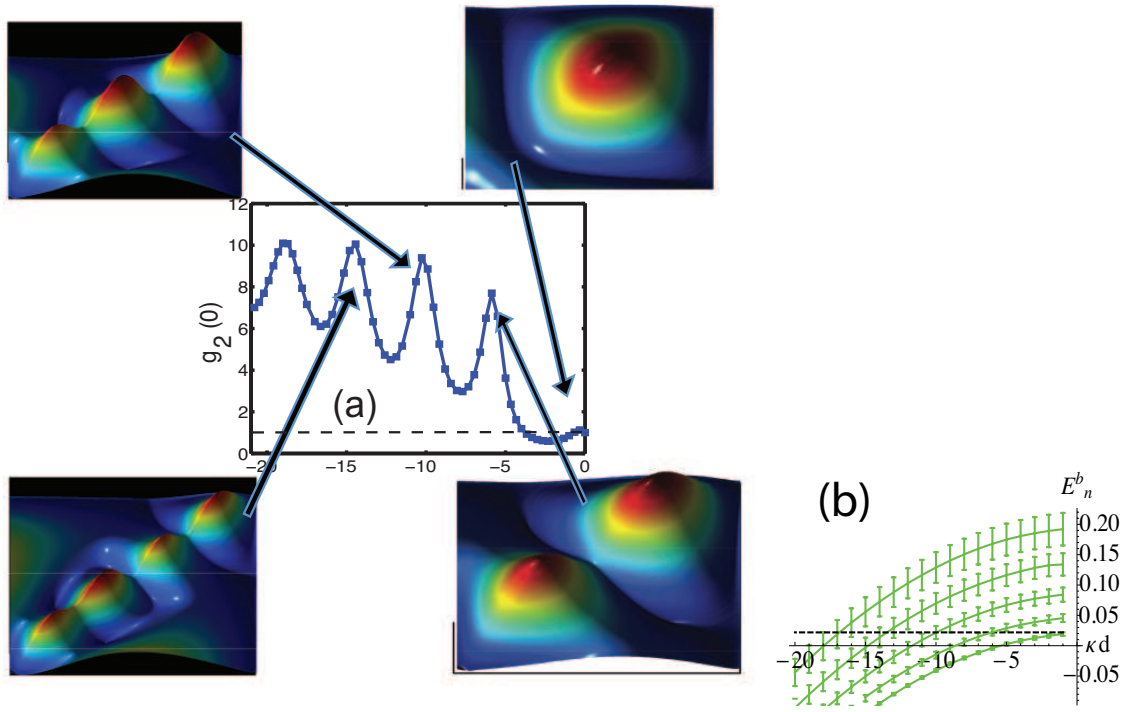

Figure 3.18: (a) Output correlation function $g_2(\tau = 0)$ as a function of nonlinearity: When the negative nonlinear strength is changed to higher values and g_2 exhibits resonances at certain values of $\kappa d \simeq (0, 6, 10, 14, ...)$. In this plot the system size is $d = 30$, however, for other system size same behaviors were observed around similar values of κd. The two-photon wavefunction ($|\phi(z_1, z_2)|$) for four values of nonlinearity is shown. (b) Corresponding bound state energies (green-solid) which become resonant with incoming photon energy (black-dotted) for specific nonlinearities. We have assumed no dissipation ($\Gamma' = \Gamma = 0$) in these plots.

3.7.3 Dissipative Regime ($\kappa = i|\kappa|$)

In this section, we study the transport properties of the system in the presence of nonlinear absorption, and calculate its effect on the transmitted light and its correlation functions.

A purely absorptive nonlinearity arises when the detuning Δ_2 is set to zero in our atomic system (see Fig. 3.1(a)). This nonlinear loss also leads to anti-bunching in the transmitted field, as multi-photon components become less likely to pass through

the waveguide without being absorbed. Linear absorption, on the other hand, affects transmission of single- and multi-photon components equally. Fig. 3.19 and Fig. 3.20 show how two-photon and one-photon states are transported differently in the nonlinear absorptive system (realistic linear losses are included in this calculation).

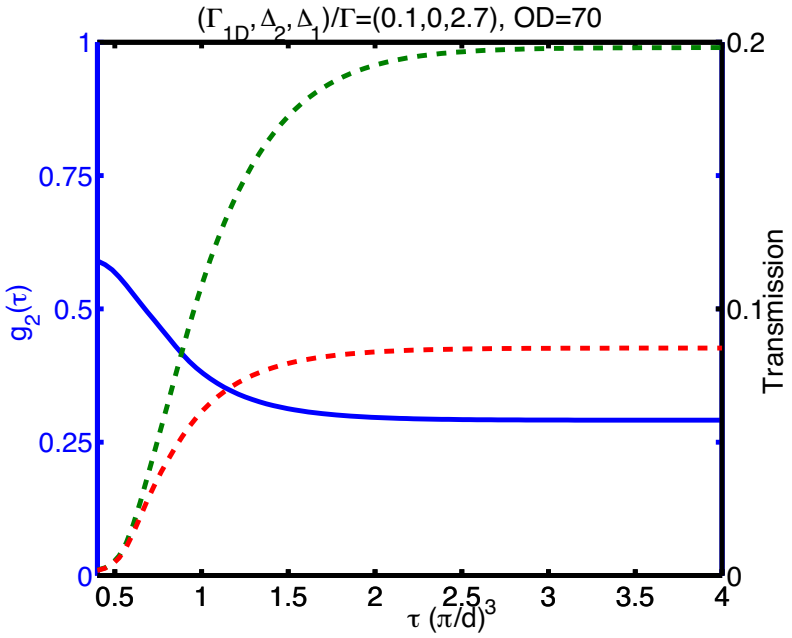

Figure 3.19: $g_2(\tau = 0)$ reaches the steady-state after a time interval which is set by the bandwidth of the system, one-photon state (green) is partially transmitted while the two-photon state (red) is strongly attenuated due the nonlinear absorption. This plot has been generated for a system with $\Gamma_{1D}/\Gamma = 10\%$ an OD=70.

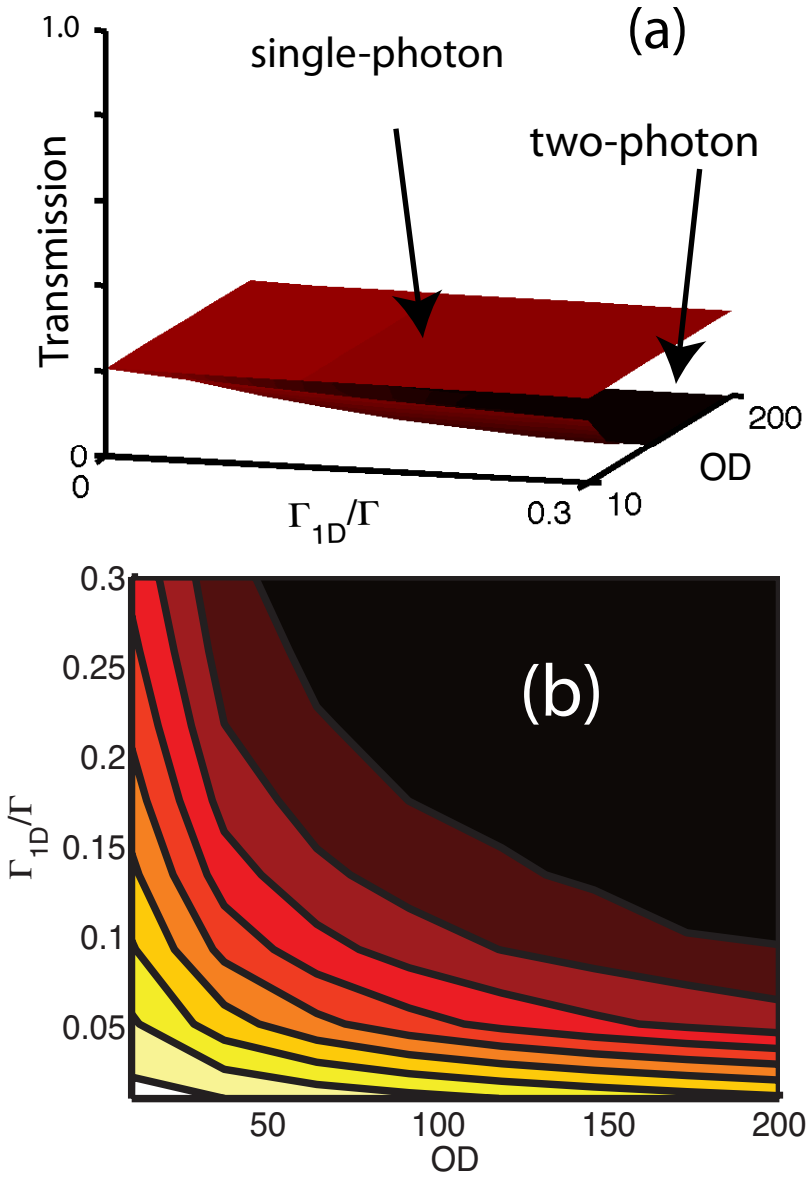

Figure 3.20: (a) one-photon state is partially transmitted (T_1) while the two-photon state transmission (T_2) is suppressed due the nonlinear absorption. This suppression is more pronounced for higher optical density and cooperativity. (b) Correlation function $g_2(\tau = 0)$ of the transmitted light when the frequency is set to the single-photon transmission resonance with $T \simeq 20\%$ and $\frac{\Delta_2}{\Gamma} = 0$.

We note that the two-photon wavefunction is attenuated due the nonlinear absorption, while it is not deformed, as shown in Fig. 3.21. In an experimental realization of such a system with $\Gamma_{1D}/\Gamma = 10\%$, an optical coherent length of $d \simeq 20$ is enough to yield a relatively large anti-bunching ($g_2 < 0.3$). In order to have high transmission ($T_1 = 20\%$) for single photons an optical density of $OD \simeq 70$ is required.

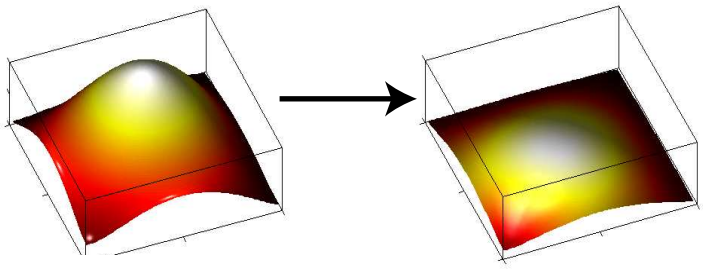

Figure 3.21: In the presence of the nonlinear absorption ($\frac{\Delta_2}{\Gamma} = 0$), the two-photon wave function is strongly suppressed comparing to the absence of the nonlinear absorption ($\Delta_2 \gg \Gamma$). These plots has been generated for a system with $\Gamma_{1D}/\Gamma = 10\%$, $T_1 \simeq 20\%$ and OD=70.

All of the physics related to the photon correlation function is described again by product of the coherent optical length and the nonlinearity coefficient ($|\kappa|d$) (since the nonlinear absorption is equal to the nonlinear absorption coefficient times the length of the medium). However, for a fixed optical density, since the nonlinear transition is on resonance, the magnitude of the nonlinear coefficient $|\kappa|$ is enhanced compared to the nonlinear dispersive case. We note that in the presence of nonlinear absorption, we should also consider the effect of accompanied noise. However as we show in Appendix.C, the effect of noise for an ensemble of many atoms which are driven by a weak laser field, is negligible, and therefore, using the NLSE with a decay term is sufficient and consistent.

3.8 Conclusions

We have developed a technique to study few-photon quantum dynamics inside 1D nonlinear photonic system. This technique allows us to study the system even in regimes where nonlinearities are significant even at a few-photon level, where we find that the behavior of the system deviates significantly from estimates based on classical formalism. Specifically, when the system is driven by classical light, the strong optical nonlinearity manifests itself in the correlation functions of the outgoing transmitted light. In particular, when the interaction between photons is effectively repulsive, the suppression of multi-photon components results in anti-bunching of the transmitted field and the system acts as a single-photon switch. In the case of attractive interaction, the system can exhibit either anti-bunching or bunching, associated with the resonant excitation of bound states of photons by the input field. These effects can be observed by probing statistics of photons transmitted through the nonlinear fiber.

Chapter 4

Single photon switch in a nonlinear optical fiber

4.1 Introduction

Photons are promising candidates for information carriers since they interact weakly with the environment and therefore can be transmitted over long distances. However, due to this weak interaction between light and matter, the mediated interaction between photons are usually very weak and therefore, physical systems that enable single photons to interact strongly with each other are extremely valuable for many emerging applications. Such systems are expected to facilitate the construction of single-photon switches and transistors, networks for quantum information processing [150, 37], and the realization of strongly correlated physics using light [79, 36]. An all-optical switch is the optical analogue of an electronic transistor [27]. In particular, in a single-photon gate, the transmission of a *target* photon is controlled by a single

control photon.

One potential approach to meditate strong interaction between photons involves the use of high-finesse optical microcavities containing a small number of resonant atoms that mediate the interaction between photons [134]. Their nonlinear properties are relatively straightforward to analyze or simulate because they involve very few degrees of freedom (i.e., a single optical mode) [84, 23, 147]. Recently, an alternative approach has been suggested, involving the use of atoms coupled to propagating photons in tight one-dimensional optical waveguides. Here, the nonlinearities are enhanced due to the confinement of photons near the diffraction limit and the subsequent increase in the atom-photon interaction [18, 102, 63, 150, 93, 121, 11]. In such systems, because of the light confinement in the transverse direction to a small area say A, the interaction between a single photon and a single atom is enhanced. In particular, the probability of such interaction scales as $p \simeq \lambda^2/A$, where λ is the wavelength of the light. In a typical system, this probability which also represents the fidelity of such a single-photon gate, is only a few percent [11].

In this chapter, we present an efficient scheme to implement a single-photon gate in a system where cold atoms are trapped inside the hollow core of a photonic-crystal fiber (PCF). Here, we show that coherent manipulation of light and atom can increase the effective interaction time between two photons. In particular, we demonstrate that the fidelity of such scheme increases by a factor which scales with the system optical density.

4.2 Description of the scheme

In this section, we present our scheme to realize a single-photon gate (SPG) for photons, based on the ideas of Ref. [7]. The idea is to first store a *control* photon [see Fig. 4.1] inside the medium using conventional EIT methods, by mapping it into a coherent spin wave excitation ($|s_+\rangle\langle g_+|$), and then transferring the stored spin coherence into another set of states ($|g_{+2}\rangle\langle g_+|$) using a microwave π- pulse (one can later recover the photon by reversing the process). Next, the control fields $\Omega_\pm$ are turned on. For the level configuration shown in Fig. 4.1 consisting of states $|g_+\rangle$ and $|s_+\rangle$ and the two coupled excited states, it can be shown that the coupled fields $\mathcal{E}_\pm$ obey the a linear Schrödinger equation [182]. In particular, the system behaves as an effective cavity and exhibits a set of linear transmission resonances as shown in Ref. [74]. Note, however, that if a control photon was successfully transferred into state $|g_{2+}\rangle$, it now effectively acts as an additional atomic scatterer inside the cavity which is capable of blocking the "bare cavity" transmission. Specifically, suppose a flying *target* photon of very narrow frequency, centered around the resonant transmission frequency (δ_{res}), is sent into the fiber at the input ($z = 0$). In absence of the control photon (switch OFF), the target photon will be transmitted with the probabilities calculated previously [74] (see Chapter 3). On the other hand, when the control photon is present (switch ON), the target photon will be entirely reflected.

The transport properties of the target photon can be evaluated from considering the transfer matrix of the waveguide and the scatterer. We define $M(\delta_{res}, z)$ to be the transfer matrix for propagation through distance z of the waveguide at the resonant transmission frequency δ_{res}. The waveguide transfer matrix can be derived from linear

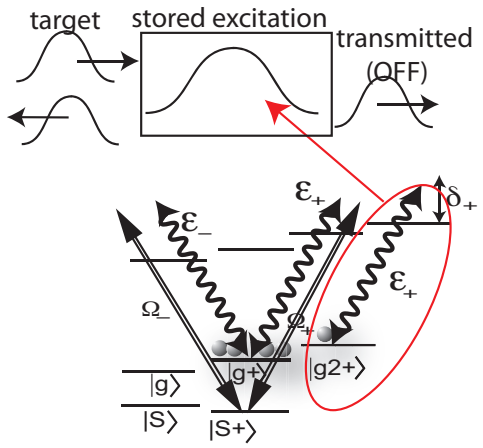

Figure 4.1: SPG scheme: In the absence of the control photon (OFF), the target photon is entirely transmitted. In the presence of the control photon (ON), the forward going field of the target photon resonantly interacts with the stored excitation through a closed transition and gets reflected. Since the backward field interacts very weakly with the corresponding transition, it is not shown.

coupled-mode equations describing the system (see Appendix D). M_a represents the transfer matrix of the photonic field interacting with a single atomic scatterer in one dimension (e.g. see Ref. [37]). Since the forward and backward fields independently couple to the scatterer, the matrix takes the form $M_a = \begin{pmatrix} t_+ & 0 \\ 0 & t_-^{-1} \end{pmatrix}$. A magnetic field is applied so that the nonlinear transition becomes resonant with the forward field (while the backward field becomes nearly uncoupled). Therefore, the phases are given by corresponding values: $t_+ = 1 - \frac{\Gamma_{1D}}{\Gamma - 2i\delta_+} \rightarrow \frac{\Gamma - \Gamma_{1D}}{\Gamma}$ and $t_- \simeq 1$ where Γ_{1D} and Γ are the guided and the total spontanoues emission rates, respectively. In the absence of the control photon, both phases are zero.

We evaluate the fidelity of such gate by calculating the transmittivity and reflectivity in the OFF and ON modes, respectecivly. More precisely, when the control excitation is not present (switch OFF as in Fig. 4.1), the target photon will be al-

most transmitted $T^{OFF} = |t^{OFF}_{total}|^2 \simeq 1$. The transmittivity can be evaluated from the corresponding transfer matrix:

$$M^{OFF}_{total} = M(\delta_{res}, d). \tag{4.1}$$

On the other hand, when the control photon is present (switch ON as in Fig. 4.1), the target photon is reflected. For simplicity, we suppose that the control photon is well-localized in the middle of the fiber ($z = \frac{d}{2}$), which is achievable with high optical depth (the fidelity in fact does not depend too strongly on position provided that it does not sit near the edges of the system). Therefore, the total transfer matrix of the system is

$$M^{ON}_{total} = M(\delta_{res}, d/2) M_a M(\delta_{res}, d/2). \tag{4.2}$$

The target photon will be reflected and the reflection coefficient will be given by $R^{ON} = |r^{ON}_{total}| \simeq 1$. To obtain a simple expression for the fidelity, we assume the optical density is large ($OD \gg 1$) and the single-atom cooperativity is small ($\frac{\Gamma_{1D}}{\Gamma} \ll 1$) and we introduce $\alpha = d\frac{\Gamma}{\Delta}$ to characterize the linear absorption of the system. Therefore, we can approximate the transmittivity in the OFF mode and the reflectivity in the ON mode:

$$T^{OFF} = 1 - \frac{\alpha}{4} \quad , \quad R^{ON} = 1 - \frac{8\pi^2}{\alpha OD \Gamma_{1D}/\Gamma}. \tag{4.3}$$

We can find the optimized value of α, by equating the above expressions and find the fidelity at a given optical density and single-atom cooperativity:

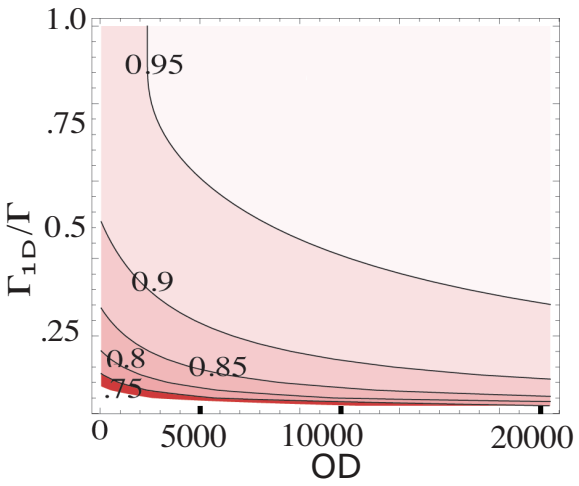

Figure 4.2: Single-photon gate fidelity: the fidelity improves by increasing OD and single-atom cooperativity.

$$\mathcal{F} \simeq 1 - \pi\sqrt{\frac{2\Gamma}{OD\Gamma_{1D}}} \tag{4.4}$$

Note that in order to include the Clebsch-Gordon coefficient, the single atom cooperativity should be multiplied by the corresponding branching ratio (see Appendix E).

Fig. 4.2 shows the fidelity of such a gate, which improves for higher optical density and waveguide coupling efficiency. A fidelity of 90% can be achieved, for instance, with $OD \simeq 5000$ and $\frac{\Gamma_{1D}}{\Gamma} = 0.3$. Contrary to the scheme presented in Ref. [7], our scheme does not require the target photon to fit inside the fiber all at once, which minimizes the effects of pulse dispersion. Moreover, this scheme allows a coherent control over both individual photons, a feature which is absent in a typical 1D single-photon switch [150, 36]. Therefore, this system can be used as a SPG without using a cavity (for a similar scheme involving an optical cavity, see Ref. [51]).

4.3 Discussion

In this section, we show that our scheme is efficient and does not lead to any residual entanglement between the control and target photon. In particular, in an ideal gate, we expect that in the presence of a control photon, the target photon will be entirely reflected without experiencing any distortion in its wave packet. Any residual entanglement between the control photon (i.e., atomic spin wave) and the target photon will result in reduction of the gate fidelity.

First, we investigate the dependance of the target photon reflection on the position of the control excitation. In particular, if the control photon is not located in the middle of the waveguide (i.e., at the anti-node), its coupling to the system will be reduced. Therefore, the reflection of the target photon will be decreased. Fig. 4.3, shows the smooth position dependence of the reflection. The gate works more efficiently if the control photon is situated at the center of the system where the reflection is maximized with respect to z. Since the stored atomic spin only couples to the forward and the backward field separately, the reflection coefficient does not have any oscillating terms proportional to e^{2ikz}. Therefore, the reflection coefficient has a smooth position dependence which is completely due to the dispersion of double-V system as shown in Fig. 4.3.

Second, we investigate the bandwidth of the single-photon gate. In the presence of the control photon, the target photon will be reflected only for certain frequencies. This is shown in Fig. 4.4. We observe that the reflection spectrum is much broader than the transmission spectrum around the resonances of interest i.e. $\sqrt{\delta}d = n\pi$, where n is an odd integer. If n is an even integer, a control photon in the middle of

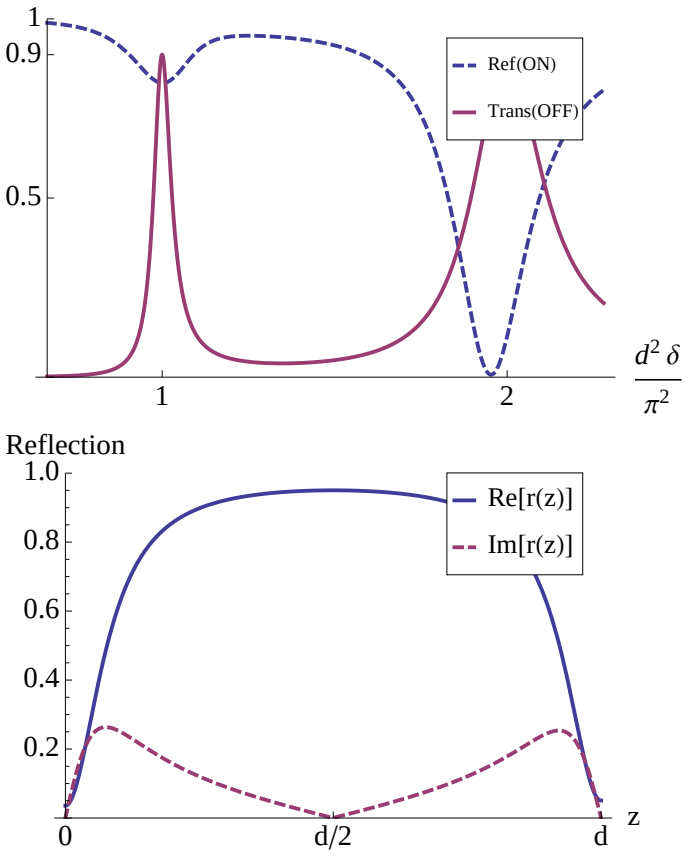

Figure 4.3: (a) Reflection spectrum when the control photon is positioned at z=d/4. (b) Reflection dependence on the position of the control photon. For these plots $OD = 5000, \Gamma_{1D}/\Gamma = 0.3$.

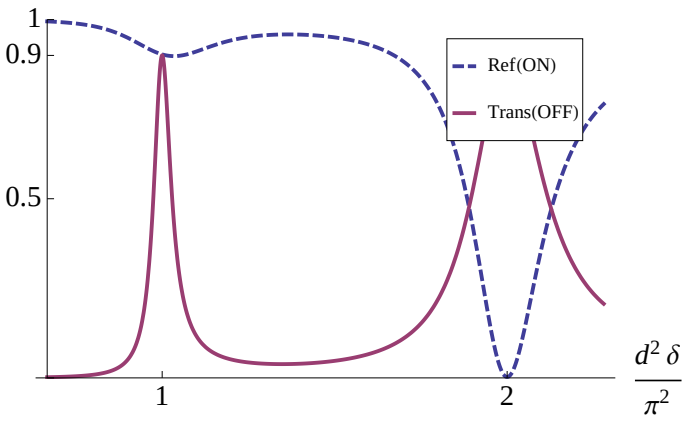

Figure 4.4: Reflectivity ($R = |r|^2$) and transmittivity ($T = |t|^2$) spectrum when the switch is ON (dashed) or OFF (solid), respectively. For this plot: $OD = 5000, \Gamma_{1D}/\Gamma = 0.3$.

the system coincides with the node of the effective cavity, therefore, the system will behave as if the control photon is not present. Below, we show that the broadness of reflection spectrum is important to establish a perfect gate without having residual entanglement.

Finally, we show that the presented scheme does not lead to any residual entanglement and the control and the target photons remain separable after the gate. In an experimental realization, both target and control photons have finite bandwidth. The general state of the two-photon state at any time is given by a two-parameter wave function $\phi(z_1, z_2)$ or equivalently $\phi(t, z_2)$. Initially, two photons are separable and wave function is only nonzero for $z_1 < z_2$. We are interested to find the state of the system after we bounced the target photon off the nonlinear system.

We start by Fourier transforming the incoming photon. With the help of the transfer matrix formalism, one can find the reflection/transmission coefficient as a function of frequency and the position of the control photon $r(\delta, z_2)$. Then, we evaluate the

reflection of each component off the delta-scatterers located at different positions according to the wave function of the control photon. Therefore, the state of the system before scattering will be:

$$\begin{aligned}\phi(t,z_2) &= \phi_1(t)\phi_2(z_2) = \frac{1}{\sqrt{2\pi}}\int d\delta e^{-i\delta t}\tilde{\phi}(\delta)\phi_2(z_2) &(4.5)\\ &= \frac{1}{\sqrt{2\pi}}\int dz_0\int d\delta e^{-i\delta t}\tilde{\phi}(\delta)\phi_2(z_0)\delta(z_0-z_2) &(4.6)\end{aligned}$$

and the reflected part of the wave function can be written as,

$$\begin{aligned}\phi_R(t,z_2) &= \frac{1}{\sqrt{2\pi}}\int dz_0\int d\delta e^{-i\delta t}\tilde{\phi}(\delta)\phi_2(z_0)\delta(z_0-z_2)r(\delta,z_0) &(4.7)\\ &= \frac{1}{\sqrt{2\pi}}\int d\delta e^{-i\delta t}\tilde{\phi}(\delta)\phi_2(z_2)r(\delta,z_2). &(4.8)\end{aligned}$$

Due to the dependence of the reflection coefficient on the target photon frequency and the control photon position, the above state is not necessarily separable. However, for the case of our interest, photons stay separable due to the following argument. In the absence of the control photons, the target photons should be entirely transmitted. Therefore, the bandwidth of the target photon should fit inside the transmission window. However, as mentioned earlier, the reflection spectrum is smooth over the transmission bandwidth. Since the imaginary part is small, therefore $r = \sqrt{|R|}$ and consequently the reflection coefficient does not depend on the target photon frequency: $r(\delta, z_2) \simeq r(\delta_{res}, z_2)$. Hence, from Eq.(4.8), we will have

$$\phi_R(t,z_2) \simeq \phi_1(t)\phi(z_2)r(\delta_{res},z_2) \quad (4.9)$$

On the other hand, as pointed out earlier, $r(\delta_{res}, z_2)$ has a very smooth dependence on position around $z_2 = d/2$ and the reflection is nearly perfect, i.e. $r(\delta_{res}, z_2) \simeq 1$. Therefore, the target photon is entirely reflected and it is not entangled to the control photon.

4.4 Conclusions

We presented a scheme to perform a single-photon gate in a nonlinear optical fiber. For that, we evaluated the transport of a single photon in a nonlinear fiber where another photon is previously stored in form of an atomic spin excitation. In particular, by using the double-V level scheme, we avoided rapidly oscillating terms in atomic coherences and photon electric field. We showed that a high fidelity gate is achievable for large optical densities. In the end, separability and entanglement issues were discussed.

Chapter 5

Optical bistability at low light level due to collective atomic recoil

5.1 Intoduction

Motivated by potential applications to quantum information science [84, 114, 50, 142], there have been intense experimental efforts to realize strong nonlinear interactions between dilute atomic ensembles and weak optical fields. Methods to achieve such quantum nonlinear couplings in dissipation-free media have relied mainly on two approaches. First, the interaction time and the coupling between the atoms and the photons can be enhanced by placing the atoms within a high finesse cavity [134], an approach that comes at the expense of considerable experimental complexity and low bandwidth. Alternatively, near-resonant light propagating through optically dense media can also result in strong nonlinear interactions. In order to limit the dominant linear absorption, this latter approach requires the use of a coherent multiphoton

process such as EIT [113]. An added benefit of such a multiphoton process is the enhancement of the interaction time due to slow group velocities. However, since EIT relies on quantum interference between the internal states of an atom, it is fairly sensitive to inhomogenous optical and magnetic fields.

In this Letter, we demonstrate nonlinear optical effects due to the interaction between weak pulses of light and the collective motion of an ultracold slow-light medium. Using the motional degrees of freedom to create a highly dispersive gas alleviates the sensitivity to external fields. As shown in recent studies [168, 167], the implementation of a recoil-induced resonance (RIR) in an optically dense anisotropic gas allows for strong atom-light interaction due to the combination of slow group velocities and transverse confinement of the optical fields within the atomic medium. Due to this strong coupling, we observe optical bistability at input powers as low as 20 pW, an upper bound limited mainly by the photodetector efficiency.

The motion of delocalized atoms under the influence of two or more light fields can mediate the conversion of atomic kinetic energy into radiation [40]. These processes, termed 'recoil-induced resonances', can be described in terms of stimulated Raman transitions between different momentum classes of the atomic ensemble [73]. For an optically thin medium, the atom-light interaction has little effect on the momentum distribution of the gas and a perturbative analysis reveals that the probe field experiences weak absorption (gain) for positive (negative) detuning relative to the pump field.

In contrast, as the optical density of the atomic gas increases, the strong atom-light coupling leads to large optical gain [168] and significant effects on the momentum

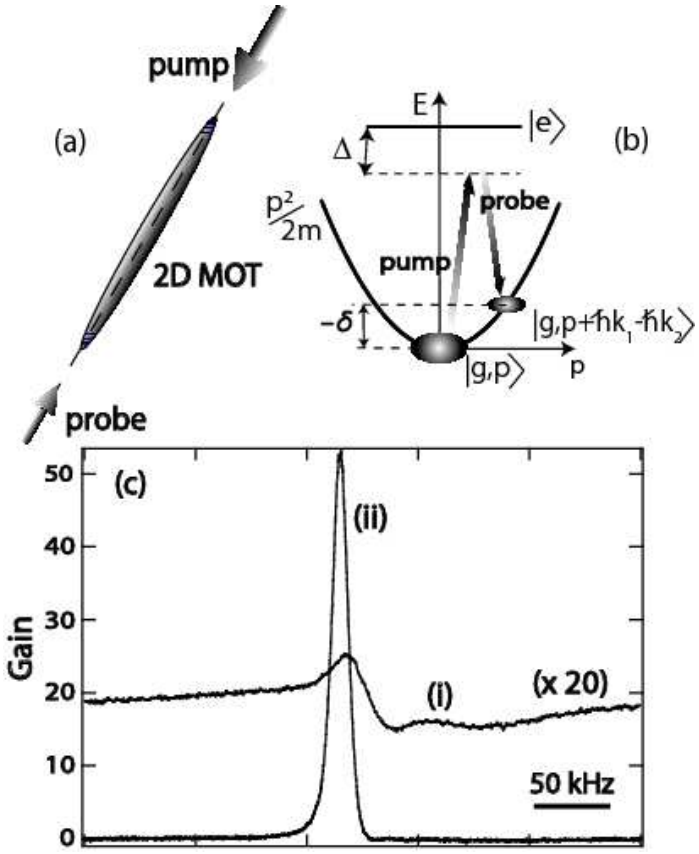

Figure 5.1: (a) Schematic indicating the pump and probe beams used for the RIR. (b) The energy levels relevent to the RIR. (c) Absorption spectrum of a probe beam around the RIR for longitudinal optical densities of ~ 10 (i) and ~ 40 (ii).

distribution of the atomic gas. The strong amplification of the probe field and its subsequent back-action on the collective motional states of the gain medium results in a nonlinear optical response even for weak incident beams. In this work, this back-action is evidenced by the observation of optical bistability in the probe transmission.

5.2 Experimental observation

The experimental scheme to create a strongly dispersive ultracold gas using the RIR is described in previous work [168]. About 5×10^8 ^{87}Rb atoms are confined in a highly anisotropic magneto-optic trap at typical temperatures of ~ 20 μK. In this trap, the atom cloud assumes the shape of a cylinder with approximate radial (longitudinal) extent of 200 μm (3 cm). The pump and probe beams for the RIR share the same linear polarization and are directed along the long axis of this cylinder to take advantage of the large optical depth (OD) along this axis. The Rabi frequency of the pump beam was typically $\Omega_1/\Gamma = 1.5$ where Γ is the natural linewidth of this transition. At low OD, the transmission spectrum of the RIR exhibits a characteristic dispersion-shaped spectrum with gain (absorption) for detuning $\delta < 0$ ($\delta > 0$). At higher OD, the probe is almost completely extinguished on the absorption side of the resonance leaving the gain peak as the only distinguishable feature (Fig. 1).

For an atomic gas with high OD, Fig. 2(a) shows the probe transmission as the pump-probe detuning is scanned across the RIR. Depending on the sign of this detuning chirp, there a shift in the resonance as well as in the maximum gain. This hysteretic nature of the transmission diminishes as the OD is lowered to less than ~ 10. At larger cooperativity, the atomic ensemble and the light fields form a strongly

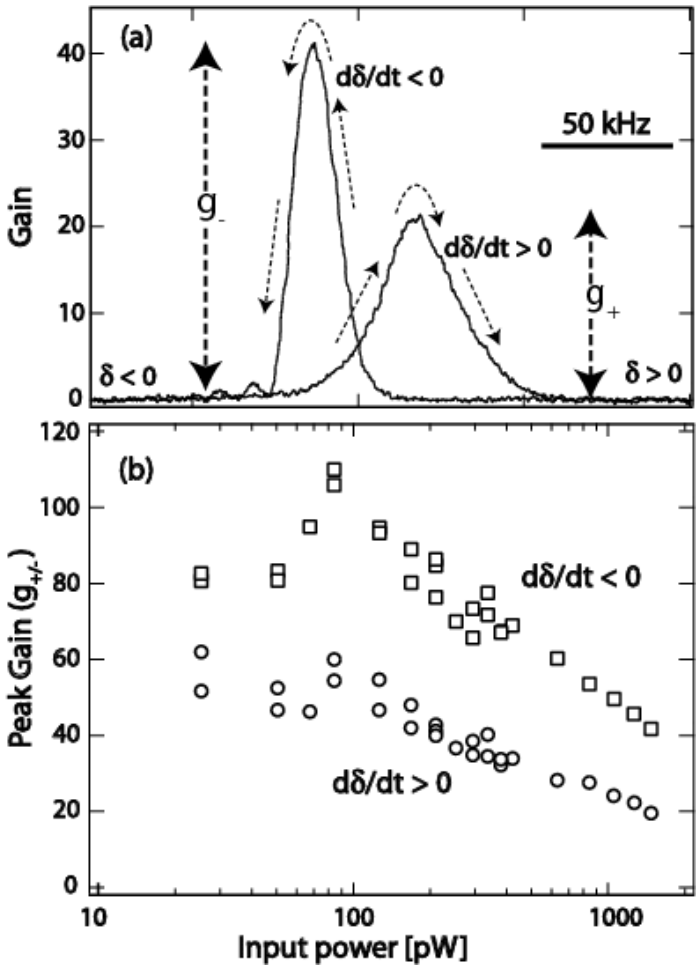

Figure 5.2: (a) Absorption bistability due to the interaction between the probe and the collective motion of the atomic gas. Depending on the sign of the detuning chirp ($d\delta/dt$), the transmission indicates a shift in both the resonance and the peak amplification (g_+, g_-). (b) Peak probe amplification indicates a bistable response down to the detection limit of the input probe power.

coupled system and the probe interacts with an atomic ensemble whose motional coherences and momentum distribution is the cumulative result of prior interactions with the light fields. As seen in Fig. 2(b), the bistable response ($g_-/g_+ > 1$) persists down to the detection limit (~ 20 pW) of the input probe power.

In order to understand this behavior, we first note that the amplification of the probe is accompanied by the transfer of atoms from a momentum p to a momentum $p + 2\hbar k$ (Fig. 1(b)). Thus, as the detuning is scanned across the gain side of the RIR, atoms at various momenta are brought into resonance with the light fields and transferred to higher momentum states. Crucially, in the case of a negative chirp ($d\delta/dt < 0$), these transferred atoms are brought *closer* to resonance with the light fields as the detuning is scanned. Thus, in this process, atoms are progressively swept up the momentum ladder due to the time-varying detuning, resulting in both an enhanced amplification and a shift in the location of the RIR. In contrast, for a positive chirp ($d\delta/dt > 0$), the atoms are transferred to states that are *farther* from resonance and the probe transmission resembles that obtained for a static thermal distribution.

5.3 Theoretical model

To quantitatively explain these observations, we use a theoretical model that describes two classical light fields that are coupled to the motional degrees of freedom of an elongated ensemble of two-level atoms. To mimic the experiment, the atoms are assumed to be tightly confined in the radial dimension. Accordingly, only the atomic momentum along the long axis is relevent and the Hamiltonian can be written as

[118]

$$\begin{aligned}\mathcal{H} &= \sum_k [\frac{\hbar^2 k^2}{2m} c_g(k)^\dagger c_g(k) + (\frac{\hbar^2 k^2}{2m} + \hbar\omega_0) c_e(k)^\dagger c_e(k) \\ &\quad + i\hbar \sum_{j=1,2} (g_j a_j^* e^{i\omega_j t} c_g(k-k_j)^\dagger c_e(k) - h.c.)] \end{aligned} \tag{5.1}$$

where $c_g(k)(c_e(k))$ are the annihilation operators of ground (excited) state atoms with momentum $\hbar k$, ω_0 is the transition frequency of the two-level atoms, $g_1(g_2)$ is the atom-light coupling coefficient and $a_1(a_2)$ is the normalized electric field of the pump (probe) beams. In the far-detuned limit, the excited states can be adiabatically eliminated and the equation for the coherences and populations of the different momentum classes in the ground state are

$$\begin{aligned} & \frac{d}{dt}\rho(p,p') = 4i\omega_r(p'^2 - p^2)\rho(p,p') \\ + \;& i\frac{g_1 g_2 a_1^*}{\Delta} a_2 e^{-i\delta t}(\rho(p+1,p') - \rho(p,p'-1)) \\ + \;& i\frac{g_1 g_2 a_1}{\Delta} a_2^* e^{+i\delta t}(-\rho(p,p'+1) + \rho(p-1,p')) \end{aligned} \tag{5.2}$$

where $\rho(p,p') \equiv \langle c_g^\dagger(k') c_g(k)\rangle$, ω_r is the recoil frequency and $\delta = \omega_2 - \omega_1$ is the detuning. Also, using the slowly-varying envelope and single-mode approximations, the evolution of the probe amplitude can be written as

$$\frac{d}{dt}a_2 = iN\frac{g_1 g_2}{\Delta} a_1 e^{i\delta t} \sum_p \rho(p-1,p) - \frac{\kappa}{2}(a_2 - a_{in}). \tag{5.3}$$

Retaining only first-order coherence terms between momentum classes, the above equations can be written as a set of coupled equations for the population $\Pi_p = \rho(p,p)$, the first-order coherence $\eta_p \equiv \rho(p+1,p)e^{i\delta t}$ and the probe amplitude a_2.

$$\dot{\Pi}_p = [-i\beta^* a_2(-\eta_p + \eta_{p-1}) + c.c.] - \gamma_{pop}(\Pi_p - \Pi_{th,p})$$

$$\begin{aligned}
\dot{\eta}_p &= i(4\omega_r(p^2-(p+1)^2)-\delta(t)+i\gamma_{coh})\eta_p \\
&- i\beta a_2^*(\Pi_{p+1}-\Pi_p) \\
\dot{a}_2 &= i\beta N\sum_p \eta_{p-1}^* - \frac{\kappa}{2}(a_2-a_{in})
\end{aligned} \tag{5.4}$$

where $\gamma_{pop}(\gamma_{coh})$ are the population (coherence) relaxation rates respectively and $\beta = g_1 g_2 a_1/\Delta$. The thermal population distribution $\Pi_{th,p}$ is given by Maxwell-Boltzman distribution. The decay rate of photons is approximated by the free-space rate $\kappa = c/L$ with L the longitudinal extent of the atomic gas. These coupled equations describe the rich dynamics that ensue as a consequence of the collective atom-light interaction and a time-dependent pump-probe detuning.

5.4 Comparison between the model and the experiment

Numerical simulations of the bistability based on this model show excellent agreement with the experimental results over a wide range of parameters of pump detuning and chirp rate (Fig. 3). In these simulations, parameters such as the pump detuning, OD of the atomic gas and scan rate of the two-photon detuning were held fixed at the experimental values.

The observation of a bistable transmission requires that the momentum coherences established as a result of the atom-light interaction persist as the detuning is scanned across the RIR. In practice, off-resonant light scattering causes the thermalization of the momentum distribution thereby suppressing the bistability. This competing process leads to a limiting rate for the scan rate ($d\delta/dt$) below which the atomic

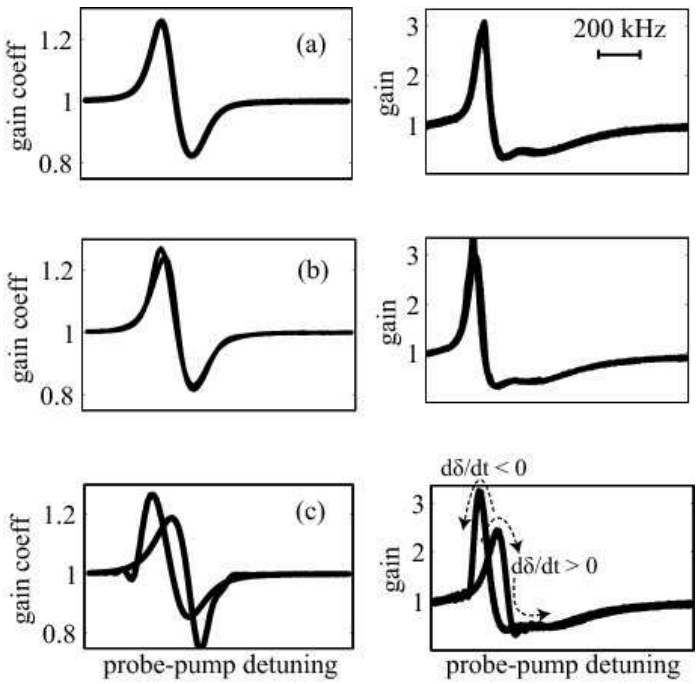

Figure 5.3: Numerical simulations based on the theoretical model match the experimental results over a wide range of parameters. Panels on the left show the numerical simulations for the gain coefficient given by $exp(-2Re[\alpha]L)$ where α is the absorption coefficient and panels on the right show the observed experimental gain of the probe transmission across the RIR, both versus two-photon detuning.(a), (b) and (c) correspond to transmission spectra obtained by chirping the two-photon detuning at scan rates of 0.1, 0.5 and 2.5 MHz/ms, respectively.

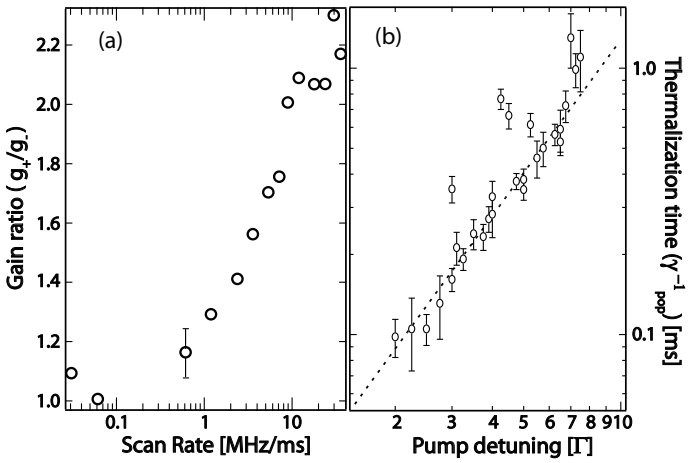

Figure 5.4: (a) The ratio of peak gain (g_-/g_+) indicates a limiting scan rate $d\delta/dt \approx 0.5$ MHz/ms below which decoherence and thermalization of the momentum distribution suppress optical bistability. This data was obtained at a pump detuning $\Delta \sim -4\,\Gamma$. (b) Thermalization time (γ_{pop}^{-1}) *vs* the pump detuning. A fit to the data (dashed line) indicates a power-law dependence $\gamma_{pop}^{-1} \propto \Delta^{\alpha}$ with $\alpha = 1.57 \pm 0.09$.

momentum distribution is quasi-static and the transmission becomes non-hysteretic (Fig. 4(a)). A bistable transmission was observed for scan rates as low as 500 kHz/ms, corresponding to moving across the RIR in 100 μs, much longer than the mean photon scattering time of $< 1\,\mu$s. This observation of long-lived momentum coherences is consistent with previous studies of the RIR [104, 40].

An independent measure of the influence of off-resonant scattering on the probe transmission was obtained by determining the thermalization time (γ_{pop}^{-1}) of the atomic momentum distribution. For this, the probe was switched on for 100 ms at an intensity of 0.1 mW/cm^2 and at a two-photon detuning that corresponded to the peak gain of the RIR. The probe intensity was then reduced to $\sim 10^{-3}$ mW/cm^2 within a few microseconds. Following this reduction in intensity, the probe transmission indicated a gain that was initially very small but gradually relaxed to a higher equilibrium value. This relaxation was interpreted as being due to the thermalization of the

momentum distribution to repopulate those states that were depleted due to the initially intense probe. Under the assumption that the final probe intensity was too small to significantly modify the atomic distribution, the time scale over which the probe transmission reaches a steady state should reflect the thermalization time. Consistent with the observation of bistability at relatively slow scan rates, we measure thermalization times on the order of a few hundred microseconds (Fig. 4(b)).

The numerical simulations used the measured value of γ_{pop} (Fig. 4(b)) while allowing the value of γ_{coh} to vary. In order to obtain the best match with the experimental results, we typically found that γ_{coh} was required to be greater than γ_{pop}. However, both quantities were much smaller than the photon scattering rate. This suppression is in agreement with earlier observations [170, 40, 104, 39]. A possible explanation lies in the fact that in the presence of an optical potential ($U \propto 1/\Delta$), in the limit of large detuning, both γ_{coh} and γ_{pop} can be suppressed due to Lamb-Dicke confinement. The estimated scaling of the suppressed decay rate with the detuning should be $\gamma_{eff} \propto \gamma_{scatt}/\sqrt{U} \propto \Delta^{-3/2}$ where γ_{scatt} is the photon scattering rate. The experimental data (Fig. 4(b)) also suggests a similar scaling(1.57 ± 0.09).

The observation of optical bistability at low input powers suggests prospects of all-optical control using weak pulses of light. For instance, this scheme lends itself rather easily to a low light level all-optical switch wherein the detuning of a few-photon probe is controlled in order to switch a more intense output beam. The largest scan rates, $d\delta/dt = 30$ MHz/ms at which bistability was observed and typical values of the momentum coherence time $\gamma_{coh}^{-1} \sim 100\,\mu$s together yield an estimate of the switching time $\tau = \gamma_{coh}/(d\delta/dt) = 0.3\ \mu$s. This is commensurate with previous measurements

of all-optical switching using a RIR [168]. Combining this with the lowest probe powers ($P \sim 20$ pW) and typical beam waists (100 μm) used in this work, we obtain a typical photon number $\tau P/(hc/\lambda) \sim 25$ and a remarkably low switching energy density [42, 180] of 7×10^{-5} photons/$(\lambda^2/2\pi)$ to operate this all-optical switch.

5.5 Conclusions

In conclusion, we demonstrate optical nonlinearities due to a coherent interaction between weak light fields and the collective motion of a strongly dispersive atomic gas. Since the atomic momentum is relatively insensitive to external magnetic or electric fields, such systems may be promising candidates for applications in low-light level nonlinear optics including the robust generation of correlated photons [160] and quantum memories [146]. Further, there is a close connection between the phenomenon discussed here and collective atomic recoil effects inside a cavity such as spontaneous self-organization of the atomic medium [89], collective recoil lasing [105] and and the generation of atom-photon entanglement [130].

Bibliography

[1] J Abo-Shaeer, C Raman, J Vogels, and W Ketterle. Observation of vortex lattices in bose-einstein condensates. *Science*, 292(5516):476, Apr 2001.

[2] A Abrikosov. Magnetic properties of superconductors of the second group. *Sov. Phys.-JETP*, 5:1174, Jan 1957.

[3] A V Akimov, A Mukherjee, C L Yu, D E Chang, A S Zibrov, P R Hemmer, H Park, and M D Lukin. Generation of single optical plasmons in metallic nanowires coupled to quantum dots. *Nature*, 450(7168):402–406, 2008.

[4] Ehud Altman, Eugene Demler, and Mikhail D Lukin. Probing many-body states of ultracold atoms via noise correlations. *Physical Review A*, 70(1):013603, Jul 2004.

[5] P Anderson. The resonating valence bond state in la2cuo4 and superconductivity. *Science*, 235(4793):1196, Mar 1987.

[6] A André. Nonclassical states of light and atomic ensembles: generation and new applications. *Ph. D. Thesis*, Jan 2005.

[7] A André, M Bajcsy, A S Zibrov, and M D Lukin. Nonlinear optics with stationary pulses of light. *Phys. Rev. Lett.*, 94(6):063902, 2005.

[8] A André and M D Lukin. Manipulating light pulses via dynamically controlled photonic band gap. *Phys. Rev. Lett.*, 89(14):143602–143602, Sep 2002.

[9] M Atatüre, J Dreiser, A Badolato, and A Imamoglu. Observation of faraday rotation from a single confined spin. *Nature Physics*, 3:101–106, Jan 2007.

[10] J E Avron, R Seiler, and B Simon. Homotopy and quantization in condensed matter physics. *Phys. Rev. Lett.*, 51(1):51–53, Jul 1983.

[11] M Bajcsy, S Hofferberth, V Balic, T Peyronel, M Hafezi, A. S Zibrov, V Vuletic, and M. D Lukin. Efficient all-optical switching using slow light within a hollow fiber. *Physical Review Letters*, 102(20):203902, May 2009.

[12] M Bajcsy, A S Zibrov, and M D Lukin. Stationary pulses of light in an atomic medium. *Nature*, 426(6967):638, Dec 2003.

[13] Leon Balents, Lorenz Bartosch, Anton Burkov, Subir Sachdev, and Krishnendu Sengupta. Putting competing orders in their place near the mott transition. *Phys. Rev. B*, 71(14):144508, Apr 2005.

[14] M A Baranov, Klaus Osterloh, and M Lewenstein. Fractional quantum hall states in ultracold rapidly rotating dipolar fermi gases. *Phys. Rev. Lett.*, 94(7):070404, Feb 2005.

[15] J Bardeen, L. N Cooper, and J. R Schrieffer. Microscopic theory of superconductivity. *Physical Review*, 106(1):162–164, Apr 1957.

[16] J. G Bednorz and K Muller. Possible high tc superconductivity in the ba-la-cu-o system. *Z. Physik B - Condensed Matter*, 64(2):189–193, Jun 1986.

[17] J Bellissard, A Van Elst, and H Schulz Baldes. The noncommutative geometry of the quantum hall effect. *J. MATH. PHYS.*, 35(10):5373, Jan 1994.

[18] F Benabid, J C Knight, G Antonopoulos, and P St J Russell. Stimulated raman scattering in hydrogen-filled hollow-core photonic crystal fiber. *Science*, 298(5592):399–402, 2002.

[19] P R Berman. Comparison of recoil-induced resonances and the collective atomic recoil laser. *Physical Review A*, 59(1):585–596, Jan 1999.

[20] Paul R Berman, editor. *Cavity Quantum Electrodynamics (Advances in Atomic, Molecular and Optical Physics)*. Academic Press, 1994.

[21] M V Berry. Quantal phase factors accompanying adiabatic changes. *Proc. R. Soc. A*, 382:45, 1984.

[22] Rajiv Bhat, M Krämer, J Cooper, and M J Holland. Hall effects in bose-einstein condensates in a rotating optical lattice. *Phys. Rev. A*, 76(4):043601, Oct 2007.

[23] K M Birnbaum, A Boca, R Miller, A D Boozer, T E Northup, and H J Kimble. Photon blockade in an optical cavity with one trapped atom. *Nature*, 436(7047):87–90, 2005.

[24] P Blakie, R Ballagh, and C Gardiner. Theory of coherent bragg spectroscopy of a trapped bose-einstein condensate. *Physical Review A*, 65(3):033602, Jan 2002.

[25] I Bloch, J Dalibard, and W Zwerger. Many-body physics with ultracold gases. *Reviews of Modern Physics*, 80(3):885–964, 2008.

[26] A Bohm, A Mostafazdeh, H Koizumi, Q Niu, and J Zwanziger. *The Geometric Phase in Quantum Systems: Foundations, Mathematical Concepts, and Applications in Molecular and Condensed Matter Physics*. Springer, 2003.

[27] Robert W. Boyd. *Nonlinear optics*. Academic Press, Jan 2008.

[28] Vincent Bretin, Sabine Stock, Yannick Seurin, and Jean Dalibard. Fast rotation of a bose-einstein condensate. *Phys. Rev. Lett.*, 92(5):050403, Feb 2004.

[29] A Brunello, F Dalfovo, L Pitaevskii, S Stringari, and F Zambelli. Momentum transferred to a trapped bose-einstein condensate by stimulated light scattering. *Phys. Rev. A*, 64(6):063608, Nov 2001.

[30] V L Bulatov. Ground state and excitations of a one-dimensional bose gas on a finite interval. *Theoretical and Mathematical Physics*, 75(1):433–439, 1988.

[31] Pasquale Calabrese and Jean-Sébastien Caux. Correlation functions of the one-dimensional attractive bose gas. *Phys. Rev. Lett.*, 98(15):150403, 2007.

[32] F E Camino, W Zhou, and V J Goldman. Transport in the laughlin quasiparticle interferometer: Evidence for topological protection in an anyonic qubit. *Phys. Rev. B*, 74(11):115301, Sep 2006.

[33] F E Camino, Wei Zhou, and V J Goldman. Aharonov-bohm superperiod in a laughlin quasiparticle interferometer. *Phys. Rev. Lett.*, 95(24):246802, Dec 2005.

[34] Gretchen Campbell, Jongchul Mun, Micah Boyd, Patrick Medley, Aaron Leanhardt, Luis Marcassa, David Pritchard, and Wolfgang Ketterle. Imaging the mott insulator shells by using atomic clock shifts. *Science*, 313(5787):649, Aug 2006.

[35] T Chakraborty and P. Pietilainen. *The Quantum Hall Effects: Fractional and Integral*. Springer, 1996.

[36] D E Chang, V Gritsev, G Morigi, V Vuletic, M D Lukin, and E A Demler. Crystallization of strongly interacting photons in a nonlinear optical fibre. *Nature Physics*, 4(11):884, Sep 2008.

[37] Darrick E Chang, Anders S Sørensen, Eugene A Demler, and Mikhail D Lukin. A single-photon transistor using nanoscale surface plasmons. *Nat. Phys.*, 3(11):807–812, 2007.

[38] N R Cooper, N K Wilkin, and J M F Gunn. Quantum phases of vortices in rotating bose-einstein condensates. *Physical Review Letters*, 87(12):120405, Aug 2001.

[39] J.-Y Courtois and G Grynberg. Probe transmission in one-dimensional optical molasses: Theory for linearly cross-polarized cooling beams. *Physical Review A*, 46(11):7060–7078, Dec 1992.

[40] J.-Y Courtois, G Grynberg, B Lounis, and P Verkerk. Recoil-induced resonances in cesium: An atomic analog to the free-electron laser. *Physical Review Letters*, 72(19):3017–3020, May 1994.

[41] Maxime Ben Dahan, Ekkehard Peik, Jakob Reichel, Yvan Castin, and Christophe Salomon. Bloch oscillations of atoms in an optical potential. *Phys. Rev. Lett.*, 76(24):4508–4511, Jun 1996.

[42] Andrew Dawes, Lucas Illing, Susan Clark, and Daniel Gauthier. All-optical switching in rubidium vapor. *Science*, 308(5722):672, Apr 2005.

[43] I H Deutsch, R J C Spreeuw, S L Rolston, and W D Phillips. Photonic band gaps in optical lattices. *Phys. Rev. A*, 52(2):1394–1410, Aug 1995.

[44] Peter Domokos, Peter Horak, and Helmut Ritsch. Quantum description of light-pulse scattering on a single atom in waveguides. *Phys. Rev. A*, 65(3):033832, Mar 2002.

[45] Elizabeth A Donley, Neil R Claussen, Sarah T Thompson, and Carl E Wieman. Atom-molecule coherence in a bose-einstein condensate. *Nature*, 417(6888):529, May 2002.

[46] Russell J. Donnelly. *Quantized vortices in helium II.* Cambridge University Press, Jan 1991.

[47] T Dorlas. Orthogonality and completeness of the bethe ansatz eigenstates of the nonlinear schroedinger model. *Communications in Mathematical Physics*, Jan 1993.

[48] P D Drummond, R M Shelby, S R Friberg, and Y Yamamoto. Quantum solitons in optical fibres. *Nature*, 365(6444):307–313, 1993.

[49] Peter Drummond. Lecture notes: Quantum theory of nonlinear optics. http://www.physics.uq.edu.au/people/drummond/NOTES/lecture.pdf, 2001.

[50] L M Duan, L M Duan, M D Lukin, M D Lukin, J I Cirac, J I Cirac, P Zoller, and P Zoller. Long-distance quantum communication with atomic ensembles and linear optics. *Nature*, 414(6862):413, Nov 2001.

[51] L-M Duan and H J Kimble. Scalable photonic quantum computation through cavity-assisted interactions. *Phys. Rev. Lett.*, 92(12):127902, 2004.

[52] Stephan Dürr, Thomas Volz, Andreas Marte, and Gerhard Rempe. Observation of molecules produced from a bose-einstein condensate. *Phys. Rev. Lett.*, 92:020406, 2004.

[53] L Fallani, C Fort, N Piovella, M Cola, F. S Cataliotti, M Inguscio, and R Bonifacio. Collective atomic recoil in a moving bose-einstein condensate: From superradiance to bragg scattering. *Physical Review A*, 71(3):033612, Mar 2005.

[54] M Fleischhauer and M D Lukin. Dark-state polaritons in electromagnetically induced transparency. *Phys. Rev. Lett.*, 84(22):5094–5097, May 2000.

[55] Michael Fleischhauer and Jonathan P Marangos. Electromagnetically induced transparency: Optics in coherent media. *Reviews of Modern Physics*, 77(2):633–673, Jul 2005.

[56] Michael Fleischhauer, Johannes Otterbach, and Razmik G Unanyan. Bose-einstein condensation of stationary-light polaritons. *Physical Review Letters*, 101(16):163601, Oct 2008.

[57] S Folling, Fabrice Gerbier, Artur Widera, Olaf Mandel, Tatjana Gericke, and Immanuel Bloch. Spatial quantum noise interferometry in expanding ultracold atom clouds. *Nature*, 434(7032):481, Mar 2005.

[58] Edwardo Fradkin. *Field Theories of Condensed Matter System*. Westview Press, 1991.

[59] Ilya Fushman, Dirk Englund, Andrei Faraon, Nick Stoltz, Pierre Petroff, and Jelena Vuckovic. Controlled phase shifts with a single quantum dot. *Science*, 320(5877):769–772, 2008.

[60] C W Gardiner and M J Collett. Input and output in damped quantum systems: Quantum stochastic differential equations and the master equation. *Phys. Rev. A*, 31(6):3761–3774, Jun 1985.

[61] M Gaudin. *La Fonction d'onde de Bethe*. Collection du Commissariat à l'énergie atomique. Série scientifique, Paris, Jan 1983.

[62] Jordan M Gerton, Dmitry Strekalov, Ionut Prodan, and Randall G Hulet. Direct observation of growth and collapse of a bose-einstein condensate with attractive interactions. *Nature*, 408(6813):692, Dec 2000.

[63] Saikat Ghosh, Jay E Sharping, Dimitre G Ouzounov, and Alexander L Gaeta. Resonant optical interactions with molecules confined in photonic band-gap fibers. *Physical Review Letters*, 94(9):093902, 2005.

[64] Vitalii L Ginzburg. Superconductivity and superfluidity (what was done and what was not). *Physics-Uspekhi*, 40:407, Apr 1997.

[65] Stefano Giovanazzi, Axel Görlitz, and Tilman Pfau. Tuning the dipolar interaction in quantum gases. *Phys. Rev. Lett.*, 89(13):130401, Sep 2002.

[66] M Girardeau. Relationship between systems of impenetrable bosons and fermions in one dimension. *J. MATH. PHYS.*, 1(6):516–523, 1960.

[67] S M Girvin. Off-diagonal long-range order, oblique confinement, and the fractional quantum hall effect. *Physical Review Letters*, 58(12):1252–1255, Mar 1987.

[68] S M Girvin, A H MacDonald, and P M Platzman. Magneto-roton theory of collective excitations in the fractional quantum hall effect. *Phys. Rev. B*, 33(4):2481–2494, 1986.

[69] Philippe Grangier, Daniel F Walls, and Klaus M Gheri. Comment on ıstrongly interacting photons in a nonlinear cavityȷ. *Phys. Rev. Lett.*, 81(13):2833, Sep 1998.

[70] Andrew D Greentree, Charles Tahan, Jared H Cole, and Lloyd C L Hollenberg. Quantum phase transitions of light. *Nat Phys*, 2(12):856–861, 2006.

[71] Markus Greiner, Olaf Mandel, Tilman Esslinger, T Hansch, and Immanuel Bloch. Quantum phase transition from a superfluid to a mott insulator in a gas of ultracold atoms. *Nature*, 415(6867):39, Jan 2002.

[72] Axel Griesmaier, Jörg Werner, Sven Hensler, Jürgen Stuhler, and Tilman Pfau. Bose-einstein condensation of chromium. *Phys. Rev. Lett.*, 94(16):160401, Apr 2005.

[73] J Guo, P. R Berman, and B Dubetsky. Recoil-induced resonances in nonlinear spectroscopy. *Physical Review A*, 46(3):1426–1437, Aug 1992.

[74] M Hafezi, D E Chang, V Gritsev, E A Demler, and M D Lukin. Photonic quantum transport in a nonlinear optical fiber. *in prepration*, 2009.

[75] Mohammad Hafezi, Anders S Sørensen, Eugene A Demler, and Mikhail D Lukin. Fractional quantum hall effect in optical lattices. *Phys Rev A*, 76(2):023613, Jan 2007.

[76] F D M Haldane. Finite-size studies of the incompressible state of the fractionally quantized hall effect and its excitations. *Phys. Rev. Lett.*, 54(3):237–240, Jan 1985.

[77] F D M Haldane. Many-particle translational symmetries of two-dimensional electrons at rational landau-level filling. *Phys. Rev. Lett.*, 55(20):2095–2098, Nov 1985.

[78] S. E Harris and Y Yamamoto. Photon switching by quantum interference. *Physical Review Letters*, 81(17):3611–3614, Oct 1998.

[79] Michael J Hartmann, Fernando G S L Brandao, and Martin B Plenio. Strongly interacting polaritons in coupled arrays of cavities. *Nat. Phys.*, 2(12):849–855, 2006.

[80] Y Hatsugai. Characterization of topological insulators: Chern numbers for ground state multiplet. *Journal of the Physical Society of Japan*, 74:1374–1377, 2005.

[81] DR Hofstadter. Energy levels and wave functions of bloch electrons in rational and irrational magnetic fields. *Phys. Rev. B*, 14(6):2239–2249, 1976.

[82] Christina J Hood, H J Kimble, and Jun Ye. Characterization of high-finesse mirrors: Loss, phase shifts, and mode structure in an optical cavity. *Phys. Rev. A*, 64(3):033804, Aug 2001.

[83] J Hwang, M Pototschnig, R Lettow, G Zumofen, A Renn, S Gotzinger, and V Sandoghdar. A single-molecule optical transistor. *Nature*, 460(7251):76, Jul 2009.

[84] A Imamoğlu, H Schmidt, G Woods, and M Deutsch. Strongly interacting photons in a nonlinear cavity. *Phys. Rev. Lett.*, 79(8):1467–1470, Aug 1997.

[85] A Imamoğlu, H Schmidt, G Woods, and M Deutsch. Erratum: Strongly interacting photons in a nonlinear cavity [phys. rev. lett. 79, 1467 (1997)]. *Phys. Rev. Lett.*, 81(13):2836, Sep 1998.

[86] Atac Imamoğlu and Yoshihisa Yamamoto. *Mesoscopic Quantum Optics*. Wiley-Interscience, 1999.

[87] D Jaksch, C Bruder, J I Cirac, C W Gardiner, and P Zoller. Cold bosonic atoms in optical lattices. *Phys. Rev. Lett.*, 81(15):3108–3111, Oct 1998.

[88] D Jaksch and P Zoller. Creation of effective magnetic fields in optical lattices: the hofstadter butterfly for cold neutral atoms. *New J. Phys.*, 5:Art. No. 56, 2003.

[89] J Javaloyes, M Perrin, G. L Lippi, and A Politi. Self-generated cooperative light emission induced by atomic recoil. *Physical Review A*, 70(2), Aug 2004.

[90] F X Kärtner and H A Haus. Quantum-mechanical stability of solitons and the correspondence principle. *Phys. Rev. A*, 48(3):2361–2369, Sep 1993.

[91] N Katz, R Ozeri, J Steinhauer, N Davidson, C Tozzo, and F Dalfovo. High sensitivity phonon spectroscopy of bose-einstein condensates using matter-wave interference. *Phys. Rev. Lett.*, 93(22):220403, Nov 2004.

[92] Jacob B. Khurgin and Rodney S. Tucker, editors. *Slow Light: Science and Applications*. CRC, Jan 2008.

[93] Fam Le Kien and K Hakuta. Correlations between photons emitted by multiatom fluorescence into a nanofiber. *Phys. Rev. A*, 77(3):033826, Mar 2008.

[94] T Kinoshita, T Wenger, and DS Weiss. Observation of a one-dimensional tonks-girardeau gas. *Science*, 305(5687):1125–1128, 2004.

[95] A Kitaev. Fault-tolerant quantum computation by anyons. *Annals of Physics*, 303(1):2–30, Jan 2003.

[96] A Kitaev. Anyons in an exactly solved model and beyond. *Annals of Physics*, 321(1):2–111, Jan 2006.

[97] K. V Klitzing and M Pepper. New method for high-accuracy determination of the fine-structure constant based on quantized hall resistance. *Physical Review Letters*, 45(6):494–497, Aug 1980.

[98] Jonathan C Knight and Jonathan C Knight. Photonic crystal fibres. *Nature*, 424(6950):847, Aug 2003.

[99] M Kohmoto. Topological invariant and the quantization of the hall conductance. *Annals of Physics*, 160(2):343–354, Jan 1985.

[100] Takeo Kojima. Ground-state correlation functions for an impenetrable bose gas with neumann or dirichlet boundary conditions. *Journal of Statistical Physics*, 88(3):713–743, 1997.

[101] A Kol and N Read. Fractional quantum hall effect in a periodic potential. *Phys. Rev. B*, 48(12):8890–8898, Sep 1993.

[102] O Kolevatova. Guiding high-intensity laser pulses through hollow fibers: self-phase modulation and cross-talk of guided modes. *Optics Communications*, 217(1-6):169–177, Mar 2003.

[103] V E Korepin, N M Bogoliubov, and A G Izergin. *Quantum Inverse Scattering Method and Correlation Functions*. Cambridge University Press, 1993.

[104] M Kozuma, Y Imai, K Nakagawa, and M Ohtsu. Observation of a transient response of recoil-induced resonance: A method for the measurement of atomic motion in an optical standing wave. *Physical Review A*, 52(5):R3421–R3424, Nov 1995.

[105] D Kruse, C Von Cube, C Zimmermann, and Ph. W Courteille. Observation of lasing mediated by collective atomic recoil. *Physical Review Letters*, 91(18), Oct 2003.

[106] Y Lai and H A Haus. Quantum theory of solitons in optical fibers. i. time-dependent hartree approximation. *Phys. Rev. A*, 40(2):844–853, Jul 1989.

[107] Y Lai and H. A Haus. Quantum theory of solitons in optical fibers. ii. exact solution. *Physical Review A*, 40(2):854–866, Jul 1989.

[108] R B Laughlin. Anomalous quantum hall effect: An incompressible quantum fluid with fractionally charged excitations. *Phys. Rev. Lett.*, 50(18):1395–1398, May 1983.

[109] R. B Laughlin. Quantized motion of three two-dimensional electrons in a strong magnetic field. *Phys. Rev. B*, 27(6):3383–3389, Mar 1983.

[110] Patrick A Lee and Xiao-Gang Wen. Doping a mott insulator: Physics of high-temperature superconductivity. *Reviews of Modern Physics*, 78(1):17–85, Jan 2006.

[111] Elliott H Lieb and Werner Liniger. Exact analysis of an interacting bose gas. i. the general solution and the ground state. *Phys. Rev.*, 130(4):1605–1616, May 1963.

[112] H. Y Ling, L Baksmaty, and N. P Bigelow. Theory of a collective atomic recoil laser. *Physical Review A*, 63(5):053810, Apr 2001.

[113] M. D Lukin. Colloquium: Trapping and manipulating photon states in atomic ensembles. *Reviews of Modern Physics*, 75(2):457–472, Apr 2003.

[114] M. D Lukin, A. B Matsko, M Fleischhauer, and M. O Scully. Quantum noise and correlations in resonantly enhanced wave mixing based on atomic coherence. *Physical Review Letters*, 82(9):1847–1850, Mar 1999.

[115] Mikhail D Lukin, Michael Fleischhauer, Marlan O Scully, and Vladimir L Velichansky. Intracavity electromagnetically induced transparency. *Opt. Lett.*, 23(4):295–297, 1998.

[116] Olaf Mandel, Markus Greiner, Artur Widera, Tim Rom, TW Hansch, and Immanuel Bloch. Controlled collisions for multi-particle entanglement of optically trapped atoms. *Nature*, 425(6961):937, Oct 2003.

[117] C Menotti, M Krämer, L Pitaevskii, and S Stringari. Dynamic structure factor of a bose-einstein condensate in a one-dimensional optical lattice. *Phys. Rev. A*, 67(5):053609, May 2003.

[118] M. G Moore and P Meystre. Effects of atomic diffraction on the collective atomic recoil laser. *Physical Review A*, 58(4):3248–3258, Oct 1998.

[119] Erich J Mueller. Artificial electromagnetism for neutral atoms: Escher staircase and laughlin liquids. *Phys. Rev. A*, 70(4):041603, Oct 2004.

[120] S R Muniz, D S Naik, and C Raman. Bragg spectroscopy of vortex lattices in bose-einstein condensates. *Phys. Rev. A*, 73(4):041605, Apr 2006.

[121] K P Nayak, K P Nayak, P N Melentiev, P N Melentiev, M Morinaga, M Morinaga, Fam Le Kien, Fam Le Kien, V I Balykin, V I Balykin, K Hakuta, and K Hakuta. Optical nanofiber as an efficient tool for manipulating and probing atomic fluorescence. *Optics Express*, 10(5):053003, May 2008.

[122] Qian Niu, D J Thouless, and Yong-Shi Wu. Quantized hall conductance as a topological invariant. *Phys. Rev. B*, 31(6):3372–3377, Mar 1985.

[123] H Onnes. Investigations into the properties of substances at low temperatures, which have led, amongst other things, to the prepration of liquid helium. *Nobel Lecture*, Jan 1913.

[124] Masaki Oshikawa and T Senthil. Fractionalization, topological order, and quasiparticle statistics. *Phys. Rev. Lett.*, 96(6):060601, Feb 2006.

[125] Roee Ozeri, Jeff Steinhauer, Nadav Katz, and Nir Davidson. Direct observation of the phonon energy in a bose-einstein condensate by tomographic imaging. *Phys. Rev. Lett.*, 88(22):220401, May 2002.

[126] R N Palmer and D Jaksch. High-field fractional quantum hall effect in optical lattices. *Phys. Rev. Lett.*, 96(18):180407, May 2006.

[127] B Parades et al. Tonks-girardeau gas of ultracold atoms in an optical lattice. *Nature(London)*, 429(6989):277–281, 2004.

[128] B Paredes, P Fedichev, J I Cirac, and P Zoller. 1/2-anyons in small atomic bose-einstein condensates. *Phys. Rev. Lett.*, 87(1):010402, Jun 2001.

[129] R E Peierls. Zur theorie des diamagnetismus von leitungselektronen. *Z. Phys. Rev.*, 80:763, 1933.

[130] N Piovella, M Cola, and R Bonifacio. Quantum fluctuations and entanglement in the collective atomic recoil laser using a bose-einstein condensate. *Physical Review A*, 67(1), Jan 2003.

[131] N Piovella, M Gatelli, and R Bonifacio. Quantum effects in the collective light scattering by coherent atomic recoil in a bose–einstein condensate. *Optics Communications*, 194:167–173, Jan 2001.

[132] M Popp, B Paredes, and J I Cirac. Adiabatic path to fractional quantum hall states of a few bosonic atoms. *Phys. Rev. A*, 70(5):053612, Nov 2004.

[133] Richard E Prange, Steven M Girvin, and Marvin E Cage. *The Quantum Hall Effect*. Springer-Verlag, 1986.

[134] J M Raimond, M Brune, and S Haroche. Manipulating quantum entanglement with atoms and photons in a cavity. *Rev. Mod. Phys.*, 73(3):565–582, Aug 2001.

[135] K Rapedius and H. J Korsch. Barrier transmission for the one-dimensional nonlinear schrödinger equation: Resonances and transmission profiles. *Physical Review A*, 77(6):063610, Jun 2008.

[136] N Read and E Rezayi. Quasiholes and fermionic zero modes of paired fractional quantum hall states: The mechanism for non-abelian statistics. *Phys. Rev. B*, 54(23):16864–16887, Dec 1996.

[137] N Read and E Rezayi. Beyond paired quantum hall states: Parafermions and incompressible states in the first excited landau level. *Phys. Rev. B*, 59(12):8084–8092, Mar 1999.

[138] Ana Maria Rey, P Blair Blakie, Guido Pupillo, Carl J Williams, and Charles W Clark. Bragg spectroscopy of ultracold atoms loaded in an optical lattice. *Phys. Rev. A*, 72(2):023407, Aug 2005.

[139] E H Rezayi. Incompressible states of the fractionally quantized hall effect in the presence of impurities: A finite-size study. *Phys. Rev. B*, 32(10):6924–6927, Nov 1985.

[140] E H Rezayi, F D M Haldane, and Kun Yang. Charge-density-wave ordering in half-filled high landau levels. *Phys. Rev. Lett.*, 83(6):1219–1222, Aug 1999.

[141] E H Rezayi, N Read, and N R Cooper. Incompressible liquid state of rapidly rotating bosons at filling factor 3/2. *Phys. Rev. Lett.*, 95(16):160404, Oct 2005.

[142] J Ruseckas, G Juzeliūnas, P Öhberg, and M Fleischhauer. Non-abelian gauge potentials for ultracold atoms with degenerate dark states. *Physical Review Letters*, 95(1):010404, Jun 2005.

[143] K Sakoda. *Optical properties of photonic crystals (Springer series in optical sciences, vol. 80)*. Springer, 2001.

[144] H Schmidt and A Imamoglu. Giant kerr nonlinearities obtained by electromagnetically induced transparency. *Opt. Lett.*, 21:1936–1938, 1996.

[145] R J Schoelkopf, R J Schoelkopf, S M Girvin, and S M Girvin. Wiring up quantum systems. *Nature*, 451(7179):664, Feb 2008.

[146] C Schori, B Julsgaard, JL Sørensen, and ES Polzik. Recording quantum properties of light in a long-lived atomic spin state: Towardsquantum memory. *Physical Review Letters*, 89(5):57903, 2002.

[147] I Schuster, A Kubanek, A Fuhrmanek, T Puppe, P W H Pinkse, K Murr, and G Rempe. Nonlinear spectroscopy of photons bound to one atom. *Nat. Phys.*, 4:382–385, 2008.

[148] V Schweikhard, I Coddington, P Engels, V P Mogendorff, and E A Cornell. Rapidly rotating bose-einstein condensates in and near the lowest landau level. *Phys. Rev. Lett.*, 92(4):040404, Jan 2004.

[149] J T Shen and Shanhui Fan. Coherent photon transport from spontaneous emission in one-dimensional waveguides. *Opt. Lett.*, 30(15):2001–2003, 2005.

[150] Jung-Tsung Shen and Shanhui Fan. Strongly correlated two-photon transport in a one-dimensional waveguide coupled to a two-level system. *Phys. Rev. Lett.*, 98(15):153003, 2007.

[151] D N Sheng, Xin Wan, E H Rezayi, Kun Yang, R N Bhatt, and F D M Haldane. Disorder-driven collapse of the mobility gap and transition to an insulator in the fractional quantum hall effect. *Phys. Rev. Lett.*, 90(25):256802, Jun 2003.

[152] Barry Simon. Holonomy, the quantum adiabatic theorem, and berry's phase. *Physical Review Letters*, 51(24):2167–2170, Dec 1983.

[153] Anders S Sørensen, Eugene Demler, and Mikhail D Lukin. Fractional quantum hall states of atoms in optical lattices. *Phys. Rev. Lett.*, 94(8):086803, Mar 2005.

[154] D M Stamper-Kurn, A P Chikkatur, A Görlitz, S Inouye, S Gupta, D E Pritchard, and W Ketterle. Excitation of phonons in a bose-einstein condensate by light scattering. *Phys. Rev. Lett.*, 83(15):2876–2879, Oct 1999.

[155] J Steinhauer, N Katz, R Ozeri, N Davidson, C Tozzo, and F Dalfovo. Bragg spectroscopy of the multibranch bogoliubov spectrum of elongated bose-einstein condensates. *Phys. Rev. Lett.*, 90(6):060404, Feb 2003.

[156] J Stenger, S Inouye, A P Chikkatur, D M Stamper-Kurn, D E Pritchard, and W Ketterle. Bragg spectroscopy of a bose-einstein condensate. *Phys. Rev. Lett.*, 82(23):4569–4573, Jun 1999.

[157] J Strikwerda. *Finite difference schemes and partial differential equations*. SIAM: Society for Industrial and Applied Mathematics, Jan 2004.

[158] R Tao and F D M Haldane. Impurity effect, degeneracy, and topological invariant in the quantum hall effect. *Phys. Rev. B*, 33(6):3844–3850, Mar 1986.

[159] Meng Khoon Tey, Zilong Chen, Syed Abdullah Aljunid, Brenda Chng, Florian Huber, Gleb Maslennikov, and Christian Kurtsiefer. Strong interaction between light and a single trapped atom without the need for a cavity. *Nat Phys*, 4(12):924–927, 2008.

[160] James Thompson, Jonathan Simon, Huanqian Loh, and Vladan Vuletic. A high-brightness source of narrowband, identical-photon pairs. *Science*, 313(5783):74, Jul 2006.

[161] D J Thouless, M Kohmoto, M P Nightingale, and M den Nijs. Quantized hall conductance in a two-dimensional periodic potential. *Phys. Rev. Lett.*, 49(6):405–408, Aug 1982.

[162] D C Tsui, H L Stormer, and A C Gossard. Two-dimensional magnetotransport in the extreme quantum limit. *Phys. Rev. Lett.*, 48(22):1559–1562, May 1982.

[163] S Tung, V Schweikhard, and E A Cornell. Observation of vortex pinning in bose-einstein condensates. *Phys. Rev. Lett.*, 97(24):240402, Dec 2006.

[164] S J van Enk and H J Kimble. Strongly focused light beams interacting with single atoms in free space. *Phys. Rev. A*, 63(2):023809, Jan 2001.

[165] R Varnhagen. Topology and fractional quantum hall effect. *Nuclear Physics B*, 443(3):501–515, Jun 1995.

[166] M Vengalattore, M Hafezi, M. D Lukin, and M Prentiss. Optical bistability at low light level due to collective atomic recoil. *Physical Review Letters*, 101(6):063901, Jan 2008.

[167] M Vengalattore and M Prentiss. Radial confinement of light in an ultracold anisotropic medium. *Physical Review Letters*, 95(24):243601, 2005.

[168] M Vengalattore and M Prentiss. Recoil-induced resonances in the high-gain regime. *Physical Review A*, 72(2):21401, 2005.

[169] P Verkerk. Coherent and collective interactions of particles and radiation beams. *Proc. Int. School of Physics, Enrico Fermi CXXXI*, page 325, Jan 1995.

[170] P Verkerk, B Lounis, C Salomon, and C Cohen-Tannoudji. Dynamics and spatial order of cold cesium atoms in a periodic optical potential. *Physical Review Letters*, 68(26):3861–3864, Jun 1992.

[171] J M Vogels, K Xu, C Raman, J R Abo-Shaeer, and W Ketterle. Experimental observation of the bogoliubov transformation for a bose-einstein condensed gas. *Phys. Rev. Lett.*, 88(6):060402, Jan 2002.

[172] M Weidemuller and C Zimmermann, editors. *Cold atoms and molecules : a testground for fundamental many particle physics*. Wiley-VCH, Jan 2009.

[173] X G Wen. Vacuum degeneracy of chiral spin states in compactified space. *Phys. Rev. B*, 40(10):7387–7390, Oct 1989.

[174] X-G Wen. Topological orders and edge excitations in fractional quantum hall state. *Adv. Phys.*, 44:405, 1995.

[175] X G Wen and Q Niu. Ground-state degeneracy of the fractional quantum hall states in the presence of a random potential and on high-genus riemann surfaces. *Phys. Rev. B*, 41:9377, 1990.

[176] N K Wilkin and J M F Gunn. Condensation of "composite bosons" in a rotating bec. *Phys. Rev. Lett.*, 84(1):6–9, Jan 2000.

[177] K Winkler, G Thalhammer, F Lang, R Grimm, JH Denschlag, AJ Daley, A Kantian, HP Büchler, and P Zoller. Repulsively bound atom pairs in an optical lattice. *Nature*, 441:853–856, 2006.

[178] G Wrigge, I Gerhardt, J Hwang, G Zumofen, and V Sandoghdar. Efficient coupling of photons to a single molecule and the observation of its resonance fluorescence. *Nat Phys*, 4(1):60–66, 2008.

[179] F C Zhang, V Z Vulovic, Y Guo, and S Das Sarma. Effect of a charged impurity on the fractional quantum hall effect: Exact numerical treatment of finite systems. *Phys. Rev. B*, 32(10):6920–6923, Nov 1985.

[180] Jiepeng Zhang, Jiepeng Zhang, Gessler Hernandez, Gessler Hernandez, Yifu Zhu, and Yifu Zhu. All-optical switching at ultralow light levels. *Optics Letters, Vol. 32, Issue 10, pp. 1317-1319*, Jan 2007.

[181] Y Zhu, DJ Gauthier, SE Morin, Q Wu, HJ Carmichael, and TW Mossberg. Vacuum rabi splitting as a feature of linear-dispersion theory: Analysis and experimental observations. *Physical Review Letters*, 64(21):2499–2502, 1990.

[182] F E Zimmer, J Otterbach, R G Unanyan, B W Shore, and M Fleischhauer. Dark-state polaritons for multicomponent and stationary light fields. *Phys. Rev. A*, 77(6):063823, 2008.

[183] FE Zimmer, A André, MD Lukin, and M Fleischhauer. Coherent control of stationary light pulses. *Optics Communications*, 264(2):441–453, 2006.

Appendix A

EIT and band gap

In this appendix, we show that how in an EIT system, where the control field is a standing wave, a band gap structure can be developed. In particular, we show the presence of transmission resonances at the band gap edge by taking into account the full expression for the atomic susceptibilities. We show that at the band gap edge, we recover that same resonances that we presented in the main text for small detunings.

We consider a λ-level scheme, where a standing control field has coupled the forward- and backward-going probe together, as shown in Fig.A.1). Following [6], we assume the noises to be negligible, and therefore, the atomic equations of motion to the leading order in $\mathcal{E}_{\pm}$ are

$$\partial_t \hat{\sigma}_{ab}^{+} = +(i\Delta_1 - \Gamma/2)\hat{\sigma}_{ab}^{+} + i\Omega\hat{\sigma}_{ac} + ig\sqrt{2\pi}\mathcal{E}_{+} \quad (A.1)$$

$$\partial_t \hat{\sigma}_{ab}^{-} = +(i\Delta_1 - \Gamma/2)\hat{\sigma}_{ab}^{-} + i\Omega\hat{\sigma}_{ac} + ig\sqrt{2\pi}\mathcal{E}_{-} \quad (A.2)$$

$$\partial_t \hat{\sigma}_{ac} = -\gamma_0\hat{\sigma}_{ac} + i\Omega\hat{\sigma}_{ab}^{+} + i\Omega\hat{\sigma}_{ab}^{-} \quad (A.3)$$

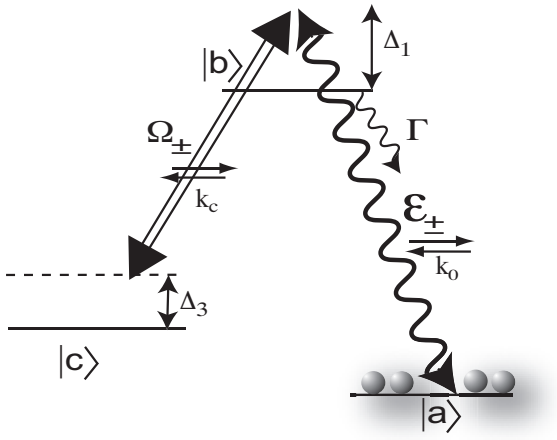

Figure A.1: In a three-level, where the control field is a standing wave, forward- and backward-going field get coupled to each other.

and the evolution equation of the photonic fields are written as:

$$(\partial_t + c\partial_z)\mathcal{E}_+ = i\Delta K\mathcal{E}_+ + ig\sqrt{2\pi}n_0\hat{\sigma}^+_{ab} \tag{A.4}$$

$$(\partial_t - c\partial_z)\mathcal{E}_- = i\Delta K\mathcal{E}_- + ig\sqrt{2\pi}n_0\hat{\sigma}^-_{ab}. \tag{A.5}$$

By taking the Fourier transform of the atomic equation of motion, one can solve for atomic polarization and obtain the self- and cross-susceptibilities. We can define a unit length based on the absorption length $L_{abs} = \frac{c\Gamma}{2\pi g^2 n_0}$, and write the field equation as:

$$\partial_{\tilde{z}}\mathcal{E}_+ = i\tilde{\Delta}_3\mathcal{E}_+ + i\chi_s(\delta)\mathcal{E}_+ + i\chi_c(\delta)\mathcal{E}_- \tag{A.6}$$

$$-\partial_{\tilde{z}}\mathcal{E}_- = i\tilde{\Delta}_3\mathcal{E}_- + i\chi_s(\delta)\mathcal{E}_- + i\chi_c(\delta)\mathcal{E}_+$$

where the self- and cross susceptibilities and the detuning are given by:

$$\chi_s(\delta) = i\frac{\Gamma}{\Gamma'}\frac{\Gamma'\Gamma_0+\Omega^2}{\Gamma'\Gamma_0+2\Omega^2} \quad (A.7)$$

$$\chi_c(\delta) = -i\frac{\Gamma}{\Gamma'}\frac{\Omega^2}{\Gamma'\Gamma_0+2\Omega^2} \quad (A.8)$$

$$\tilde{\Delta}_3 = \frac{\Delta_3}{\Gamma}\frac{\Gamma^2}{2\pi g^2 n_0} = \frac{\delta}{\eta}\frac{\Gamma}{|\Delta_1|} \quad (A.9)$$

where $\Gamma' = \Gamma/2 - i\Delta_1 - i\Delta_3$, $\Gamma_0 = \gamma_0 - i\Delta_3$ and Δ_3 is the two-photon detuning which is related to the dimensionless two-photon detuning in the main text ($\Delta_3 = 2\frac{\Omega^2}{\Delta_1}\delta$). We note that in most cases, $\tilde{\Delta}_3$ is very small for slow group velocities ($\frac{\Gamma^2}{2\pi g^2 n_0} = (\frac{\Gamma}{\Omega})^2\frac{\Omega^2}{2\pi g^2 n_0} \ll 1$), and therefore the corresponding term can be neglected for simplicity.

In order to obtain transmission and reflection coefficient, one should solve the couple mode equations Eq.(A.6) with proper boundary conditions. Therefore, we consider a system which is driven with a weak coherent field at ($z = 0$). Therefore, the boundary conditions can be set to,

$$\mathcal{E}_+(z=0) = \mathcal{E}_0 \quad (A.10)$$

$$\mathcal{E}_-(z=d) = 0. \quad (A.11)$$

We evaluate the transmission coefficient ($\mathcal{E}_+(z=d)/\mathcal{E}_0$), and the reflection coefficient ($\mathcal{E}_-(z=0)/\mathcal{E}_0$) by numerical methods using BVP5C in Matlab. In particular, we are interested in the Raman regime, in other words the detuning is very large $|\Delta_1| \gg \Gamma$ and also we assume $\Delta_1 < 0$. First, we consider the case where the EIT width is smaller than the one-photon detuning, i.e. $\Omega \ll |\Delta_1|$. Fig.A.2 shows the reflectivity and transmittivity of the system for different optical densities. In the regime with low optical density, the spectrum corresponds to a shifted Raman transition at

$\Delta_3 \simeq 2\frac{\Omega^2}{\Delta_1}$ and an EIT window around $\Delta_3 \simeq -\Delta_1$. In higher optical densities, the system develops a band gap for $-\Omega \leq \Delta_3 \leq 0$. Fig.A.2 shows that in media with higher optical density, the band gap becomes more prominent.

As we discussed in the main text, we are interested in the band gap edge where the transmission peaks are present and the system acts like an effective cavity. Fig.A.3 shows a close-up of the transmittivity and reflectivity spectrum in Fig.A.2(c) at the band gap edge. We can observe that several resonances occur at the edge due to the finite size of the system. By positioning at the one of the transmission peaks, the system behaves as an effective cavity, where the decay rate of the cavity will be given by the width of the transmission peak. Therefore, the present results, including the full susceptibilities of the system, is consistent with the model presented earlier where we had approximated the system to be around $\Delta_3 = 0$.

We add that alternatively, one can assume a strong control field so that the EIT windows would be smaller than the one-photon detuning $\Omega > |\Delta_1|$. Similar to the previous case $\Omega < |\Delta_1|$, the system develops a band gap. As shown in Fig.A.4, the band gap is formed between $-\Omega \lesssim \Delta_3 \lesssim \Omega$, similar to modulated EIT with AC-stark shift as discussed in Ref.[8].

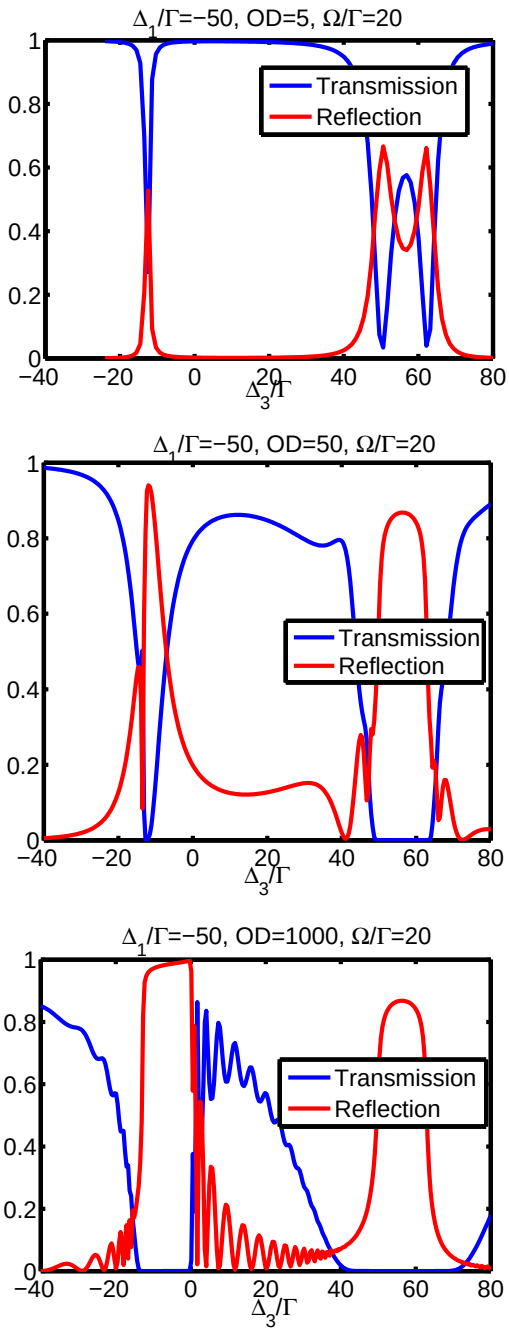

Figure A.2: By increasing OD, the band gap structure becomes more pronounced

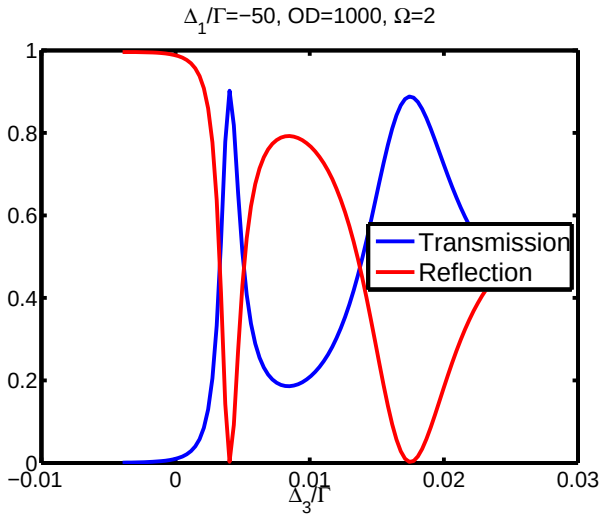

Figure A.3: Transmission resonances at the edge of the band gap

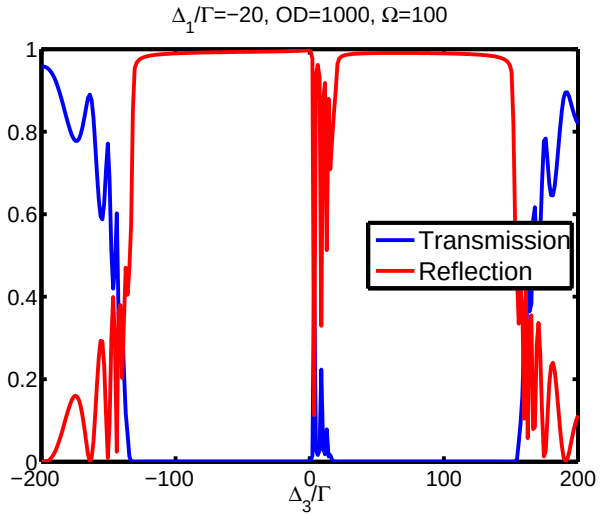

Figure A.4: Band gap structure for strong control fields ($\Omega > \Delta_1$)

Appendix B

Numerical methods

In this section, we describe the numerical methods that have been used to simulate the evolution of the photonic quantum state and the related correlation functions, in the limit where we truncate the Hilbert space to two photons or less (Chapter 3). The partial differential equations for the one-photon and two-photon wave functions (3.30, 3.31) are turned into difference equations by discretizing space and time, and are evolved forward in time using the Du Fort-Frankel scheme [157]. This algorithm is is explicit in time – *i.e.*, the next time step function is explicitly given by the past time function – and is also unconditionally stable. We note that the system under investigation is open and it is driven out of equilibrium, therefore, conventional analytical methods for approaching the NLSE such as Bethe ansatz or quantum inverse scattering [103] are not applicable here.

The one-photon wave function can be easily integrated and solved analytically. However, we describe how to obtain the one-photon wave function numerically and then generalize this technique to obtain the two-photon wave function. First, we

mesh space and time and reduce the differential equations to a difference equation. If we choose the time step k and the space step h, the discretized time and space will be $x = z/h$ and $s = t/k$ and the system length $d = Nh$. Then following the Du Fort-Frankel scheme [157], the evolution equation takes the form:

$$\frac{\theta(x,s+1)-\theta(x,s-1)}{2k} = \frac{i}{2mh^2}\left[\theta(x+1,s)+\theta(x-1,s)-\theta(x,s+1)-\theta(x,s-1)\right] \tag{B.1}$$

where the position take all values inside the boundary ($2 \leq x \leq N-1$). By rearranging the above equation, the explicit form of the equation can be obtained

$$(1+\frac{ik}{mh^2})\theta(x,s+1) = \frac{ik}{mh^2}\left[\theta(x+1,t)+\theta(x-1,t)-\theta(x,s-1)\right]+\theta(x,s-1) \tag{B.2}$$

Therefore inside the boundaries, the wave function at time $s+1$ can be obtained knowing the wave function at time s and $s-1$. The boundary condition at $z = 0$ -i.e. $x = 1$, will be given by

$$\frac{\theta(1,s+1)+\theta(2,s+1)}{2} - i\frac{\theta(2,t+1)-\theta(1,s+1)}{2mh} = \alpha \tag{B.3}$$

Or equivalently,

$$\theta(1,s+1) = \frac{\alpha + (-\frac{1}{2}+\frac{i}{2mh})\theta(2,s+1)}{\frac{1}{2}+\frac{i}{2mh}} \tag{B.4}$$

and similarly for the boundary condition at $z = d$ -i.e. $x = N$, we have

$$\frac{\theta(N,s+1)+\theta(N-1,s+1)}{2} + i\frac{\theta(N,s+1)-\theta(N-1,s+1)}{2mh} = 0 \tag{B.5}$$

which gives

$$\theta(N,s+1) = \frac{(-\frac{1}{2}+\frac{i}{2mh})\theta(N-1,s+1)}{\frac{1}{2}+\frac{i}{2mh}}. \tag{B.6}$$

Therefore, by having the above boundary conditions and the initial condition $\theta(x, s = 1) = 0$, the wave function can be calculated at any time inside the boundaries ($2 \leq$

$x \leq N-1$). The order of accuracy of the Du Fort-Frankel scheme is given by $O(h^2)+O(k^2)+O(k^2h^{-2})$ and it is consistent as k/h tends to zero [157].

Similarly, we can write a difference equation for the two-photon wave function. The δ-interaction can be approximated by a Gaussian distribution. The space domain is meshed so that $\Delta z_1 = \Delta z_2 = h$. The evolution equation for the two-photon wave function reads

$$\left(1+\frac{2ik}{mh^2}\right)\phi(x,y,s+1) = \frac{ik}{mh^2}\left[\phi(x+1,y,s)+\phi(x-1,y,s)\right] \quad \text{(B.7)}$$

$$+ \frac{ik}{mh^2}\left[\phi(x,y+1,s)+\phi(x,y-1,s)\right] \quad \text{(B.8)}$$

$$- 2\frac{ik}{mh^2}\phi(x,y,s-1)+\phi(x,y,s-1) \quad \text{(B.9)}$$

$$- 2k\frac{2i\kappa}{\sigma\sqrt{2\pi}}\mathrm{Exp}\left(-\frac{(\mathrm{x}-\mathrm{y})^2}{2\sigma^2}\right)\phi(\mathrm{x},\mathrm{y},\mathrm{s}) \quad \text{(B.10)}$$

The boundary condition at $z=0$ will be given by

$$\frac{\phi(1,y,s+1)+\phi(2,y,s+1)}{2} - i\frac{\phi(2,y,s+1)-\phi(1,y,s+1)}{2mh} = \frac{\alpha}{2}\theta(y,s+1), \quad \text{(B.11)}$$

where σ is the length scale characterizing the distance of the two-photon interaction. Approximating the delta-function with a Gaussian is valid if $\sigma \ll d$. On the other hand, we should have $h \ll \sigma$ so that the Gaussian function would be smooth. Or equivalently,

$$\phi(1,y,s+1) = \frac{\frac{1}{2}\alpha\theta(y,s+1)+(-\frac{1}{2}+\frac{i}{2mh})\phi(2,y,s+1)}{\frac{1}{2}+\frac{i}{2mh}} \quad \text{(B.12)}$$

and similarly for the boundary condition at $z=d$, we have

$$\frac{\phi(N,y,s+1)+\phi(N-1,y,s+1)}{2} + i\frac{\phi(N,y,s+1)-\phi(N-1,y,s+1)}{2mh} = 0 \quad \text{(B.13)}$$

which gives

$$\phi(N,y,s+1) = \frac{(-\frac{1}{2}+\frac{i}{2mh})\phi(N-1,y,s+1)}{\frac{1}{2}+\frac{i}{2mh}}. \quad \text{(B.14)}$$

Once the wave function is known at any point in time and space, we can evaluate the correlation functions. In particular, the two-photon correlation function $g_2(d, \tau = 0)$ is given by Eq. (3.45), where the first and the second derivatives at anytime are given by the following expressions,

$$\partial^{(1)}\phi(d,d) = \frac{1}{2mh}[\phi(N,N) - \phi(N-1,N)] \tag{B.15}$$

$$\partial^{(1)}\partial^{(2)}\phi(d,d) = \frac{1}{4m^2h^2}[\phi(N,N) - \phi(N-1,N) \tag{B.16}$$

$$- \phi(N,N-1) + \phi(N-1,N-1)]. \tag{B.17}$$

Note that in evaluation of $g_2(\tau)$, once the first photon is detected the two-photon wave function collapses to zero. This seems to be contradictory with the driven boundary condition Eq.(3.38) where the two-photon state at the boundaries is proportional to the one-photon wave function which is not zero. This apparent inconsistency occurs because we have neglected higher number photon states in our truncation. However, this inconsistency only leads to higher order corrections to $g_2(\tau)$ in the input field amplitude α, which is assumed to be weak ($\alpha \ll 1$).

Appendix C

Effect of noise

In this appendix, we investigate the effect of noise in the NLSE system introduced in Chapter 3. We first show the origin of the nonlinear noise and then argue that the noise is negligible for the regime of our interest where many atoms are present and the system is weakly driven. In particular, every time a two-photon is absorbed, an atom has undergone a transition from the state $|a\rangle$ to the state $|d\rangle$. The excited atom first emits a photon and goes to the state $|c\rangle$. The emitted photon can either be in the guided mode or in a mode which is not guided. In the former case, the photon emission is already taken into account by $\mathcal{E}_{\pm}$, as long as the regime of validity of NLSE is greater than Γ_{1D} (which is usually the case). In the former case, the photons leaves the system and therefore does not interfere with the desired guided mode. Therefore, no noise is produced so far. Now, the atom can relax from the state $|c\rangle$ into $|a\rangle$ by absorbing a control photon and subsequently emitting a second photon either in the guided or non-guided mode. However, if the emission of the first emitted photon was not in the guided mode, the emission of the second photon in

the waveguide can introduce a noise, because it does not carry any phase correlation with the field inside the medium. Although, this noise can in principle interfere with the photonic field of our interest, we show that in the limit of large number of atoms and small number of excitations (photons), this noise effect is negligible. For that, we review the emission of the noise photon in further detail to include the effect of many atoms. In an atomic ensemble, the interaction between atoms and photon is enhanced by $\sqrt{N}$, where N is the number of atoms. As shown in Fig.C.1, atoms in the ground state ($|a\rangle = |a_1 a_2 ... a_N\rangle$) are coupled to a symmetric state with a single excitation ($|b\rangle = \frac{1}{\sqrt{N}} \sum_{i=1}^{N} |a_1 a_2 ... b_i ... a_N\rangle$) by a coupling constant equal to $g\sqrt{N}$. However, the single excitation ($|c\rangle = \frac{1}{\sqrt{N}} \sum_{i=1}^{N} |a_1 a_2 ... c_i ... a_N\rangle$) is weakly coupled to the corresponding excited state ($|d\rangle = \frac{1}{\sqrt{N}} \sum_{i=1}^{N} |a_1 a_2 ... d_i .... a_N\rangle$) with the coupling constant g. There could be also two-photon excitation which is presented by ($|cc\rangle = \sqrt{\frac{2}{N(N-1)}} \sum_{i \neq j}^{N} |a_1 a_2 ... c_i .. c_j . a_N\rangle$). Now, we want to track the source of noise. For simplicity, let's assume that the system starts in the ground state with n+2 photon: ($|a, n+2\rangle = |a_1 a_2 ... a_N, n+2\rangle$), then one of the atoms can make a transition to the excited state $|d, n\rangle$, by absorbing two photons. Due to the spontaneous emission out of the waveguide, this state relaxes into ($|c', n\rangle = |a_1 a_2 ... c_i ... a_N, n\rangle$) where i corresponds to an arbitrary single atom (circle in Fig. C.1). We note that such states are orthogonal to symmetric state with single excitation ($|c\rangle$) in the limit $N \gg 1$. Now in return, this atom can go back to the ground state by emitting one photon into the waveguide ($(|c', n\rangle \rightarrow (|b', n\rangle \rightarrow |a, n+1\rangle)$). The atom-photon coupling for this process is g (dashed curvy line in Fig.C.1), since we are dealing with only one excitation. Due to the incoherent nature of the spontaneous emission out of the guided mode (from

$|d, n\rangle \rightarrow |c', n\rangle$ transition), the extra photon (from $|b, n\rangle \rightarrow |a, n+1\rangle$ transition) does not have any phase relationship with the starting photonic state inside the waveguide. Therefore, this process adds a noise to the guided photonic mode.

However, when there is a large number of atoms inside the cavity $N \gg 1$, the atom-photon coupling for the non-symmetric state is very small and the noise is negligible. In other words, while the coherent process coupling strength scale with $\sqrt{N}$, the noise due to dipole radiation of few exited atoms is very weak and therefore the noise effect scales down with $\sqrt{N}$. Hence, given that the noise effect is not important, using the previous formalism where the nonlinear absorption is treated as a decay term in the NLSE, is consistent within the model.

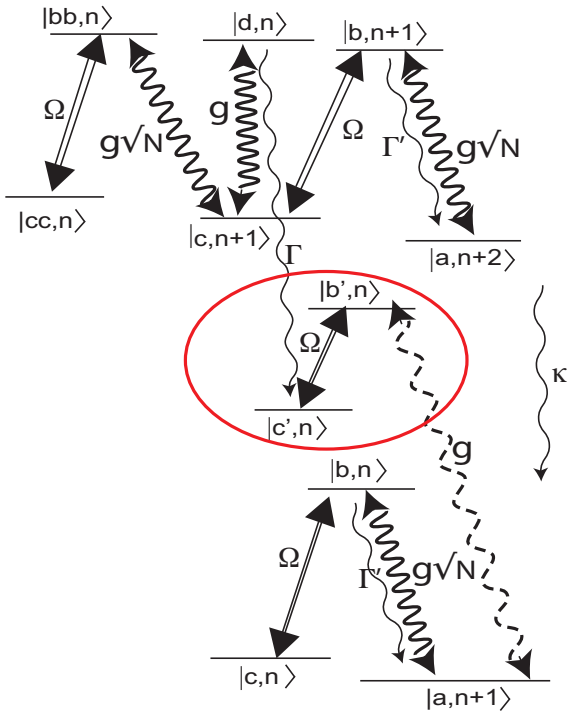

Figure C.1: Level diagram of the atom-photon system. Two-photon absorption is accompanied by an emission of a photon out of the guided mode. Subsequently, the atom decays into a single atom state (red circle) which has a small overlap with spin wave state when $N \gg 1$.

Appendix D

Photon-Photon interaction in Double-V system

In this appendix, we show that the stationary pulses of light can be achieved by counter-propagating control fields in an EIT system and expand the derivation of the transfer matrix introduced in Chapter 4. In particular, we illustrate that how such stationary pulses can be obtained without neglecting the rapidly oscillating atomic coherences [7, 8] by generalizing a scheme introduced in Refs.[182, 56].

Specifically, we consider a double-V system where the counter propagating probe fields ($\mathcal{E}_{\pm}$) are coupled to counter-propagating control fields ($\Omega_{\pm}$), as shown in Fig. D.1. Note that for both the probe and the control channel, forward and backward lights have different polarizations (e.g., the forward-propagating probe field is σ_+ polarized). Using the rotating wave approximation, the Hamiltonian of the system in the rotating frame is written as,

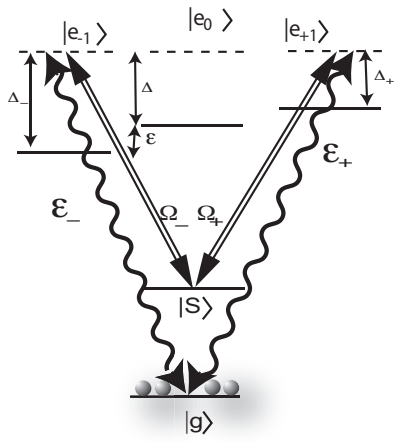

Figure D.1: Double-V system

$$H = -\int dz(\Delta_+\sigma_{e_+,e_+} + g\sqrt{2\pi}\mathcal{E}_+\sigma_{e_+,g} + \Omega_+\sigma_{s,e_+} \tag{D.1}$$

$$+ \Delta_-\sigma_{e_-,e_-} + g\sqrt{2\pi}\mathcal{E}_-\sigma_{e_-,g} + \Omega_-\sigma_{s,e_-}) \tag{D.2}$$

where $\Delta_\pm = \Delta \mp \epsilon$ is the detuning of the control field from the exited states.

The evolution of the slowly varying electric fields is given by Maxwell equations:

$$\begin{aligned}(\partial_t + c\partial_z)\,\mathcal{E}_+ &= i\sqrt{2\pi}gN\sigma_{g,e+}\\ (\partial_t - c\partial_z)\,\mathcal{E}_- &= i\sqrt{2\pi}gN\sigma_{g,e-}.\end{aligned}$$

Furthermore, one can write the evolution equation of the entire photon-atom system, $X^\top = (\mathcal{E}_+, \mathcal{E}_-, \sigma_{gs}, \sigma_{g,e+}, \sigma_{g,e-})$, in a compact form:

$$\frac{\partial}{\partial t}X = -iH_{eff}X \tag{D.3}$$

where the effective Hamiltonian, in Fourier domain for space, is

$$H_{eff} = \begin{pmatrix} -ck & 0 & 0 & -g\sqrt{2\pi}N & 0 \\ 0 & +ck & 0 & 0 & -g\sqrt{2\pi}N \\ 0 & 0 & 0 & -\Omega & -\Omega \\ -g\sqrt{2\pi} & 0 & -\Omega & -i\Gamma/2-(\Delta-\epsilon) & 0 \\ 0 & -g\sqrt{2\pi} & -\Omega & 0 & -i\Gamma/2-(\Delta+\epsilon) \end{pmatrix} \tag{D.4}$$

where Γ accounts for the decay rate of the excited states. The dynamics of the system in double-V scheme is essentially the same as in N-level scheme described in Ref.[8, 12, 36]. However, in this derivation, we have not used the secular approximation to neglect the rapidly oscillating atomic coherences. Such system yields five eigenstates which their energies is shown in Fig. D.2. In particular, one solution has zero energy at $ck = 0$, which we call the *dark state polariton* [54] and has the form:

$$\Psi = \frac{1}{\sqrt{2\Omega^2 + g^2 N}} \left[\Omega(\mathcal{E}_+ + \mathcal{E}_-) - g\sqrt{N}\sigma_{g,s}\right]. \tag{D.5}$$

We note that at $ck = 0$, the dark state polariton is separated by a gap from the other energy eigenstates. In the limit, where $\epsilon \to 0$, this gap is equal to $\frac{1}{2}(-\Delta + \sqrt{8\pi g^2 N + \Delta^2 + \Omega^2})$. The energy of such states at small values of ck is quadratic in momentum and therefore, we can write the evolution of such states in form of a Schrödinger equation:

$$(i\partial_t + \frac{1}{2m}\partial_z^2)\Psi(z,t) = 0 \tag{D.6}$$

Other eigenstates has nonzero energies, and by adiabatically eliminating them one finds: $\sigma_{g,s} \simeq -\frac{g\sqrt{N}}{\Omega}(\mathcal{E}_+ + \mathcal{E}_-)$. In the slow light limit, $g^2 N/\Omega^2 \gg 1$, the effective mass

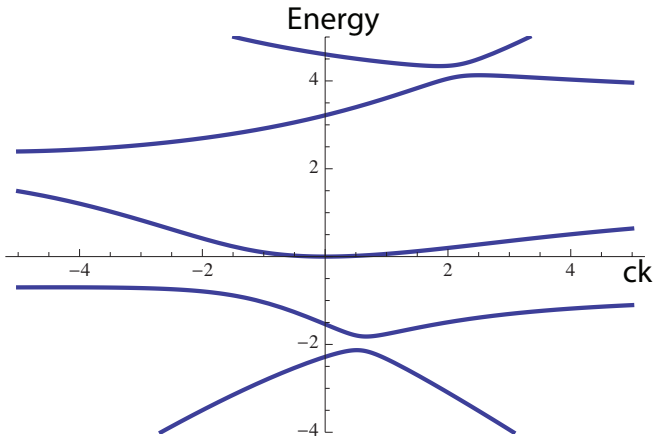

Figure D.2: Energy spectrum of a double-V system as a function of momentum (ck). ($\Delta = -2, \epsilon = 1, g^2N/\Omega^2 = 1, \Gamma = 0$). Dark state polariton solution (third band) has zero energy at $ck = 0$ and possesses a quadratic dispersion.

is given by: $\frac{1}{2m} = -\frac{c^2\Delta\Omega^2}{2\pi(g^2N)^2}\left(1 + \frac{i\Gamma}{2\Delta}\right)$ which is independent of ϵ and the dark state polariton takes the simple form of $\Psi = \frac{g\sqrt{N}}{\Omega}(\mathcal{E}_+ + \mathcal{E}_-)$. If we assume $\epsilon, g\sqrt{N} \ll \Delta$, the energy gap between the dark state polariton and the neighboring states will be equal to $2\pi g^2 N/\Delta$, in the slow light regime.

As mentioned before, the Schrödinger equation in Eq. (D.6) is equivalent to the Schrödinger equation as in the N-level scheme [36]. However, in this case no secular approximation on rapidly oscillating atomic coherences is used.

In the following, we evaluate the transport properties of a stationary pulse system. The transfer matrix formalism allows us to obtain the transport properties of light through the system in the linear regime. Moreover, since in our gate scheme, the control photon is stored and its dynamics is frozen in time, such formalism is also useful to evaluate the effect of photon-photon nonlinearity.

Following Ref.[12, 74] (see Chapter 3), the counter-propagating dark-state polari-

tons ($\Psi_\pm$) inside the waveguide obey a set of linear equations of motion,

$$(\pm c\partial_z + \partial_t)\,\Psi_\pm + \frac{\eta}{2}\partial_t\,(\Psi_+ + \Psi_-) = \mp\frac{\xi}{2}\,(\Psi_+ - \Psi_-)\,. \tag{D.7}$$

Working now in the frequency domain, because the system is linear, one can define a transfer matrix $M(\omega, z)$ that relates the fields $\Psi_\pm(z'+z,\omega)$ to the fields $\Psi_\pm(z',\omega)$ at some previous position z' $(0 < z, z' < L)$,

$$\begin{pmatrix} \Psi_+(z'+z,\omega) \\ \Psi_-(z'+z,\omega) \end{pmatrix} = M(\omega,z) \begin{pmatrix} \Psi_+(z',\omega) \\ \Psi_-(z',\omega) \end{pmatrix}. \tag{D.8}$$

By solving the propagation equations of Eq. (D.7), it is possible to obtain the elements of $M(\omega, z)$. Switching now to the dimensionless units defined in earlier work [74] (i.e., time and space in units of t_{coh}, L_{coh} introduced in Chapter 3), we find that

$$\begin{aligned}
M &= \begin{pmatrix} M_{11} & M_{12} \\ M_{21} & M_{22} \end{pmatrix}, \qquad (D.9)\\
M_{11} &= \cos\, z\sqrt{\tilde{\delta}} + \frac{i}{2\sqrt{\tilde{\delta}}}(1 + i\frac{\Gamma}{2|\Delta|} + \delta)\sin\, z\sqrt{\tilde{\delta}},\\
M_{12} &= \frac{i(\delta - 1 - i\frac{\Gamma}{2|\Delta|})}{2\sqrt{\tilde{\delta}}}\sin\, z\sqrt{\tilde{\delta}},\\
M_{21} &= -M_{12},\\
M_{22} &= \cos\, z\sqrt{\tilde{\delta}} - \frac{i}{2\sqrt{\tilde{\delta}}}(1 + i\frac{\Gamma}{2|\Delta|} + \delta)\sin\, z\sqrt{\tilde{\delta}},
\end{aligned}$$

where $\tilde{\delta} = \delta(1 + i\Gamma/|2\Delta|)$, δ is the two-photon detuning in our re-scaled units, and the imaginary part accounts for the small imaginary component of the mass $m{\approx}1/2$. The reflection and transmission coefficients can generally be related to the transfer matrix elements by $r = -M_{21}/M_{22}$, $t = M_{11} - M_{12}M_{21}/M_{22}$. In particular, for the above solutions of M_{ij} and a system of length $z = d$, we recover the previously derived

transmission and reflection amplitudes [74],

$$t(d,\delta) = \frac{2i\sqrt{\tilde{\delta}}}{2i\sqrt{\tilde{\delta}}\cos[d\sqrt{\tilde{\delta}}] + (1 + i\frac{\Gamma}{2|\Delta|} + \delta)\sin[d\sqrt{\tilde{\delta}}]}, \tag{D.10}$$

$$r(d,\delta) = \frac{(1 + i\frac{\Gamma}{2|\Delta|} - \delta)\sin[d\sqrt{\tilde{\delta}}]}{2i\sqrt{\tilde{\delta}}\cos[d\sqrt{\tilde{\delta}}] + (1 + i\epsilon + \delta)\sin[d\sqrt{\tilde{\delta}}]}. \tag{D.11}$$

In the absence of losses ($\Gamma \ll |\Delta|$), the first transmission resonance occurs at $(\pi/d)^2$ and in real units $\delta_{res} = (\frac{\pi}{d})^2 \frac{2\Omega^2}{|\Delta|}$. We note that in the regime of our interest ($OD \gg 1000$), the transmission resonance happen very close to two-photon Raman resonance ($\delta_{res} \ll |\Delta|$.) A finite loss both shifts the resonance frequency δ_{res} by a small amount and reduces the transmittivity from its peak value of 1. Note that fixing OD and the desired transmittivity $T_{peak} = |t|^2$ on (shifted) resonance allows one to solve for the corresponding detuning [74].

Appendix E

Strategy for single photon gate

In this appendix, we investigate the implementation of the single-photon switch scheme presented in Chapter 4 in a realistic situation. In particular, we consider a realistic electronic level structure for the atom and discuss required parameters such as optical density, single-atom cooperativity and magnetic field to obtain a high fidelity gate.

We describe the scheme for a realistic atomic level structure as shown in Fig. E.1. The main idea is similar to the scheme of Fig. 4.1. Specifically, we first store the first photon in $|s\rangle$ and then transfer it to $|g_-\rangle$, either by a microwave or Raman $\pi-$pulse. In this situation, $\mathcal{E}_+$ and $\mathcal{E}_-$ can interact with the single excitation through $|e_0\rangle \leftrightarrow |g_-\rangle$ and $|e_{-2}\rangle \leftrightarrow |g_-\rangle$ transitions, respectively.

Note that the "excited" atom only couples to forward-going (σ_+ polarized) and backward-going (σ_- polarized) field. Therefore, the fast oscillating terms (e^{i2kz}) due to reflection (i.e., forward-going (σ_- polarized) and backward-going (σ_+ polarized) electric fields), do not lead to undesirable interference, contrary to the scheme of

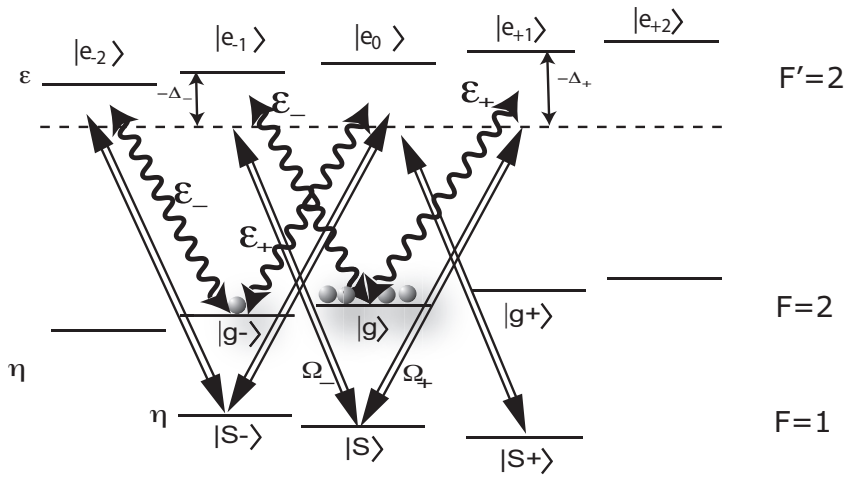

Figure E.1: Single-photon gate: The detailed level diagram where both the forward- and backward-propagating electric field interact with the stored excitation, i.e. $\mathcal{E}_+$ through $|g-\rangle \rightarrow |e_0\rangle \rightarrow |s-\rangle$ and $|g-\rangle \rightarrow |e_0\rangle \rightarrow |s+\rangle$ transitions and $\mathcal{E}_-$ through $|g-\rangle \rightarrow |e_{-2}\rangle \rightarrow |s-\rangle$. The zeeman shift is tuned such that only the backward field is coupled to the excitation and the forward field is entirely off-resonant. Therefore, the system simplifies to the level diagram shown in Fig. 4.1(a).

Ref. [7]. Therefore, the corresponding transfer matrix will look like,

$$\begin{aligned} M_a &= \begin{pmatrix} t_+ & 0 \\ 0 & t_-^{-1} \end{pmatrix}, t_\pm = 1 + r_\pm \\ r_+ &= \zeta_+ \frac{-\Gamma_{1D}}{(\Gamma - 2i\Delta'_+) + \frac{\Omega^2}{-2i\delta^1_+} + \frac{\Omega^2}{-2i\delta^2_+}} \\ r_- &= \zeta_- \frac{-\Gamma_{1D}}{(\Gamma - 2i\Delta'_-) + \frac{\Omega^2}{-2i\delta_-}} \end{aligned}$$

where $\zeta_\pm$ are Clebsch-Gordon coefficient corresponding to strength of dipole transitions $|g_-\rangle \rightarrow |e_{-2}>, |e_0\rangle$. Detuning parameters are defined as,

$$\delta^1_+ = \delta_- = \delta_{res} - 2\eta, \delta^2_+ = \delta_{res}, \Delta'_+ \simeq \Delta'_- \simeq \Delta \tag{E.1}$$

where (ϵ, η) correspond to Zeeman shift of the excited and ground states, respectively.

We have assumed $\Delta \gg \epsilon, \eta$. We should later optimize these Zeeman shifts so that the single excitation resonantly interacts with the backward field i.e. $r_- = -\zeta_- \Gamma_{1D}/\Gamma$. On the other hand, the excitation will be far off-resonant for the forward field, therefore r_+ is essentially zero.

We note that the above equations can be seen as a generalization of transmission coefficients for two-level atoms coupled to 1D waveguides [37, 149]. In the two-level atom case, reflection and transmission coefficients are given by $t = 1 + r, r = \frac{-\Gamma_{1D}}{\Gamma - 2i\Delta}$. In our case, due the presence of the control field, we should also include the effect Raman transitions (or EIT). Moreover, we note that only transmission coefficients are important (corresponding to forward-propagating $\mathcal{E}_+$ and backward-propagating $\mathcal{E}_-$) and reflections can be ignored. The reason is that the reflection terms (backward-propagating $\mathcal{E}_+$ and forward-propagating $\mathcal{E}_-$) have fast oscillating terms (e^{2ikz}), which result in destructive interference of them after traveling over a wavelength distance.

If the required Zeeman shift is present, the target photon interacts resonantly with the stored spin excitation. This interaction is enhanced since the target photon will be trapped inside the system because of the stationary pulse effect [12, 74]. Using the transfer matrix introduced earlier, we can characterize such enhancement and consequently evaluate how much of a target photon in the presence of a control photon (switch ON) will be reflected. We set the transmittivity for switch OFF mode and the reflectivity for switch ON mode to be equal. This quantity is the fidelity of the gate. Then, for a fixed optical density and single-atom cooperatively, we optimize the single-photon detuning to obtain the highest fidelity.

Fig. E.2 shows the fidelity as a function of OD and single-atom cooperatively.

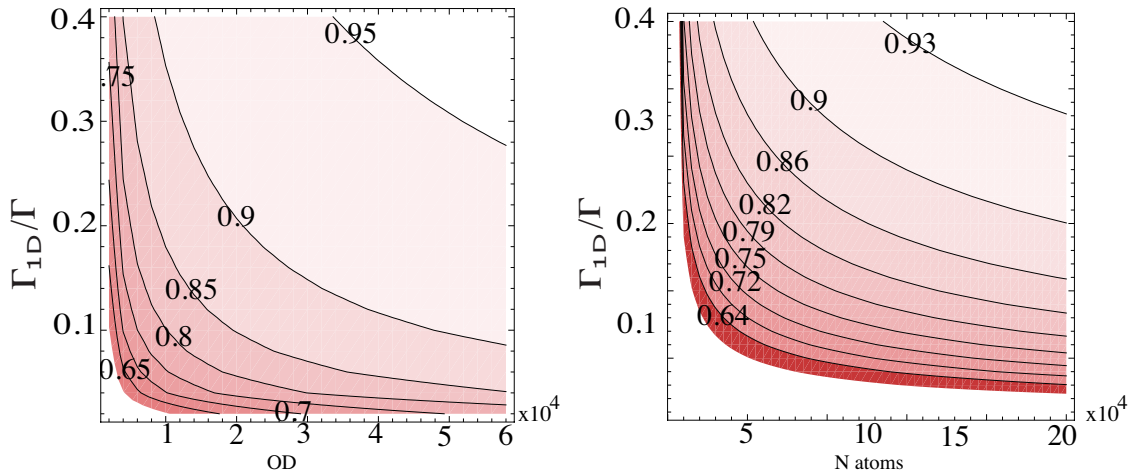

Figure E.2: Fidelity of the gate for the scheme presented in Fig. E.1. Reflectivity and transmittivity are set to be equal to obtain the optimized α. (D1 Clebsch-Gordon coefficient are included)

For example, a 90% fidelity for OD=50000 ($N_{atoms} = 5 \times 10^5$) is achieved when $\Gamma_{1D}/\Gamma = 0.1$. More importantly, both Fig. E.2(b) and Eq. (4.4) show that the fidelity improves linearly with single-atom cooperativity (Γ_{1D}/Γ) while it only improves with square root of the atom number $\sqrt{N_{atoms}}$. Therefore, although using smaller fiber core may reduce the number of loaded atoms, it improves the overall fidelity. For example, with $\Gamma_{1D}/\Gamma = 0.3$ only $N_{atoms} \simeq 5.3 \times 10^4$ ($OD = 16,000$) is needed to perform the gate.

In the following, we discuss the required parameters such as detuning and magnetic field to obtain a high fidelity gate.

First, we consider the case in the absence of a stored excitation. The system has a finite linear absorption proportional to $\alpha = d\frac{\Gamma}{\Delta}$. Therefore, for a given optical density ($OD = \alpha(\frac{\Delta}{\Gamma})^2$), one can find the detuning (Δ) such that the transmittivity is set to a desired value say $T_{peak} = 90\%, \alpha = 0.43$ [74]. Note that the first transmission

resonance at the band edge, $\delta_{res} = (\frac{\pi}{d})^2 \frac{2\Omega^2}{\Delta}$, is a function of the control field (Ω).

Next, we optimize the Zeeman shift so that the transition ($|e_{-2}\rangle \leftrightarrow |g_{-}\rangle$) interacts strongly with the backward field. We can estimate its value by the following argument. We note the control field Rabi frequency is smaller than the single photon detuning ($\Omega \ll \Delta$), in order to have the band gap structure and the resonances at the edge, in the first place. This means that the forward/backward field almost form a Raman transition with their corresponding control field $\delta_{res} \ll \Delta$ [74]. Therefore, in order to maximize the coupling between the backward electric field and the control spin excitation, the backward field should be on resonance with either the one-photon $|e_{-2}\rangle \leftrightarrow |g_{-}\rangle$ transition or the corresponding Raman transition. The former case requires a rather large Zeeman shift of the order of single-photon detuning ($\epsilon \simeq \Delta$, more specifically $\eta - 2\epsilon = \Delta$). However, the latter case only requires a small Zeeman shift so that the backward field and the control field form a resonant Raman transition (more specifically $\eta = \delta_{res}/2 - \Omega^2/8\Delta \simeq -\Omega^2/8\Delta$). This solutions will give $r_{-} = -\zeta_{-}\Gamma_{1D}/\Gamma$, regardless of the control field amplitude (Ω). Moreover, $r_{+} \simeq 0$ due to the shifted double-EIT resonance structure.

As an example of experimental realization, we consider a ^{87}Rb system with optical density $OD = 50000$ and a small cooperatively $\Gamma_{1D}/\Gamma = 10\%$. Then, in the switch OFF mode, a 90% transmission can be achieved by choosing $\Delta = -170\Gamma$. Consequently, for a control field of $\Omega = 10\Gamma$, the resonance frequency is $\delta_{res} = 10^{-4}\Gamma$ and a small magnetic field ($\eta = 0.07\Gamma \rightarrow B \simeq 3.7$ Gauss) is required to bring the two-photon transition to resonance and achieve a 90% reflection in the switch ON mode.

So far only the interaction of the atom with the backward field was optimized, i.e. r_- was maximized. One may be tempted to optimize the control field amplitude (Ω) to bring the ($|e_0\rangle \leftrightarrow |g_-\rangle$) transition also to resonance with the forward field and maximize r_+. However, this requires fine tuning of a very strong control field. Furthermore, this strong field may entirely deform the band-gap structure [74].

Moreover, we note that in the current estimates the Clebsch-Gordon coefficients are included, therefore, the effective single atom cooperatively for a single transition is reduced comparing to the simple estimate of Sec. 4.2. Note that if we ignore Clebsch-Gordon coefficients, the required optical density is lowered almost three folds to OD=5000 (for $\Gamma_{1D}/\Gamma = 0.3$) and the number of required atoms is reduced almost six-folds $N_{atoms} = 17,000$, consistent with the analytical estimate of fidelity in Eq. (4.4).

Appendix F

Vacuum Rabi splitting in electromagnetically induced photonic crystal

In this appendix, we show the analogy between single-mode and the transfer matrix formalism to describe the physics of Rabi splitting. Although Rabi splitting is derived primarily in cavity QED context, however it is not inherently a quantum phenomenon and can be described by a simple classical treatment. A conventional way to classically approach such a problem is the following: First, we treat atoms as damped oscillators which are coupled to the light inside a cavity. Then, in each round trip, we take into account the absorption and dispersion of the intra cavity field due the interaction. Finally, we obtain the steady-state solution of the field inside the cavity. Such treatment can predict the position and the width of Rabi splitted peaks, identical to results of cavity QED approaches such as the dressed states formalism

(see for example Ref.[181]).

Here, we present a classical method to evaluate Rabi splitting using transfer matrix approach. This approach reproduces the same results as the other approaches. However, this approach also allows us to consider the position dependence of the coupling between atoms and the cavity field. Moreover, we can study the forward- and backward-going fields inside the cavity separately and we can investigate their coupling to atoms in some details.

The transfer matrix of a mirror can be written as:

$$M_{mirror} = \frac{1}{t}\begin{pmatrix} t^2 - r^2 & r \\ -r & 1 \end{pmatrix} \tag{F.1}$$

where t and r are reflection and transmission coefficient, respectively. They satisfy the following relations: $|t|^2 + |r|^2 = 1$ and $r^*t + t^*r = 0$ (e.g. $r = \sqrt{R}$, $t = i\sqrt{1-r^2}$). In a realistic situation mirror have high reflectivity: $R = |r^2| \simeq 1$ and consequently an empty cavity made by two of such mirrors has a finesse $\mathcal{F} = \pi/(1-R)$ [82]. The free propagation of light on a distance z along the cavity axis is characterized by,

$$M_{free}(z) = \begin{pmatrix} e^{ikz} & 0 \\ 0 & e^{-ikz} \end{pmatrix} \tag{F.2}$$

For the moment, in other to reproduce the same result as the "round trip" treatment, we assume the effect of the atom is purely a dispersive and/or absorptive effect and the atom does not couple forward and backward-propagating fields. Therefore, the transfer matrix which characterizes the interaction of light and a single two-level system is given by (using slowly varying approximation $\Gamma_{1D} \ll |\Gamma - 2i\Delta|$):

$$M_{atom} = \begin{pmatrix} e^{\theta_a} & 0 \\ 0 & 1 \end{pmatrix}$$
$$\theta_a = -\frac{\Gamma_{1D}}{\Gamma - 2i\Delta}$$

where g denotes the atom-photon coupling strength and $\Delta = \omega - \omega_a$. Assuming that the atomic resonance is close to the first fundamental mode of the cavity, we have $\Gamma_{1D} = g^2 L/c$ which is the spontaneous rate into the guided mode in 1D waveguide context [44, 149]. We should note that the above expression is not always valid. Since an atom interacts with the total electric field, which is the sum of forward and backward-going fields, the effect of the coupling between these fields at each scattering should be considered. In such cases, the transfer matrix takes the form:

$$M_{atom} = \frac{1}{t_a} \begin{pmatrix} t_a^2 - r_a^2 & r_a \\ -r_a & 1 \end{pmatrix}$$
$$r_a = -\frac{\Gamma_{1D}}{\Gamma - 2i\Delta}, t_a = \frac{\Gamma - \Gamma_{1D} - 2i\Delta}{\Gamma - 2i\Delta}$$

Note that if the single atom position is random over a wavelength, the reflection term picks up a random phase e^{ikz}, which leads to a destructive interference.

Now, we can easily evaluate the transmission properties of a cavity containing an atom. For simplicity, we assume that the atoms is located in the middle of the cavity $z = L/2$. Therefore, the transfer matrix of the entire system is equal to:

$$M_{total} = M_{mirror} M_{free}(L/2) M_{atom} M_{free}(L/2) M_{mirror} \tag{F.3}$$

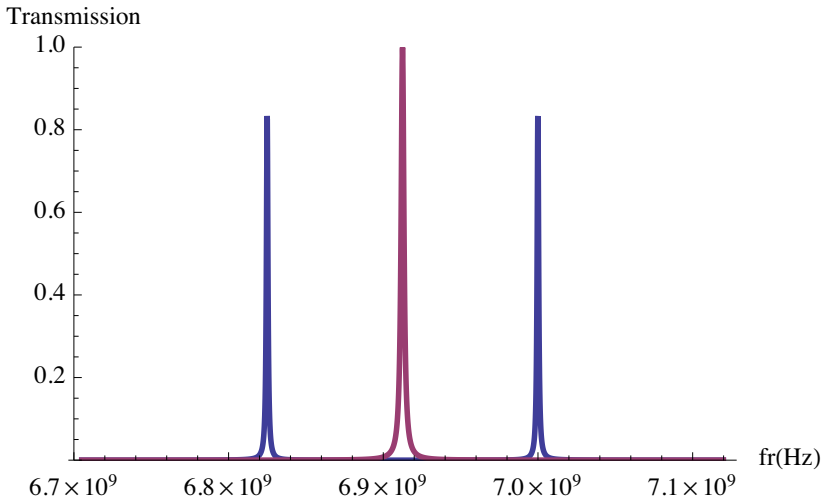

Figure F.1: Vacuum Rabi splitting. Purple represents the bare cavity and blue represents the cavity coupled to an atom. ($2g/2\pi = 350MHz, \kappa/2\pi = 800kHz, \Gamma/2\pi = 200kHz$) Numbers correspond to circuit QED with superconducting qubit Ref.[145]

Furthermore, we assume the atom is resonant with the cavity $\omega_a = \omega_c = \frac{n\pi c}{L}$. Then, the transmittivity is given by

$$T(\Delta) = \frac{(-1+R)^2}{e^{\frac{8g^2\Gamma L/c}{\Gamma^2+4\Delta^2}} + R^2 - 2e^{\frac{4g^2\Gamma L/c}{\Gamma^2+4\Delta^2}} R\cos\left[2\frac{L}{c}\Delta\left(1-\frac{4g^2}{\Gamma^2+4\Delta^2}\right)\right]} \tag{F.4}$$

similar to the result of a round trip approach (see e.g. Ref.[181]). If we neglect the effect of atomic absorption, we can find the location of the new transmission resonances by finding zeros of the cos function argument which gives us: $\Delta = 0, \pm\frac{1}{2}\sqrt{4g^2+\Gamma^2}$. The first solution corresponds to the dip in the cavity transmission and the second and the third solutions, i.e. $\pm g$ (in the limit of strong coupling), correspond to Rabi splitted peaks (see Fig. F.1).

The above results are for an atom located in the middle of the cavity, therefore, the atom is strongly coupled to the first fundamental mode of the cavity which has

an anti-node at the position of the atom. This is in contrast to the case of the second fundamental mode of the system where the cavity field has a node in the middle and therefore the atom is decoupled from the photonic field. In a single-mode cavity QED treatment or a round trip approach, one has to use extra care to make sure that such effects are included. However, the transfer matrix formalism, by construction, allows us to automatically evaluate transmission properties of light when atoms are located at arbitrary positions. For an atom positioned at z, the transfer matrix takes the form:

$$M_{total} = M_{mirror} M_{free}(z) M_{atom} M_{free}(L-z) M_{mirror}. \tag{F.5}$$

Note that the Rabi splitting is due the frequency dependent dispersive behavior of the scatterer. Therefore, one should not expect Rabi splitting when the phase introduced to the intra cavity field is fixed and frequency independent. For example, one can assume that the cavity is largely detuned from the atomic transition ($\Delta_0 \gg \kappa, \Gamma$). In this situation, the atom couples to light with a fixed dispersion and produces a shift to the cavity resonance equal to $\frac{g^2}{\Delta_0}$ (see Fig. F.2).

Here, we assumed that the cavity field only couples to forward propagating field. However, in general, not only both fields interact with the atom separately (diagonal element in the atom transfer matrix), but also the atom can couple them to each other (off-diagonal element in the atom transfer matrix). In Chapter 4, these effects are included.

In the following, we study the effect of adding a scatterer inside our cavity-like system (the single-photon gate in Chapter 4), on the transmission spectrum. We

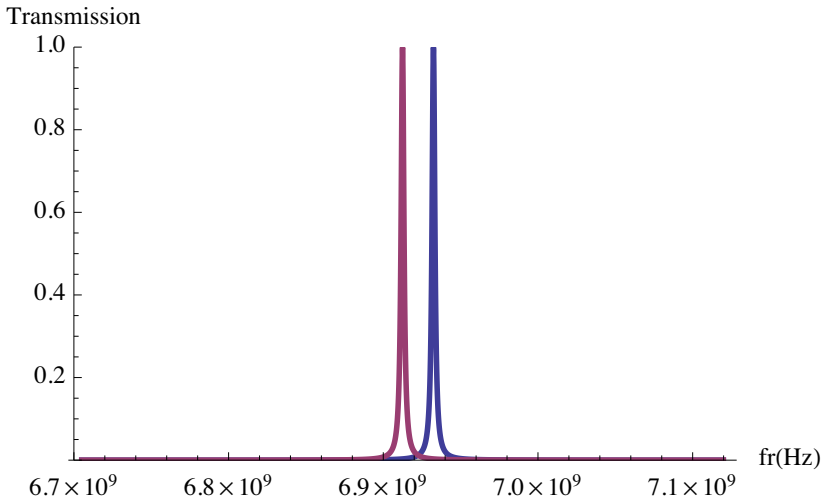

Figure F.2: Cavity resonance is shifted due to dispersive interaction between cavity and atom. $(2g/2\pi = 8MHz, \kappa/2\pi = 800kHz, \Delta_0/2\pi = 200kHz, \Gamma \ll \kappa, g)$.

investigate under what conditions one should expect a Rabi splitting, similar to cavity QED physics.

In the single-photon gate, the excited atom has two resonances, one single-photon resonance due a two-level transition with a characteristic width Γ , and a detuned Raman transition width a characteristic width of $\frac{\Omega^2}{\Delta^2}\Gamma$. By tuning the Zeeman shift, the backward (or forward) electric field of the target photon can become resonant with both of them. However, since tuning it to the Raman transition requires smaller magnetic field, we consider this case. As we said before, in order to the maximize the interaction with an atom (i.e. maximize the scattering from an atom), the Zeeman shift should be such that the frequency of the target photon becomes resonant with the atom. On the other hand, since the bandwidth of the photon (which is set by the band gap edge structure) is much smaller than the width of atomic resonances, we can safely consider that the impact of an atom on the photon is constant across

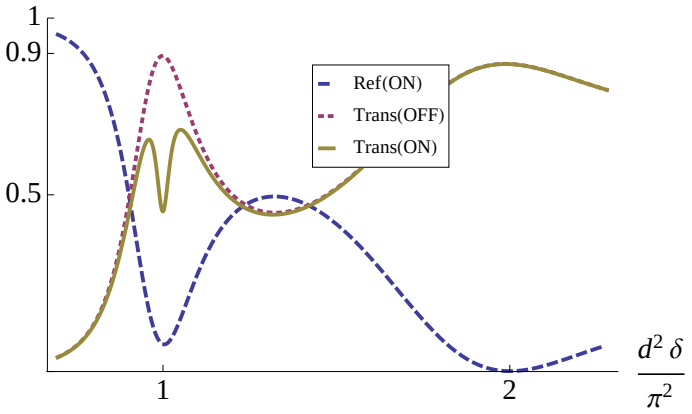

Figure F.3: The reflectivity ($R = |r|^2$) and the transmittivity ($T = |t|^2$) spectrum when the switch is ON or OFF, $OD = 300, \Gamma_{1D}/\Gamma = 0.1$. Since in low OD, the transmission bandwidth at the band gap edge becomes comparable to the single-atom Raman bandwidth ($\frac{\Omega^2}{\Delta^2}\Gamma$), Rabi splitting is observed in contrast to Fig. 4.4.

the frequency range of the first few transmission resonances at the band gap edge. We check this approximation more precisely. The first transmission resonance at the band gap each is given by $\delta_{res} = \frac{\pi^2}{OD}\alpha\frac{2\Omega^2}{|\Delta|}$ and the atomic resonance width is $\gamma = \frac{\Omega^2}{\Delta^2}\Gamma$. In a typical situation, we have: $\Delta \simeq 100\Gamma, \alpha = .4, OD = 30,000$. Therefore, we readily see that atomic resonance is much broader than the transmission bandwidth: $\delta_{res}/\gamma = 0.03$. This approximation is better satisfied for higher optical densities. Note that the numerical calculation for the fidelity is carried out without this approximation and they are exact. Therefore, the scatterer only suppresses the transmission peak rather than Rabi splitting the transmission resonance (see e.g. Fig. 4.4).

On the other hand, if we assume a comparatively low OD, the above assumption breaks down and we see the well-known Rabi splitting as shown in Fig. F.3.

Appendix G

Theoretical model for collective atomic recoil

G.1 Introduction

We develop a theoretical model to investigate optical nonlinearities due to collective motion of atoms. This model is important to study the recoil-induced resonance (RIR) and optical bistability due to collective interaction between weak pulses of light and external degrees of freedom of an ultracold slow-light medium. Since the conventional light storage or the nonlinear optical systems use atomic ground state coherence [113, 55], there are susceptible to the external magnetic and electric perturbation. However, using the motional degrees of freedom to create a highly dispersive gas and to mediate photon-photon interaction alleviates the sensitivity to external electric and magnetic field perturbations.

The motion of delocalized atoms under the influence of two or more light fields can

mediate conversion of the atomic kinetic energy into radiation[73]. These processes, termed 'recoil induced resonances' have been described both in terms of stimulated Raman scattering between different momentum classes of the atomic ensemble and in terms of Rayleigh scattering of the light fields off a periodic density modulation of the atomic distribution [169]. In the case of an optically thin sample of ultracold atoms illuminated by a strong pump beam and a weak probe, a perturbative analysis reveals that the probe experiences gain (loss) for red (blue) detunings relative to the pump [40]. The width of these features is proportional to the temperature of the atomic distribution. In this dilute limit, the amplification of the probe has little effect on the momentum distribution of the gain medium. In contrast, as the optical thickness of the gain medium increases, the probe can be amplified by around two orders of magnitude[168]. This can result in significant effects on the momentum distribution of the gain medium and in a variety of dynamical processes involving feedback between the gain medium and the amplified probe.

Further, there is a close connection between the phenomenon discussed here and collective atomic recoil effects inside a cavity such as spontaneous self-organization of the atomic medium [89], collective recoil lasing [105].

The absorption and the consequent emission of a photon result in a momentum recoil on a single atom. Once this simple phenomenon occurs for an ensemble of nearby atoms, a rich variety of behavior will occur. The collective behavior of atoms and photons has been a subject of tremendous research for more than a decade, yet new theoretical and experimental work are underway. A general theory was devised by Moore *et al.* [118] to study the center-of-mass motion in the collective atomic

recoil laser (CARL) and Berman [19] developed a framework for compare RIR and CARL. Later, Ling *et al.* [112] improved the theory by incorporating some relaxation parameters for the light field and the atomic momentum state but the origin of these relaxations and also the distinction between the coherent momentum transfer and diffusive population relaxation was not considered. On the other hand, there had been some efforts to investigate the mechanical behavior of an elongated BEC (similar to our MOT case) interacting with a pump and a probe light field [53]. By increasing the intensity of a the probe beam, a transition from the pure superradiant regime to the Bragg scattering regime (similar to Rabi oscillations in a two-level system) was observed [53]. The observations can be explained either through a CARL-BEC formalism (generalized Gross-Pitaevskii equation [53]) or the formalism explained here in the limit of low temperature. Not surprisingly, both formalism yield the same results.

Here, we develop a theoretical model to study the collective mechanical behavior of atoms interacting with light. This single model allows us to derive results consistent to previous work, by exploring different regimes. Moreover, this model is used to explain the absorptive bistability observed in our recent experiment [166]. Specifically, we consider an elongated atomic ensemble and investigate the atomic motion in the elongated direction while interacting with two light fields propagating along the elongation axes. The atomic ensemble can also be placed in a low finesse ring cavity to interact with a single mode of light inside the cavity.

G.2 Model

The system can be described by quantizing both the internal and external degrees of freedom of the atoms while treating the light fields classically. Accordingly, the Hamiltonian can be written as a sum over the contribution of different momentum classes, $\mathcal{H} = \sum_k \mathcal{H}_k$:

$$\begin{aligned}\mathcal{H}_k &= \frac{\hbar^2 k^2}{2m} c_g(k)^\dagger c_g(k) + \left(\frac{\hbar^2 k^2}{2m} + \hbar\omega_0\right) c_e(k)^\dagger c_e(k) \\ &\quad + i\hbar \sum_{j=1,2} (g_j a_j^* e^{i\omega_j t} c_g(k-k_j)^\dagger c_e(k) - H.c.)\end{aligned} \tag{G.1}$$

where $c_g(k)[c_e(k)]$ are the annihilation operators of ground (excited) state atoms with momentum $\hbar k$, $g = \mu(\omega/2\hbar\epsilon_0 V)^{1/2}$ is the atom-light coupling coefficient and $a_1(a_2)$ is the normalized electric field of the pump (probe) beams. We assume that the atoms are bosonic and therefore the following commutation relations hold,

$$[c_g(k), c_g(k')^\dagger] = [c_e(k), c_e(k')^\dagger] = \delta_{k,k'}. \tag{G.2}$$

The other commutators are zero. The equations of motion for the density matrix can be derived from $\dot{\rho}_{mn}(k,k') = \frac{i}{\hbar}\langle[\mathcal{H}, \hat{\rho}_{mn}(k,k')]\rangle$ where $\rho_{mn}(k,k') = \langle\hat{\rho}_{mn}(k,k')\rangle = \langle c^\dagger_{n,k'} c_{m,k}\rangle$. Hence, the evolution of the ground state density matrix elements is given by

$$\begin{aligned}&\frac{d}{dt}\rho_{gg}(k,k') = i\frac{\hbar(k'^2 - k^2)}{2m}\rho_{gg}(k,k') \\ &+ \sum_{j=1,2} g_j a_j^* e^{i\omega_j t}\rho_{eg}(k+k_j, k') + g_j a_j e^{-i\omega_j t}\rho_{ge}(k, k'+k_j)\end{aligned} \tag{G.3}$$

and the density matrix elements for the ground-excited state coherence is given by

$$\frac{d}{dt}\rho_{eg}(k,k') = i\left[\frac{\hbar(k'^2-k^2)}{2m} - \omega_0\right]\rho_{eg}(k,k') + \sum_{j=1,2} g_j a_j e^{-i\omega_j t}(\rho_{ee}(k,k'+k_j) - \rho_{gg}(k-k_j,k')) \tag{G.4}$$

In the limit of large pump detunings and weak excitation i.e. $ga_i \ll \Delta$, the excited state can be adiabatically eliminated by introducing the parameters $\rho_{eg} = \tilde{\rho}_{eg}e^{-i\omega_1 t}$ and $\delta = \omega_2 - \omega_1 = \omega_{probe} - \omega_{pump}$. In this case,

$$\tilde{\rho}_{eg}(k,k') \approx \frac{i}{\Delta}(g_1 a_1 \rho_{gg}(k-k_1,k') + g_2 a_2 e^{-i\delta t}\rho_{gg}(k-k_2,k')) \tag{G.5}$$

where $\Delta = \omega_0 - \omega_1$ is the pump detuning for the exited state. Thus, the evolution of the ground state populations and coherences are given by

$$\begin{aligned}\frac{d}{dt}\rho(p,p') &= 4i\omega_r(p'^2-p^2)\rho(p,p') \\ &+ i\frac{g_1 g_2 a_1^*}{\Delta}a_2 e^{-i\delta t}[\rho(p+1,p') - \rho(p,p'-1)] \\ &+ i\frac{g_1 g_2 a_1}{\Delta}a_2^* e^{+i\delta t}[-\rho(p,p'+1) + \rho(p-1,p')]\end{aligned} \tag{G.6}$$

where $\rho(p,p') = \rho_{gg}(k,k')$. Here, we have assumed that $|k_1| = |k_2| = k_0$ and the recoil frequency $\omega_r = \hbar k_0^2/2m$ and that the pump and the probe propagate are counter propagating i.e. $|\vec{k_1} - \vec{k_2}|/2k_0 = 1$ and $p = k/2k_0$.

On the other hand, the dynamics of the probe amplitude can be obtained using Maxwell's equations with the slowly varying envelope approximation,

$$(c^2k_2^2 - \omega_2^2)a_2 - 2i(c^2k_2\partial_z a_2 + \omega_2\partial_t a_2) = \frac{\mu\omega_2^2}{i\hbar g\epsilon_0}\tilde{P}_2 \tag{G.7}$$

where

$$\tilde{P}_2(z,t)e^{ik_2 z - i\omega t} = \frac{N\mu}{V}\sum_k \tilde{\rho}_{eg}(k+k_2,k) \tag{G.8}$$

By redefining ω_2 to take into account the linear dispersion, the time evolution of the probe beam, in the single-mode approximation, can be written as,

$$\partial_t a_2(z,t) = iN\frac{g_1 g_2}{\Delta} a_1 e^{+i\delta t} \sum_p \rho(p-1,p) \tag{G.9}$$

Therefore, the coherent dynamics of atom-photon interaction can be deduced by series of coupled equation given by Eqs. (G.6, G.9). We treat the incoherent part of interaction such as inelastic photon scattering and atomic collision, as extra damping terms both in photonic and atomic dynamics. Because of the decoherence among different momentum classes, we consider that only the first order coherence of the form $\eta(p) \equiv \rho(p+1,p)e^{i\delta t}$, are important. We neglect the higher order coherence among different momentum classes. Therefore, we obtain a set of coupled equations describing the dynamics of the ground state populations, coherences and the amplitude of the probe field:

$$\begin{aligned}
\partial_t \Pi(p) &= 2\Im[\beta^* a_2(-\eta(p)+\eta(p-1))] - \gamma_{pop}(\Pi(p)-\Pi_{th}(p)) \\
\partial_t \eta(p) &= i(4\omega_r(p^2-(p+1)^2) - \delta(t) + i\gamma_{coh})\eta(p) \\
&- i\beta a_2^*(\Pi(p+1)-\Pi(p)) \\
\partial_t a_2 &= i\beta N \sum_p \eta^*(p-1) - \kappa/2(a_2 - a_{in})
\end{aligned} \tag{G.10}$$

where $\gamma_{pop}(\gamma_{coh})$ are the population (coherence) relaxation rates respectively. The coupling coefficient is $\beta = g^2 a_1/\Delta$, and Π_{th} is the initial thermal distribution of the atoms. The cavity decay rate in the free space limit can be approximate by the inverse time needed for a photon to traverse the atomic ensemble i.e. $\kappa \simeq c/L$ where L is the length of the ensemble. We have also assumed that $g_1 = g_2 = g$.

These coupled equations describe a rich dynamics that ensue as a consequence of the high-gain RIR and can explain optical bistabilities due to momentum coherence.

But before elaborating on the experiment, to clarify the physics of these equation, we explore different limiting regimes of interaction between light and the motional degrees of freedom of atoms depending on the decoherence rate and width of the momentum distribution Δp. First, we consider the regime where all coherences among different momentum classes are absent either because of high temperature ($\sqrt{mk_BT} \simeq \Delta p \gg \hbar k$) or any other source of decoherence. Therefore only populations in different momentum states governs the dynamics. We show that the dynamics of the system can be described by a classical diffusive model where momentum population transfer occurs among momentum classes (Sec. G.3). In contrast to the first regime, in Sec. G.4, we analyze the sub-recoil temperature regime ($\Delta p \ll \hbar k$) in the strong coherent limit. A Bose-Einstein condensate falls into this regime. We show that the system dynamics can be reduced to a set simple three coupled differential equations. Depending on the probe intensity, we can deduce the superradiance and Rabi oscillation behaviors from these equations. On the other hand, the intermediate temperature regime ($\Delta p \sim \hbar k$) where the momentum coherence is still present, is the relevant case to our experiment which is used to explain the observed bistable behavior (Sec.5.2).

In this section for simplicity, the pump is considered to be non depleted (which is a fulfilled approximation for low optical densities)and therefore the dynamics of the a_1 is neglected. However, in the numerical simulation of Sec.5.4, the depletion of the pump is taken into account since the high gain limit the pump is depleted.

G.3 Limit of large decoherence: Population diffusion

In a regime where the coherence relaxation rate γ_{coh} is very large i.e. $\gamma_{coh} \gg |\beta a_2|$, the coherence between different momentum states can be adiabatically eliminated to obtain

$$\eta(p) \approx \beta a_2^* \frac{\Pi(p+1) - \Pi(p)}{4\omega_r[p^2 - (p+1)^2] - \delta + i\gamma_c} \tag{G.11}$$

We note that we have assumed the two-photon detuning is changing slowly comparing to the decoherence rate, i.e. $\dot{\delta}/\delta \ll \gamma_c$. Therefore, the detuning can be considered constant on this time scale. By plugging the momentum coherence back into the population equation, we obtain a diffusion equation for the population of different momentum states:

$$\begin{aligned} \frac{\partial}{\partial t}\Pi(p) &= -\gamma_{pop}\Pi(p) \\ &- 2\beta^2|a_2|^2 \frac{\gamma_{coh}[\Pi(p) - \Pi(p+1)]}{\gamma_{coh}^2 + (-\delta + 4\omega_r[p^2 - (p+1)^2])^2} \\ &- 2\beta^2|a_2|^2 \frac{\gamma_{coh}[\Pi(p) - \Pi(p-1)]}{\gamma_{coh}^2 + (-\delta + 4\omega_r[(p-1)^2 - p^2])^2} \end{aligned} \tag{G.12}$$

On the other hand, the dynamics of the probe is given by

$$\frac{\partial}{\partial t}a_2 = iN\beta^2 a_2 \sum_p \frac{\Pi(p+1) - \Pi(p)}{-\delta + 4\omega_r[p^2 - (p+1)^2] - i\gamma_{coh}} - \frac{\kappa}{2}(a_2 - a_{in}) \tag{G.13}$$

In the limit of a large momentum spread, the propagation of the probe field is characterized by a gain coefficient

$$g(\delta) = -iN\beta^2 a_2 \int \frac{\Pi(k + 2k_0) - \Pi(k)}{\delta + 4\omega_r + 2\omega_r \frac{k}{k_0} + i\gamma_{coh}} dk \tag{G.14}$$

We assume a Maxwell-Boltzmann distribution of momentum $\Pi(k) = \frac{1}{\sqrt{2\pi mkT}} e^{-\frac{k^2}{2mkT}}$. Approximating the population difference by $\Pi(k + 2k_0) - \Pi(k) \approx 2k_0 \partial_k \Pi(k)$ and the Lorentzian by a Dirac's delta-function, we recover a frequency dependent gain coefficient for the probe consistent with Ref. [40].

Moreover, it is easy to show that if the probe-pump frequency is far detuned form the recoil-induced resonance, Eq. G.13 reduces to a simple diffusion equation. In particular, when $\delta \gg k_0 \bar{v}$, where $\bar{v} = \sqrt{\frac{k_B T}{m}}$ is the characteristic spread in the velocity distribution, the right hand side of Eq. G.13 can be simplified to the second derivative of momentum distribution, i.e. $\Pi(p + 1) + \Pi(p - 1) - 2\Pi(p) \propto \partial_k^2 \Pi(k)$. Therefore, the momentum diffusion will be characterized by a diffusion coefficient $\beta^2 a_2^2 \frac{k_0^2}{\gamma_{coh}}$.

G.4 Subrecoil Limit

In the opposite limit, in an atomic ensemble with a very low temperature and negligible decoherence, the width of the momentum distribution is less than the recoil momentum. In this case, the density matrix of the system has only two relevant parameters: the population difference and the coherence between the two momentum classes p_0 and $p_0 + 1$. Introducing the parameters $\xi = \eta(p)$, $W = \Pi(p_0 + 1) - \Pi(p_0)$ and $A = -ia_2$, we obtain a closed set of equations

$$\frac{d\xi}{dt} = -i\delta'\xi + \beta A^* W - \gamma_{coh}\xi \tag{G.15}$$

$$\frac{dW}{dt} = -2\beta A\xi + c.c. \tag{G.16}$$

$$\frac{dA}{dt} = \beta N \xi^* - \frac{\kappa}{2}(A - A_{in}) \tag{G.17}$$

where $\delta' = 4\omega_r(2p_0 + 1) + \delta(t)$. These equations are consistent with the evolution equations from a Gross-Pitaevskii model [53]. This set of equations lend themselves to simple solutions in two extreme cases.

First, in the case of no input probe i.e. $A_{in} = 0$ and large attenuation in free space i.e. $\kappa \simeq c/L \gg \delta', \gamma_{coh}$, the light field can be adiabatically eliminated to obtain $A \approx 2\beta N \xi^*/\kappa$. Further, if $\delta' = 0$, the equations for the coherence and the population difference reduce to

$$\frac{d\xi}{dt} = -\gamma_c \xi + 2\frac{\beta^2 N}{\kappa}\xi W \tag{G.18}$$

$$\frac{dW}{dt} = -4\frac{\beta^2 N}{\kappa}|\xi|^2 + c.c. \tag{G.19}$$

which allow a superradiant solution of the form [131, 53],

$$W = -1 + \left(1 - \frac{2\gamma_c \kappa}{\beta^2 N}\right)\left(1 + \tanh[(\beta^2 N/\kappa - \gamma_c)(t - t_d)]\right) \tag{G.20}$$

where we have assumed that initially the total population is in the momentum state p_0. Therefore, the flux of photon which is proportional to $\kappa|\xi|^2$ exhibits a superradiance with a gain equal to $\beta^2 N/\kappa = N(g^2 a_1/\Delta)^2/\kappa$.

On the other hand, in the presence of a significant input probe beam, in other words $(g^2 a_1/\Delta)A_{in} \gg \beta^2/\kappa$, it can be assumed that the probe is not affected by the atomic dynamics. In this case, the population different is given by

$$W(t) = e^{-\gamma_c t/2}(\cos\Omega_R t + \frac{\gamma_c}{2\Omega_R}\sin\Omega_R t) \tag{G.21}$$

and the system exhibits Rabi oscillations between momentum states p_0 and $p_0+1$with a frequency $\Omega_R = \sqrt{(g^2 a_1/\Delta)^2 A_{in}^2 - \gamma_c^2/4}$.